A Direct Performance Based Seismic Design Method for Irregular Structures

Applications to **Concrete Structures**

by LUIS ALBERTO MONTOYA CORONADO

Supervised by

Jesús Miguel Bairán García

November, 2016

A dissertation submitted to the Department of
Civil and Environmental Engineering
Polytechnic University of Catalonia
For in partial fulfillment of the requirements for the degree of
Doctor of Philosophy

UNIVERSITAT POLITÈCNICA
DE CATALUNYA
BARCELONATECH

This page is left intentionally blank

To my beloved family
My parents, Alberto and Violeta
My sisters, Violeta Alexandra and Gabriela Paola

This page is left intentionally blank

ACKNOWLEDGEMENTS

All goals in life are not possible without the support of everyone around, either close as far. The support and encouragement of my beloved family was essential in this thesis, my parents Alberto and Violeta, my sisters Violeta and Gabriela. This thesis was possible because of your support. I want to express also my gratitude to my beloved wife Helen, which was essential during this long stage.

I would like to express my sincere gratitude, as well, to my supervisor and professor Jesús Bairán for all the advices, knowledges, hard and great work, and to be an excellent mentor whom I learn a lot. I also want to thanks professor Bairán for allowing to work in this research and for showing me the road and helped to get started on the path to these degrees. Of course, I want to thanks to Prof. Toni Marí, Monste Bernaus, Noemí Duarte and professor Eva Ollers, for its kind attention and help in the research group.

I'm very grateful to Professor Fabio Biondini, who accepted me as a visiting Ph.D. student at the Department of Civil and Environmental Engineering from Politècnico di Milano. All the advices, suggestions, all the knowledge and long discussion help me a lot for this thesis, many thanks to Professor Fabio Biondini and Alessandra for being excellent and kind persons. I also want to thanks Dr. Andrea Titi and Dr. Bruno Dal Lago for the good attention at the stage at POLIMI.

Also, I'm very grateful with the Catalan family Ferrer-Piqué, for the pleasant welcome and very nice long stage in this city and country. Thanks to be always as a family, as well, and being there for everything for Helen and me. Thanks a lot!

Of course, this long stage for Master's and Doctoral studies would not have been so easy without all the colleagues and friends. Thanks to Leandro Martinez and Iván Burgos, for being a great friend and making many good moments to remember. Better times will come for other memories.

A special mention must be done for all the colleagues in this research with whom I share a wonderful time during "the free" time, for the good friendship and help as well. Specially, with whom I started, the group "Despacho 2", with Dr. Ricardo Pieralisi, Dr. Amin Housseini and Dr. Renan Piccolo. Thanks also to Dr. Andres Henao and his wife Daniela for the goods weekend and very good friendships. I want to extend, of course, this acknowledgement to my other good friendships and soon very good doctors in this Department, for the good fishing tours with Ruben Lopez and Razmik Martirozyan, as well as, the Brazilian girls, Andressa Gobbi, Talita Pieroni, Mylene de Melo and Debora Carlesso. The Iranians guys, Amir and Golshid, and to Janill Marie, Edu Galeote, Luis Sanchez and Tai Ikumi. I have many people who is involved in this thesis, the degree is a memory of them all.

Finally, the present study has been partially supported by the projects PROPPOSE – "Performance based design of partially prestressed concrete structures. Proposed new methodology, experimental verification and design criteria" (BIA2012-36848)

This page is left intentionally blank

This page is left intentionally blank

ABSTRACT

Designing structures to achieve a specified performance state has gained importance on seismic design practice. Currently, several methodologies have been proposed in order to take into account for inelastic behavior of the structure in design phases. In that sense, a performance limit state can be provided that controls damage and strength demand. However, most of these methods involve iterative process that depends, in some cases, on the experience of the designer. Otherwise, many are based on the concept of equivalent single degree of freedom system, which is, only adequate for regular structures.

In this Thesis, a direct performance based seismic design methodology for irregular structure with damage control is proposed. This method is based on the superposition of two elastic spectral analyses. One strength of the method is the selection of the local distribution damage regions (by mean of plastic hinges), intentionally chosen by designer. The distribution of hinges defines the zones where damage is allowed and the desired failure mechanism in the design.

A damage parameter (α) is defined to control the damage intensity in the plastic hinges and the non-structural damage through allowable displacement or drifts. This coefficient is also used for the superposition of the two elastic solutions. In this way. It is possible to estimate the evolution of the non-linear response as this parameter varies, the adequate value of α for target performance can be easily selected.

A series of case-studies examples are developed on 2D and 3D irregular systems, both in plan and height. Moreover, the effects of higher modes of vibrations is highlighted on the design process, making possible to account for them in the final design. The method is validated through non-linear analyses, by means of incremental static analysis (pushover) and step-by-step time-history analysis. The results presented show good accuracy when predicting local damage, ductility and strength demand in design phases. Moreover, the methodology was used as

an assessment method as well, applied to a numerical example and a pseudo-dynamic test on a full-scale prototype. It was demonstrated, in both cases, the importance of the effect of higher vibration modes. In these cases, it was evidenced that, the current provisions to achieve the “strong column – weak beam” capacity criterion may not be adequate in a general basis. The proposed method allows for a more general way to obtain the overstrength factor for columns, which may be different in different stories.

RESUMEN

El diseño de estructuras para satisfacer niveles prestacionales, o de desempeño específico ha ganado interés en la ingeniería sismo resistente. Actualmente, existen varias metodologías de diseño sísmico basadas en prestaciones, en las cuales se intenta tener en cuenta el comportamiento no-lineal en las fases de diseño, controlando el nivel de daño y la demanda de resistencia a rotaciones concretas. Sin embargo, la mayoría de los métodos tienen procesos iterativos, que dependen, en algunos casos, de la experiencia del proyectista. Por otro lado, muchos están basados en el concepto de sistemas equivalentes de un grado de libertad, el cual es adecuado sólo para estructuras con esquema regular.

En esta tesis se desarrolla un método de diseño sísmico basado en prestaciones (o desempeño) para estructuras irregulares con control de daño. Este método se basa en la superposición de dos análisis espectrales elásticos, lo que hace que sea directo (no iterativo). Un punto fuerte del método es poder seleccionar los daños locales intencionalmente a través de rótulas plásticas, en el cuál el daño es permitido y el mecanismo deseado es asegurado. Se define un parámetro (α) para controlar la intensidad del daño en las rótulas plásticas y los daños no estructurales a través de desplazamientos y derivas de piso. Este coeficiente sirve, a la vez, para combinar las soluciones elásticas mediante superposición. De esta forma, se consigue estimar la variación de la respuesta no-lineal en función de dichos parámetros. Así, el valor adecuado de α para una prestación objetivo puede relacionarse fácilmente. Se desarrolla una serie de ejemplos y casos de estudios de diversos sistemas 2D y 3D sobre estructuras irregulares en planta y altura. Además, el efecto de los modos altos de vibración se hace evidente en el proceso de diseño.

El método es validado a través de análisis no-lineales en el tiempo (time-history) y mediante modelos no-lineal estático (Pushover). Los resultados presentados son considerados como buena aproximación en la predicción de daños locales y demanda de ductilidades en las fases de diseño. Por otro lado, el método también

fue utilizado como método de evaluación para un ejemplo numérico y un experimento pseudo-dinámico en un prototipo a escala real. En estos casos, se evidenció que, las actuales provisiones normativas para conseguir el criterio de capacidad de la columna fuerte – viga débil pueden no ser adecuadas o suficientes. El método propuesto permite estimar el coeficiente de sobre-resistencia a aplicar a las columnas de una forma más óptima, el cual puede ser diferente para diferentes pisos.

CONTENTS

This page is left intentionally blank

TABLE OF FIGURES

LIST OF TABLES

This page is left intentionally blank

This page is left intentionally blank

CHAPTER 1

INTRODUCTION

1.1 Background and context

In recent earthquakes, e.g. Northridge 1994, Kobe 1995, L'Aquila 2009, Canterbury 2010, Maule 2010, Ecuador 2016 and Taiwan 2016 among many others, the adequacy of capacity seismic design based on preventing structural collapse has been confirmed. However, it has also been highlighted the extensive damage levels that can be produced in the process. Currently, the goal of seismic design goes beyond preserving life safety, but also to control damage in structural and non-structural components. The allowable damage intensity should be consistent with previously selected performance objectives.

Performance – based seismic design (PBSD) is a conceptual design framework whose early developments can be tracked back to the decade of 1990's, SEOC (2000), ATC-40 (1996), FEMA 273 (1997), Bertero et al (2001), among others, wherein design criteria are expressed in terms of performance objectives selected for a structure subjected to different levels of seismic hazard. It is a powerful design approach based on the idea that performance objectives (such as immediately serviceability, damage limitation to reparable extent, and life safety) can be related to the level of structural damage and other possible indicators, as inter-story drifts and/or member deformations.

These concepts imply the need for occurrence of inelastic behavior in structural elements. Many approaches have been proposed by the research community during the late 90's and the decade of 2000. Assessment and verification methods, such as the "Capacity Spectrum Method" in the ATC-58 Project, FEMA (2012) and "N2 Method" Fajfar (2000), appeared during the early years, as well as some concepts and definitions of the objectives of the "Performance Based Design" (PBD). However, design tools and methodologies were still to be defined, making PBD mainly an iterative process, to be applied in special situations.

In order to successfully implement performance based design, practical methodologies should be developed that, in the case of earthquake performance, accounts for non-linear behavior of structures. This latter aspect is a relevant inconvenient that has limited an extended use of the performance based design paradigm.

Many researchers have worked in developing practical design methods to achieve a limit damage state by using some simplification on the non-linear dynamic performance. Some of the more extended ones are the Displacement Based Seismic Design (DBSD), and its simplified format Direct Displacement Based Design (DDBSD), proposed by Priestley & Kowalsky (2000) during the late 90's. This method is currently well extended and accepted in specialized practice

due to its simplicity and direct process. Other methodologies have also been proposed by Ayala, et al. (2012), (Franchin & Pinto, 2012), Sullivan (2011), Kappos & Stefanidou (2010), (Benavent-Climent, 2007), Chopra & Goel (2001), (Benavent-Climent, 1997) Panagiotakos & Fardis (1999), (Akiyama, 1999) among many others.

As a key aspect in PBD is the explicit and realistic consideration of the inelastic behavior, most of the existing proposals are iterative, except for the DDBSD. The simplified DDBSD is a direct approach; however, it requires substituting the structure by an equivalent single degree of freedom (SDOF) model based on plausible assumptions of the deformation shape of the 1st vibration mode. As stated by the authors, this simplification is applicable to regular structures.

The methodology that is developed in this thesis corresponds to the extension of the work of non-linear static design approach to seismic loadings. This aim requires a framework to control the dynamic characteristics of the structure after the seismic demand and its performance variation.

Although the referred design method proposed in this thesis is not restricted to concrete structures, it presents advantages when applied to this type of structures, and others materials that may exhibit limited ductility, as it particularly focuses on the selection of the zones where forces will be dissipated or redistributed, the distribution of ductility demand and how to design for it, as in Bairán & Marí (2010).

1.2 Motivation

In the recent seismic events that strike regions with constructions designed according to seismic provisions, it was observed that a large number of structures that survived the earthquakes without collapsing suffered disproportional damage levels, making reparation economically unfeasible (Pampanin, 2012).

Although, this performance is considered as adequate according to the collapse prevention requirements in current codes, rehabilitation and facilities substitution in frequent events resulted excessive economic losses. This has turned into the attention of stakeholders, insurance companies and general public and highlighted the need of multiple performance requirements for different hazard levels.

In order to provide safe and economic designs, together with adequate degree of reparability, plausible methods are needed to include residual damage and deformation as a design variables. Damage in structural and nonstructural components is strongly related to the maximum deformability and the residual displacement in local components and the overall structure. Therefore, considering residual deformation and its distribution in early design steps is crucial and implies accounting for the inelastic response.

The inelastic behavior is intended to be reached in several performance based design methods as a manner of “non-linear” design, i.e. a design procedure in which the degree of redistribution and ductility demand is a-priori selected in order to achieve a given structural performance with economic or sustainability benefits. It is possible to design a structure intended to consider real behavior, in which it has to exceed elastic branch in a force-displacement curve. In many exiting methods for design assumes a plastic structural response based in the two collapse theorems of the theory of plasticity. However, concrete structures do not show a perfect plastic or elasto-plastic behavior. On the contrary, they show limited

ductility. However, it is possible to design for higher ductility in order to satisfy the demand.

In this sense, the Concept of “non-linear design” is to account for the non-linear behavior in first design steps. That means, to design not only for resisting the elastic internal forces, but also to select a specific level of force redistribution as well as a reinforcement design for a ductility demand. In that way, it is intended to reach a reinforcement layout in which concrete structures achieve ultimate state while the internal force coincides with proposal design.

Lately, some performance based design methods are proposed with the concept of double linear analysis as in Franchin & Pinto (2012) and Bairán & Marí (2010). Where, numerous of equivalent linear analyses of seismic performance at each point in the design phases are computed, implementing an intermediate element-by-element damage assessment after the first analysis. For the latter method, a superposition of both analysis is computed to find a final response.

1.3 Objectives

The main goal of this thesis is to develop a direct performance based seismic design method applied for irregular concrete structures, where the designer may explicitly take into account the no-linear behavior in the early phases of design. A design procedure with such characteristics have been considered as “non–linear design” in (Bairán & Marí, 2010), where an adequate procedure was proposed applied to static loads enabling any degree of redistribution of the internal forces envelope that optimizes the design with adequate safety. The process is direct and is based on a double elastic analysis of the original and an auxiliary structure with perfect hinges, which are combined in a convenient manner.

A number of specific objectives must be formulated to meet the main goal. The first specific goal is to develop a numerical model algorithm enabling the necessary modal spectral dynamic analyses of the original structure and the auxiliary system with perfect hinges, being like this capable to obtain all modal properties and result to reach for a well design. Other specific objectives are described below.

- To extend the theory developed in (Bairán & Marí, 2010), accounting for dynamic and seismic loads. As well as, keeping it attractive for design practice. As it is based on linear analysis, concepts of model spectral analysis will be used.

- To look for a practical design parameters that allows controlling the damage, strength and ductility demand, so it can be used as design variable.

- To study the effects of multimodal response and derive an approach to take them into account in the design method.

- To study the effects of irregularities in height and plan in the response of the damaged system and investigate if the method can account for.

- To enable the use of different dissipating systems from the structural construction technology, i.e., Reinforced Concrete (RC), Partially Prestressed Concrete (PPC), with bonded or unbonded active reinforcement, seismic devices, etc.

- To validate the design methodology by means of up to date assessment methods, including explicitly the non-linear and dynamic behavior, namely, pushover and non-linear time-history analysis.

This page is left intentionally blank

CHAPTER 2

STATE OF THE ART

2.1 Earthquake engineering design and structural dynamics

Earthquake engineering is the discipline that solves the problem of studying the effects of earthquakes on infrastructures and designing them the service seismic events. In this problem, the demand (earthquake) is a time varying actions if posed in the frequency (or period) domain. Earthquake ground motion contains an infinity of number of frequencies deforming through a medium (soil or rock). On the other hand, all structures have their own dynamic properties and interacts with the ground motion. In seismic analysis it is necessary to work with the two types of frequency dependence mentioned above, one as a demand and the other as a response.

The modal uncoupling method is the most extended elastic seismic analysis. Besides being the fastest method, it shows a conceptual idea of the “n” shapes of independent displacement of structures, where modal superposition describe the complex vibration deformation of a multi-degree of freedom (MDOF). Those displacement shapes are called vibration modal shapes. This methodology allows to obtain two kind of structural responses: the time – history response at each interval of time and the maximum response that is calculated by means of response spectrum. In both cases, it is important to notice that this modal uncoupling method is valid only for linear structural response, i.e. constant stiffness and proportional damping matrices. Based on basics structural dynamic concepts, the motion equation is deduce in Chopra (2007), Paz (1998), Clough & Penzien (1993) among others. The equation of multi-degree of freedom for free vibration ca be written as (2.1).

$$M\ddot{u} + Ku = 0 \tag{2.1}$$

The non-trivial solution of (2.1) leads to an algebraic problem, called the Matrix Eigenvalue problem. The stiffness and mass matrices K and M are known. The problem is to determine the scalar ω_n^2 and vector $\emptyset_n$ as in Eq (2.2). The notation are, circular frequencies and Eigen vectors, respectively.

$$[K - \omega_n^2 M]\emptyset_n = 0 \tag{2.2}$$

2.1.1 Modal Spectral Analysis

Structural design is usually based in the peak values of forces and deformations over the duration of the earthquake – induced response. The peak response of a SDOF (single degree of freedom) systems can be calculated from the response spectrum. The estimation obtained is accurate enough for structural designs applications. However, the total response of a MDOF (Multi-degree of freedom) will be a combination of all peak values from all modal response. Several method exist for modal combination, as the square root of sum of squares (SRSS), proposed by Rosenblueth (1951), for well-separated natural frequencies. The maximum

response is obtained by square root of sum of square of response in each mode of vibration and is expressed by:

$$R_{max} = \sqrt{\sum_{i=1}^{n} r_i^2} \tag{2.3}$$

The complete quadratic combination (CQC) proposed by Wilson, et al. (1981) for earthquake excitations that contain a wide band of frequencies with long phases of strong shaking is define with the following equation.

$$R_{max} = \sqrt{\sum_{i=1}^{n}\sum_{j=1}^{n} r_i \cdot \alpha_{ij} \cdot r_j} \tag{2.4}$$

Where r_i and r_j are the maximum response in the i and j modes, respectivetly and α_{ij} is the correlation coefficient. . Other methods, such as the absolute sum and double sum, have been proposed for modal combination, among others.

2.1.2 Viscous Damping

The process by which the free vibration of a structure steadily diminishes in amplitude is called damping. When damping is considered, the equation of motion is:

$$\boldsymbol{M}\ddot{u} + \boldsymbol{C}\dot{u} + \boldsymbol{K}u = 0 \tag{2.5}$$

Nevertheless, it is not easy to determine the damping matrix $[\boldsymbol{C}]$. Hence, modal damping ratios are estimated using measured data from similar structures. Most of the recorded data used for damping estimation come from structures shaken bellow the inelastic range. On the other hand, recorded motions of structures that have experience significant yielding during an earthquake would provide additional damping that also include energy dissipation due to yielding. Most building codes typically defines the design response spectrum for a reference structural damping ratio of 5%. However, actual damping ratio varies for different structural materials,

systems and stress levels. In Table 2.1 some damping values for structural systems are shown (Newmark & Hall, 1982).

Table 2.1. Recommended damping values

Stress level	Type an condition of structure	Damping Ratio (%)
Working stress, no more than about ½ yield point	Bolted and riveted steel or bolted joint	5-7
	Welded steel, prestressed concrete, slightly cracked reinforced concrete	2-3
	Reinforced concrete with considerable cracking	3-5
At or just below yield point	Welded steel, prestressed concrete without complete loss in prestressed	5-7
	Reinforced concrete	7-10
	prestressed concrete with loss of prestressed	7-10
	Bolted and riveted steel, wood structures with bolted joint.	10-15

2.2 Hysteretic energy dissipation

The hysteretic energy in an element is dissipated by a structural system during a seismic event when a certain amount of nonlinearity deformation takes place. It has been recognized by several researchers as an indicator of the level of seismic force reduction through energy dissipation, e.g. Park, et al. (1987), (Benavent-Climent, 2011), Bojorquez, et al. (2011). In general, a hysteretic loop with large energy dissipation capacity at a member level are considered as a guarantee of better deformation performance of the system, implying that there is a good correlation between the dissipated hysteretic energy and the inelastic deformation demands (see Figure 2.1). However, unlike the structural stiffness, it is complex to compute the damping coefficient from the dimensions of the structure and materials properties. Thus, it is not feasible to identify all the mechanisms that dissipate vibrational energy in structures.

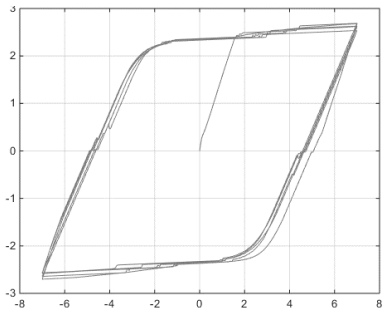

a. Reinforced concrete

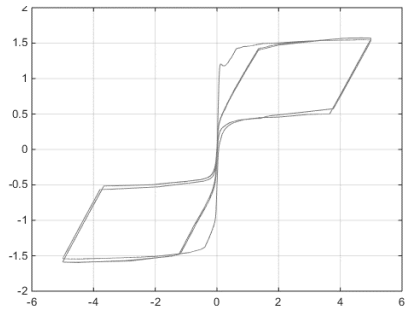

b. Partially prestressed concrete with unbonded tendons

Figure 2.1. Numerical moment – curvature hysteretic loop relation for a particular structural concrete element

2.2.1 Ductility and energy dissipation relationship

A relationship between force and deformation is needed in order to determine the amount of energy dissipation. In a single degree of freedom (SDOF) system, a complete force – displacement cycle, with load reversals, is representative of the maximum deformation demand during an earthquake. The area enclosed in the loop (Figure 2.1) is dissipated in that cycle. As an viscous damped system also dissipates energy within each cycle, an equivalent damping ratio for the nonlinear system may be derived. In Chopra (2007), this was demonstrated by considering a steady-state motion of a single degree of freedom system due to the harmonic force as in Eq. (2.6).

$$f(t) = f_o \cdot \sin \omega t \tag{2.6}$$

It can be shown that the energy dissipated in a load cycle by a damped SDOF is given by Eq. (2.7), where u_o is the maximum displacement in a cycle and $\omega_n = \sqrt{\frac{K}{M}}$ is the natural frequency of the system.

$$E_D = c \cdot \pi \cdot \omega_n \cdot u_0^2 \tag{2.7}$$

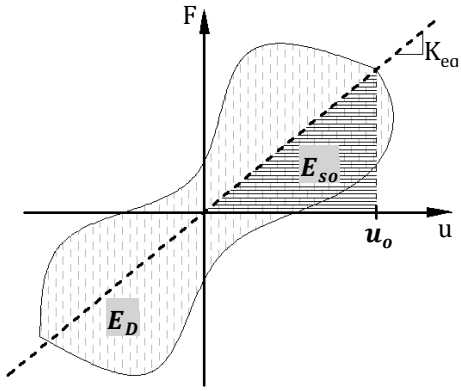

Figure 2.2. Energy dissipated E_D in a cycle of a harmonic vibration determined for any hysteretic loop

The most common method for defining equivalent viscous damping is to equate the energy dissipated in a vibration cycle of the actual structure and an equivalent viscous system (Blandon, 2004). The structure force – displacement relation may be obtained from experiments or from numerical non – linear analysis under cyclic loading. The energy dissipated in the actual section is given by the area E_D enclosed by the hysteresis loop as in Figure 2.2, as in Chopra (2007), Paz (1998), among others. By equating E_D to the energy dissipated in viscous damping given Eq. (2.7), the following relationship is obtained:

$$\xi_{hyst} = \frac{c_{eq}}{c_{cr}} = \frac{1}{4\pi}\frac{E_D}{E_{so}} \tag{2.8}$$

Where the strain energy is calculated from the equivalent stiffness as,

$$E_{so} = \frac{K_{eq} \cdot u_{max}^2}{2} \tag{2.9}$$

This formulation is widely accepted and it has been applied to model the damping in multi-degrees of freedom systems. In most performance based seismic design methods, the total damping of the structure is considered as the sum of the elastic viscous damping and the hysteretic damping as:

$$\xi_{eq} = \xi_{el} + \xi_{hyst} \tag{2.10}$$

Where the hysteretic damping (ξ_{hyst}) depends on the hysteretic rule corresponding to the structure that is being designed. The elastic damping (ξ_{el}) ratio is usually taken as 0.05; although, alternative values have been given in Table 2.1.

Jacobsen (1930) proposed the first approximate solution of the steady-state of a non-linear oscillator by defining an equivalent linear oscillator. In Jacobsen's approach, both oscillator have the same natural frequency and dissipate equal energy per cycle of a sinusoidal response. In performance based seismic design methods, Jacobsen's damping was combined with the secant stiffness as equivalent stiffness K_{eq} (see Figure 2.1). This differs from the Jacobsen's initial work in which it is used the initial stiffness. The equivalent linearization approach defined by Jacobsen's damping and the secant stiffness is referred to as the JDDS approach (Jacobsen's Damping Secant Stiffness), such combination was proposed by Rodenblueth & Herrera (1964). The JDSS approach applied to the rigid-perfectly-plastic loop (RPP) shown in Figure 2.3 yields an equivalent damping in (2.11), with an equivalent coefficient of $2/\pi$. The area A_1 is the area of the hysteretic loop, and A_2 is the area of RPP loop which encompasses the hysteretic loop of area A_1.

In the work presented by Grant, et al. (2004), it was shown that viscous and hysteretic damping should not be added directly. Instead, if the structure exhibits viscous damping which is proportional to tangent stiffness, this damping value should be reduced prior to adding it to the hysteretic component.

$$\xi_{hyst} = \frac{2}{\pi} \cdot \frac{A_1}{A_2} \tag{2.11}$$

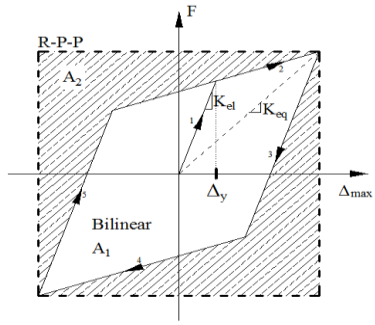

Figure 2.3. Equivalent damping for bilinear and RPP hysteretic rule

2.2.2 Equivalent hysteretic damping for different structural systems.

There exist different proposals to obtain equivalent damping for reinforced concrete structures. Blandon (2004) and Rodiguez, et al. (2012) reviewed and studied the existing approach for all type of elements, such as Priestley, et al. (2007), Kowalsky (1994), Dwairi, et al. (2007), Gulkan & Sozen (1974), Rodenblueth & Herrera (1964), among others. The work of Dwairi, et al. (2007), Priestley & Kowalsky (2000) represented the hysteretic component of response in the form:

$$\xi_{hyst} = C \cdot \left(\frac{\mu - 1}{\mu \cdot \pi}\right) \tag{2.12}$$

Where the coefficient C depends on the shape of the hysteresis loop. This type of relationship can be derived from the area-based approach of Eq. (2.10) for the Elastic Perfectly Plastic (EPP) rule. In this case, it can be shown that the factor C would be equal to 2. However some period dependency was found for effective periods $\mathrm{T_e} < 1.0\ \mathrm{second}$. In Priestley, et al. (2007), it can be found values of the C constant for different hysteretic systems (see Table 2.2).

Table 2.2. Coefficient C corresponding to structural typology

Concrete wall building, Bridges	$\xi_{eq} = 0.05 + 0.444 \cdot \left(\frac{\mu - 1}{\mu \cdot \pi}\right)$	(2.13)
Concrete frame building	$\xi_{eq} = 0.05 + 0.565 \cdot \left(\frac{\mu - 1}{\mu \cdot \pi}\right)$	(2.14)
Hybrid prestressed frame	$\xi_{eq} = 0.05 + 0.186 \cdot \left(\frac{\mu - 1}{\mu \cdot \pi}\right)$	(2.15)
Steel frame building (RO)	$\xi_{eq} = 0.05 + 0.577 \cdot \left(\frac{\mu - 1}{\mu \cdot \pi}\right)$	(2.16)
Friction slider (EPP)	$\xi_{eq} = 0.05 + 0.670 \cdot \left(\frac{\mu - 1}{\mu \cdot \pi}\right)$	(2.17)
Bilinear isolation system (BI r=0.2)	$\xi_{eq} = 0.05 + 0.519 \cdot \left(\frac{\mu - 1}{\mu \cdot \pi}\right)$	(2.18)

2.3 Seismic performance assessment

The prediction of inelastic seismic response is an essential component of performance seismic design and assessment (PBSD). Some methods, as the non – linear static analysis or the non – linear time history analysis, allow engineers to "understand" structure's behavior and progression of damage in structural elements with increasing ground motion intensity. In some way, all PBSD methods evaluate if the collapse mechanisms are produced safely in the intended manner. At the same time, they ensure that all the strength capacity is exploited.

2.3.1 Non – linear static analysis (Pushover)

In this procedure, the static loads are applied in incremental steps until a failure mechanism of the structure is reached, as described in FEMA-273 (1997). The non – linear designation comes from the fact that the various components/elements are modeled using a non – linear model, normally with concentrated plastic hinges in elements. This is one of the most widely used methods for structural seismic assessment due to its low computational cost and its ease of use in comparison with non – linear dynamic analysis. For example, it does not require selecting and scaling of ground motions records. In contrast, it can only estimate the maximum response, but not the transient one. The basic steps of a pushover analysis are describe in the Figure 2.4. (Bento, et al., 2004)

1. Model structure

2. Select pattern of distribution of loads

3. Perform a series of non – linear analyses, increasing the load distributed in the selected pattern step by step on sequentially degraded models as damage is predicted

4. Develop pushover curve as the connection of the results of base shear at every step and the corresponding top displacement

5. Determine effective dynamic properties

6. Determine demand lateral displacement for design ground motion

7. Check adequacy of elements for force and deformation demands at design lateral displacement.

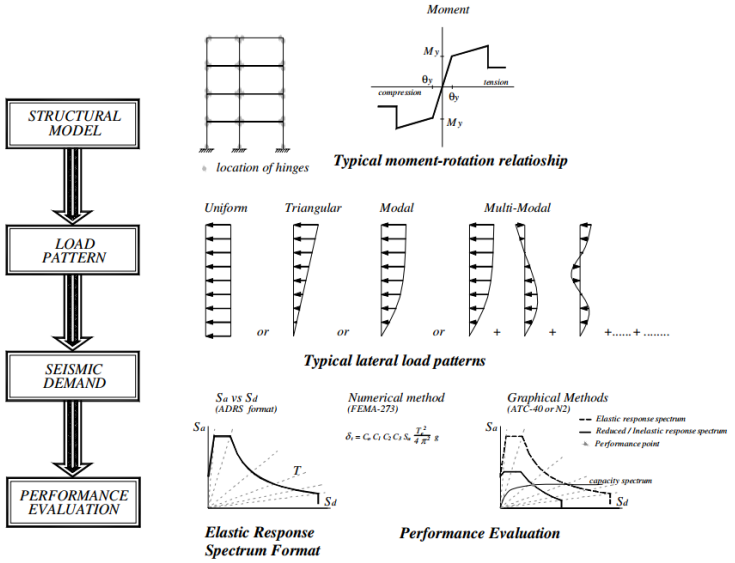

Figure 2.4. General flowchart for Non –linear Static Procedure (Bento, et al., 2004)

2.3.2 Time – History analysis

When the transient behavior is of interest, besides the peak response, there are two main analysis methods: modal superposition and direct time integration. While for the analysis of linear structures both methods are applicable, in the case of non – linear behavior, the latter method is the only option. For a non – linear analysis, a realistic enough behavior could be observed by modeling concentrated plastic hinges in elements which will provide the mechanism progress as damage takes place.

A number of numerical methods for time-integration algorithm are available. According to Dokainish & Subbaraj (1989), ideal algorithms should be unconditionally stable and second-order accurate, generate low frequency error

and low damping error, high or controllable damping for the high frequency response, be computationally efficient and self-starting or single-step.

Houbolt (1950) made one of the first attempts to develop an integration scheme for the computer analysis of aircraft dynamics. In structural dynamics problems, governing equation is a second order differential equation. The widely used solution techniques include direct integration, step-by-step time interval integration and implicit schemes (Hughes, 1987) are; those related to Newmark's method as, Newmark – β method (Newmark, 1959), $\text{Wilson} - \theta$ method (Wilson, 1968), Hilber – Hughes – Taylor (HHT) method (Hilber, et al., 1977), the Generalized-α method (Chung & Hubert, 1993).

Those techniques can be referred as one-step method with a second order accuracy, which is unconditionally stable in linear dynamics and permits an efficient variable step size variation. The Newmark – β method and Newmark family of algorithm, are widely used in numerical evaluation of the dynamic response of structures adapted to non – linear system with concentrated plastic hinges. Dahlquist (1963) showed that the constant average acceleration method is the most accurate unconditionally stable scheme.

2.4 Performance based design methods

One of the major development in seismic design has been the increased emphasis on multiple limit state design, as can be seen the "Performance based engineering" (Priestley, 2000). Design for seismic resistance has been undergoing a critical reappraisal, with the emphasis changing from "resisting" to "performance" on summing an earthquake. The concept of designing structures to achieve a specified performance limit state, defined by strain or drift limits, was first introduced. Currently, performance based design (PBD) is a design philosophy that places structures' non – linear behavior in relation to their real needs, reducing leadership to standards methods. PBD gives more freedom to design procedures,

and provides ways to compare different of methods. It opens a wide range of possibilities, techniques, methods that allows the most of material properties, structural typologies and adaptive behavior.

One relevant landmark was the capacity design principle proposed in New Zealand in 1970 by Park & Paulay (1975). It was a formal realization that the relative distribution of strength through a structure was more important than the absolute value of design base shear. It was recognized that a frame building would perform better under seismic actions if it could be assured that plastic hinges form in a particular order, so the desired failure mechanism will take place. Hence, in the case of multi-story frame buildings, the plastic hinges are to occur in beams instead columns. This was further known as "strong column – weak beam" design principle. In order to ensure this type of mechanism, brittle undesired modes want to be avoided.

Further, the research community became involved in attempts to quantify the inelastic deformation capacity of structural components, generally in terms of displacement of ductility (μ_Δ) as it is accepted as an indicator of force reduction factors ("R" or "q").

2.4.1 Non – linear static design method (Bairán, et al., 2011)

Performance based seismic design is a way to design structures taking into account its realistic behavior after yielding. A static method so called "Non – Linear Static Design" was proposed by Bairán, et al. (2011).

This methodology directly considers plastic behavior in designs phases without iterations or need for non – linear analysis. It means that the structure can not only be designed for resisting certain load, but also to produce a level of redistribution that can be decided a priori by designers. If the structure is further assessed through

non – linear analysis or experimental models, the intended inelastic behavior should be observed. Including similar distribution of plastic hinges, damage and ultimate load intended in structural design.

The method is based on two linear analyses of two structural schemes, referred as elastic structure and an auxiliary structure. To obtain the final redistribution of internal forces and deformation, the two elastic analyses are superposed in a convenient manner. The first structure is identical to a typical elastic model of the structure to be designed with the conventional process, and the external loads. In the second structure (auxiliary structure), the designer selects the plastic hinges locations. In those hinges a pair of moment vectors (representing a tensor quantity) are applied in both sides of hinges, of equal magnitude and opposite sign to bending moment that designer wants to redistribute. This means that the bending moment applied (M_R) in the second structure on an internal hinge, will be the difference between the final bending moment that designer wants to achieve after redistribution (M_{final}) and the bending moment obtained in this point in the first linear analysis (M_e), see the Figure 2.7. This method can be performed in four simple steps, as shown below and illustrated in Figure 2.5:

Step 1. Linear elastic analysis.

Step 2. Decision of hinges locations with his bending moment redistribution values.

Step 3. Structural analysis of redistribution of internal forces and obtain plastic rotation.

Step 4. Design reinforcement in plastic hinges for ductility and resistance demand.

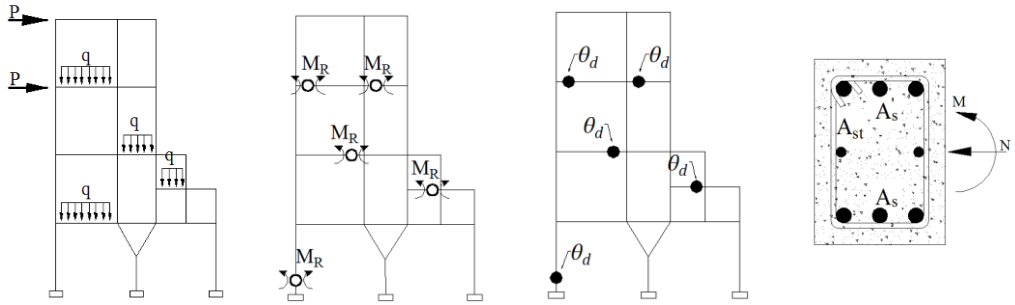

Figure 2.5. Concept of a complex structure with “Non-linear static design” method.

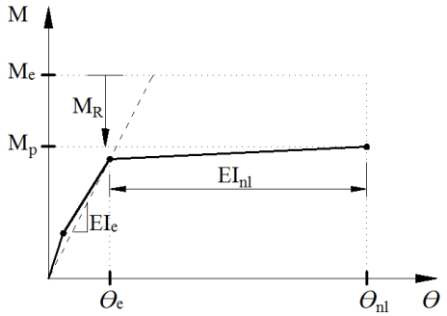

Figure 2.6. Plastic rotation produced due to redistribution moment M_R

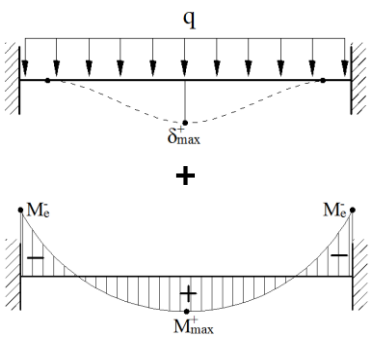

a. Linear Elastic Analysis – Bending moment diagram.

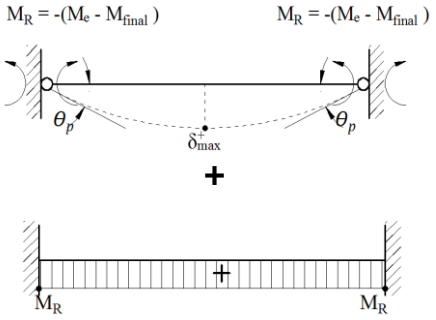

b. Linear Elastic Analysis with bending moment applied in hinges – Diagram of redistribution Bending moment.

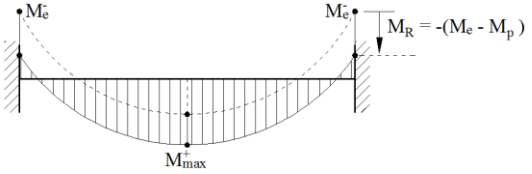

c. Final state.

Figure 2.7. Final state estimation through the two linear analyses.

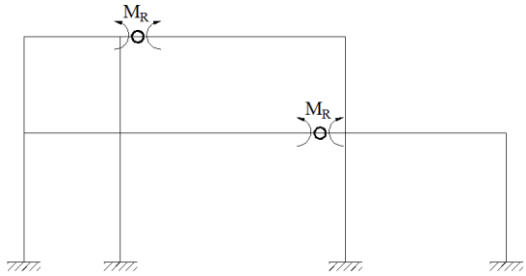

Figure 2.8. Redistribution moments applied to a complex structure.

In Figure 2.6 a moment – curvature diagram shows the reduction due to the bending moment applied on internal hinge, which follows a rotation capacity that has to be provided in the plastic capacity. In that way, the final result (Figure 2.7.c) satisfies both equilibrium and compatibility as it is the superposition of two elastic models. In a complex multi-degree of freedom (MDOF), as shown in Figure 2.8, the bending moment to be redistributed M_R will be a pair of moments vectors ($-M_R$ and M_R), self-balanced in each side of plastic hinge which were located intentionally in this specific element. Hence, equilibrium is also satisfied.

The bending moment will produce, in general, increments of elastic bending moments in other parts of the structure, that are needed to take into account those changes of internal forces. At the moment of confining internal forces of both structures, the variation of internal forces in elements, which remain elastic, it is included automatically in the final step.

The analysis of rotation in the auxiliary structure in complex MDOF structures can be deduced. However, commercial software packages does not allow for applications of moments on hinges. Therefore, an ad-hoc methodology was proposed.

The relationship between nodal forces and nodal displacements of macro-elements can be written through a matrix partition as follows in Eq. (2.19):

$$\begin{bmatrix} q_g \\ q_l \end{bmatrix} = \begin{bmatrix} K_{gg} & K_{gl} \\ K_{lg} & K_{ll} \end{bmatrix} \begin{bmatrix} d_g \\ d_l \end{bmatrix} \tag{2.19}$$

Where q_g and d_g represent forces and displacements vectors of external nodes, i.e. degrees of freedom 1 to 7 in Figure 2.9. Vectors q_l and d_l represent forces and displacements vectors degree of freedom for internal hinge in global axes.

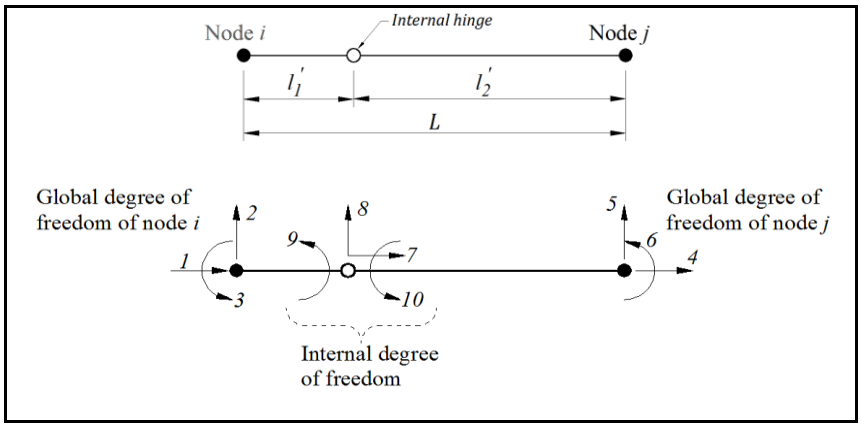

a. Macro-element with one internal hinges.

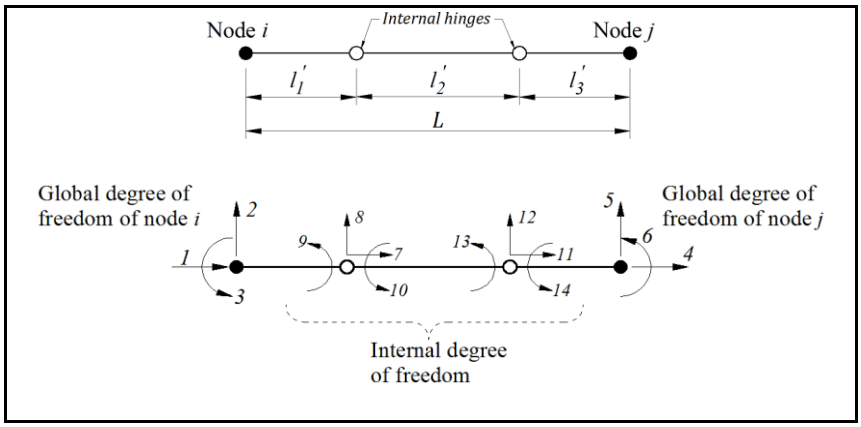

b. Macro-element with two internal hinges

Figure 2.9. Macro-elements with one or two plastic hinges.

Stiffness matrix partition is achieved by assembling the macro-element from 2 or 3 sub-elements. Figure 2.9 shows the case for an element with one and two internal hinges, respectively. For the sake of simplicity, the axial degrees of freedom are not shown. The partitioned matrix, as it is shown below, provides the bending matrix to be assembled. Where the length of the sub-assembling, l_1', l_2' and l_3', are shown in Figure 2.9.

$$K_{gg} = EI \begin{bmatrix} \frac{12}{l_1'^3} & \frac{6}{l_1'^3} & 0 & 0 \\ \frac{6}{l_1'^2} & \frac{4}{l_1'} & 0 & 0 \\ 0 & 0 & \frac{12}{l_3'^3} & -\frac{6}{l_3'^2} \\ 0 & 0 & -\frac{6}{l_3'^2} & \frac{4}{l_3'} \end{bmatrix} \tag{2.20}$$

$$K_{gg} = K_{\lg}^T = EI \begin{bmatrix} \frac{12}{l_1'^3} & \frac{6}{l_1'^2} & 0 & 0 & 0 & 0 \\ \frac{6}{l_1'^2} & \frac{4}{l_1'} & 0 & 0 & 0 & 0 \\ 0 & 0 & 0 & \frac{12}{l_3'^3} & 0 & -\frac{6}{l_3'^2} \\ 0 & 0 & 0 & \frac{6}{l_3'^2} & 0 & \frac{2}{l_3'} \end{bmatrix} \tag{2.21}$$

$$K_{gg} = K_{\lg}^T = EI \begin{bmatrix} \frac{12}{l_1'^3}+\frac{12}{l_2'^3} & -\frac{6}{l_1'^2} & \frac{6}{l_2'^2} & -\frac{12}{l_2'^3} & \frac{6}{l_2'^2} & 0 \\ -\frac{6}{l_1'^2} & \frac{4}{l_1'} & 0 & 0 & 0 & 0 \\ \frac{6}{l_2'^2} & 0 & \frac{4}{l_2'} & -\frac{6}{l_2'^2} & \frac{2}{l_2'} & 0 \\ -\frac{12}{l_2'^3} & 0 & -\frac{6}{l_2'^2} & \frac{12}{l_2'^3}+\frac{12}{l_3'^3} & -\frac{6}{l_2'^2} & \frac{6}{l_3'^2} \\ \frac{6}{l_2'^2} & 0 & \frac{2}{l_2'} & -\frac{6}{l_2'^2} & \frac{4}{l_2'} & 0 \\ 0 & 0 & 0 & -\frac{6}{l_3'^2} & 0 & \frac{4}{l_3'} \end{bmatrix} \tag{2.22}$$

All degrees of freedom are statically condensed by defining the stiffness matrix of the macro-element in Eq. (2.23). Statically equivalent forces of the redistributions internal moment are obtained for the exterior nodes, as in the Eq. (2.25). In general, macro-element condensed stiffness matrix is obtained as:

$$K_e = K_{gg} - K_{gl} \cdot K_{ll}^{-1} \cdot K_{lg} \tag{2.23}$$

The bending moment applied is

$$M_{R,i} = -\left(M_{e,i} + M_{p,i}\right) \tag{2.24}$$

Where i represents de hinge label. The equivalent nodal force vector for bending is defined from Eq. (2.25) and (2.26).

$$q_{EP} = -K_{gl} \cdot K_{ll}^{-1} \cdot q_l \tag{2.25}$$

$$q_l = \begin{bmatrix} 0 \\ M_{R1} \\ -M_{R1} \\ 0 \\ M_{R2} \\ -M_{R2} \end{bmatrix} \tag{2.26}$$

Table 2.3. Estimated effective stiffness in concrete structure in elastic zone

ELEMENT TYPE	MOMENT OF INERCIA REDUCTION FACTORS $\left({I_E}/{I_B}\right)$
Beams	0.30
Column with weak axil	0.50
Column with strong axil	0.70
Wall with weak axil	0.35
Wall with strong axil	0.50

In this process plastic hinges are considered as perfectly plastic. This hypothesis is reliable and safe enough for design phases. However, the calculated plastic rotation depend also on the stiffness in the structure in elastic zone. Therefore, if the structure is made of reinforced concrete (RC), the effects of cracking should be considered. For this reason, it is important to use an estimation of effective crack stiffness $\left(K_{fis}\right)$. This stiffness can be calculated as in Eq. (2.27).

$$\frac{K_{fis}}{EI} = \left(\frac{d}{h}\right)^3 \cdot \left[0.12 + 5.4 \cdot \eta \cdot \rho \left(1 + \frac{\rho' \cdot d'}{\rho \cdot d}\right)\right] \tag{2.27}$$

As a result of the analysis, the distribution of internal moments (M_d) and the corresponding ductility demand, in terms of required plastic hinges rotations $(\theta_{p,d})$ are obtained. Design should be made such that:

$$M_u \geq M_d; \qquad N_u \geq N_d; \qquad V_u \geq V_d \tag{2.28}$$

$$\theta_u \geq \theta_d \tag{2.29}$$

The design process, for $N_d = 0$, is as follows. Design plastic rotation is used for estimating the minimum ultimate curvature, in cross sections, through Eq. (2.30), in which (L_p) is the plastic length.

$$\emptyset_u = \emptyset_y + 2\frac{\theta_p}{L_p} \tag{2.30}$$

Therefore, it is possible to determine a limit depth of neutral axis (x_{lim}), either from the Eq. (2.31) or form direct abacuses which take into account confining reinforcement ratio as in Bairán & Marí (2010), Bairán, et al. (2011). This study provides a collection of direct design abacuses for different type of steel bars, concrete, and level of confinement.

$$\xi_{lim} = \frac{x_{lim}}{d} = \frac{\varepsilon_c}{\varepsilon_c + \varepsilon_{su}} = \frac{\varepsilon_{cu}}{c \cdot \varepsilon_y + \theta_d \cdot \frac{d}{L_p}} \tag{2.31}$$

When the confinement in concrete is needed, the confined To determine confined concrete ultimate deformation and its strength it depends on the volumetric confinement reinforcement ratio, and it will be necessary an iterative process in order to obtain confinement reinforcement and material properties to use in Eq. (2.32). It can be defined the limit moment that indicates if it is necessary to have compression steel bar reinforcement to ensure the highest possible ductility as below:

$$M_{lim} = \eta \cdot \lambda \cdot \xi_{lim} \cdot f_{cd} \cdot b \cdot d^2 \cdot \left(1 - \frac{\lambda \cdot \xi_{lim}}{2}\right) \tag{2.32}$$

Where η and λ are parameters of the equivalent compression block, see EC2 (1992). Finally, if the bending moment is smaller than Eq. (2.32) it is not necessary

to provide specific compression steel reinforcement. Further situations, where spalling or special confinement, may be needed in order to guarantee the ductility capacity (Bairán, et al., 2011); direct equations for the cases have been also developed.

2.4.2 Seismic design based on direct deformation (Kappos & Stefanidou, 2010)

A deformation – based seismic design method for 3D R/C irregular buildings using inelastic dynamics analysis was proposed by Kappos & Stefanidou (2010). The non-linear behavior of the structure is approximately and explicitly taken into account through non-linear step by step dynamic analyses of partially inelastic structural model subjected to earthquake records for multiple levels of earthquake action. At least 3 for services conditions and 3 for life safety are considered. The record are scaled in accordance with these two limit states considered in the performance criteria. The design method proposed is applicable to irregular buildings with and without shear walls and dual system with frames and walls. The steps required to implement the method are shown in the flowchart in Figure 2.10.

First, a conventional elastic analysis of the structural model considering reduced inertias in beams due to cracking and gross inertia in columns is carried out the design forces of the element sections that will exhibit damage under the service limit state. All beams are designed for bending only, considering a reduction factor to account for more general definition of the moment – rotation diagram ($M - \theta$), and the requirement of minimum reinforced specified in the design code. Subsequently, based on the available information of the properties of the structural elements (stiffness and strength). A partially inelastic model is constructed, in which inelastic deformation are accepted for all beams and columns at base whereas the rest of columns are considered to behave elastically. With this information, non – linear dynamic analyses of the structural model are carried out, considering as demand a set of no less the three earthquake records representative of the site of the structure and the services limit state considered for the design.

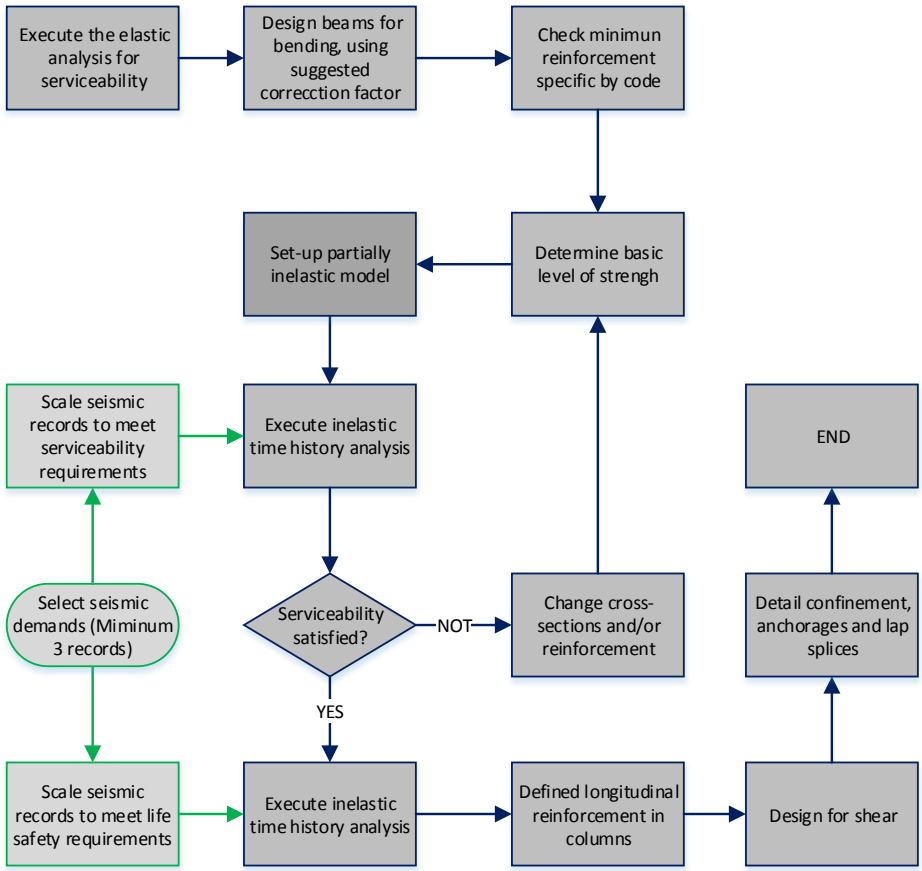

Figure 2.10. Flowchart of Seismic design method based on direct deformation, SDBDD by (Kappos & Stefanidou, 2010)

Further, it should be verified that the drift and the ductility demands obtained, lies within the range of allowed values. If this is not the cases, the proposed design must be modified until performance is in accordance with the target in the limit state. Once this condition is satisfied, a new set of non-linear dynamic analyses of the designed model is carried out, using as demands a set records consistent with the life safety limit state. With the result obtained, the columns are designed for bending and all the structural elements are designed for shear. Finally, the design of all elements is detailed so that the structural system, as a whole, can develop the inelastic levels considered in the design.

As the application of the method involves the use of results of non-linear dynamic analyses of the structures, high precision is expected. In general, better than other existing methods. However, it has as drawbacks, that to apply it, the designer must have enough knowledge and experience to carry out, and interpreting these non-linear analyses and for the selection of the earthquake records required. Moreover, the method involves a series of iterations in which the improvement of the solution with respect to previous attempt is very much dependent on the experience of the designer and it is time consuming.

2.4.3 A Displacement-Based Seismic Design Method with damage control for RC buildings (Ayala, et al., 2012)

This method was propose by Ayala, et al. (2012) and consists on a displacement based seismic design with damage control, where the targets for considering a performance level are set as displacements and a damage distribution, which are proposed by the designer. The method is based on concepts of basic structural dynamics and of a reference or equivalent single degree of freedom system, associated to a fundamental mode, with a bilinear behavior.

The main hypothesis of this method is that the non-linear capacity curve of a MDOF structure can be approximated by a bilinear curve, as shown in Figure 2.11.a. This behavior curve may be conveniently represented in the acceleration-displacement response spectrum (ADSR) format, as it is shown in Figure 2.11.b. Here, the capacity curve and the behavior curve are obtained from the results produced by two conventional modal spectral analyses, one for the elastic analysis with undamaged structure, and the other for the inelastic phase, i.e., the damaged structure. In Figure 2.11, V is the base shear, d the top displacement of the MDOF system, S_a is the pseudo-spectral acceleration equivalent to the strength per unit mass, (R). S_d is the spectral displacement and K is the stiffness. The first slope in the branch of the capacity curve (Figure 2.11.a), represents the stiffness properties of the structures in the elastic range associated to the top displacement and the

second slope branch is the corresponding inelastic range. The characteristic of this last branch are defined by the assumed damage distribution associated to the proposed maximum displacement of the given performance level.

The yield strength per unit mass (R_y) is the demand level to be met by the structural elements, which are assumed to be damaged under design conditions. The strength per unit mass (R_u) is the demand level for the elements that behave elastically under design conditions. The preliminary results publish in Mendoza Pérez (2011) show that, for the analyzed structures, stiffness values corresponding to approximately half the undamaged stiffness are acceptable.

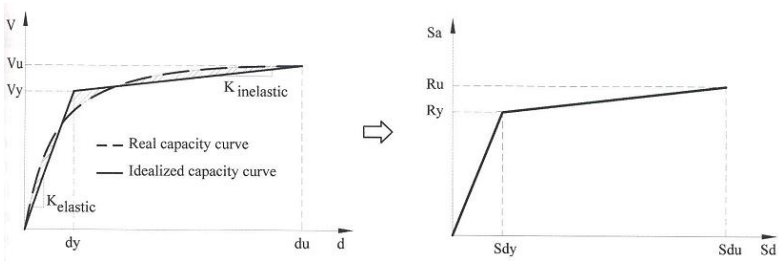

a. Bi-linearization of the capacity curve b. Behavior curve in the ADRS format

Figure 2.11. Transformation of the capacity curve to the spectral space

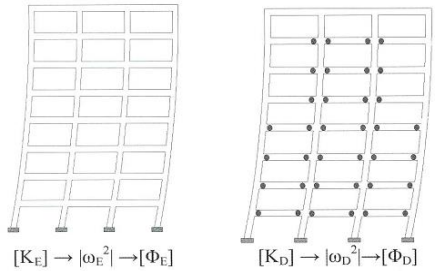

a. Undamaged model b. Damaged model

Figure 2.12. Dynamic properties of two stages of behavior propose.

The application of this seismic design method involves the following steps:

1. Obtain of a preliminary structure, considering gravitational and lateral loads.

2. Modal analysis of the un-damage model structure from elastic stiffness considering as a MDOF and obtain fundamental period "T_1".

3. For a given performance level, a rational damage distribution is defined in accordance with the characteristic of the structures.

4. Based on the prescribed story drift for the require performance level, the target roof displacement d_u, is defined by means of the displaced shape of the damage model.

5. An approximation of the yield roof displacement d_y, is calculate and the properties of the elements obtained from preliminary design through the following equation:

$$d_y = \frac{\delta_n}{\psi_n} \tag{2.33}$$

$$\delta_n = \frac{0.3 \cdot \varepsilon_y \cdot L_1 \left(\frac{I_{v1}}{L_1} + \frac{I_{v2}}{L_2} + \frac{I_{cn}}{H_n} + \frac{I_{cn+1}}{H_{n+1}}\right)}{h_{v1}\left(\frac{I_{cn}}{H_n^2} + \gamma_o \frac{I_{cn+1}}{H_{n+1}^2}\right)} \tag{2.34}$$

Where,

δ_n t is the yield inter-story drift at the floor where the maximum drift occurs;

ψ_n is the drift obtained from a modal spectral analysis of the undamaged structure at the story where maximum drift occurs, normalized by the maximum roof displacement;

ε_y is the yield strain of the reinforcement steel;

L_1 is the length of the span to the left of the node nearest to the center of the storey where maximum drift occurs;

L_2 is the length of the span to the right of such node;

H_n is the height of the storey where maximum drift occurs;

H_{n+1} is the height of the storey above the storey where the maximum drift occurs;

I_{v1} and I_{v2} are the moment of inertia of the beams in the spam 1 and 2, respectively;

I_{cn} and I_{cn+1} are the moment of inertia of the columns of the storey n and n+1; respectively and h_{v1} is the beam depth at span 1.

6. With the result of modal spectral analysis, the target yield and ultimate spectral displacement of the SDOF system corresponding to the fundamental mode are calculated, as well as its ductility, (μ), defined by Eq. (2.35).

$$\mu = \frac{S_{du}}{S_{dy}} \tag{2.35}$$

7. From the design displacement spectrum, for a given μ and α, the ultimate spectral displacement associated to (T_1), is obtained. Finally, this spectral displacement and the target spectral displacement of the frames (S_{du}), are compared. If the last value obtained close enough to the target, the design is considered satisfactory. Otherwise, the initial period of the structure, (T_1) and/or the damage distribution needs to be modified. Alternatively, the required period to satisfy the target displacement can be directly obtained from the displacement spectra.

8. If the target displacement of the structure is guaranteed, the yield strength, (R_y) for the period that satisfies the target displacement is obtained from the inelastic strength spectrum (ISS), corresponding to the values of (μ) and (α) previously calculated.

9. The ultimate strength R_u, is calculate using Eq. (2.36)

$$R_u = R_y[1 + \alpha(\mu - 1)] \tag{2.36}$$

10. Once the characteristic points of the behavior curve are defined, the behavior curve of the reference SDOF system may be drafted as it's showed in the Figure 2.13.a.

11. Three analyses need to obtain the design forces of the elements: a gravity load analysis of the un-damage structures, a modal spectral analysis of the un-damaged structure using the elastic design spectrum scaled by ratio of the strength per unit mass at the yield point to the behavior curve and the elastic pseudo-acceleration for the initial period, λ_1 as it is showed in Figure 2.13.b, and modal spectral analysis of the damaged structure using the

elastic spectrum scaled by the ratio of the difference of ultimate and yield strengths per unit mass and the pseudo-acceleration for the period of the damaged structures, λ_2 as it is showed in Figure 2.13.c.

12. Design of structural elements in accordance with the forced obtained from the analysis of the simplified models using applicable rules.

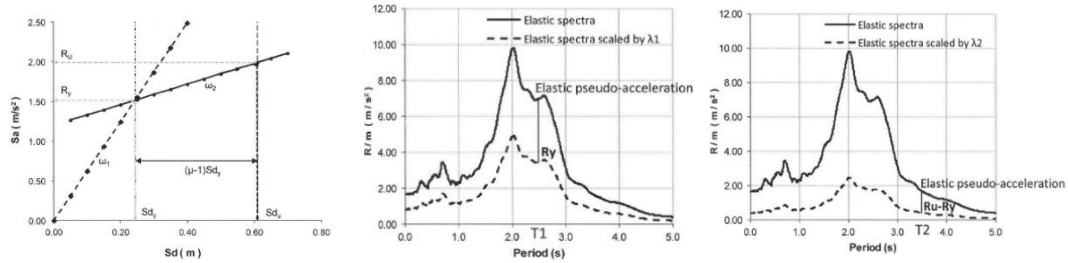

a. Behavior curve of reference SDOF system

b. Un-damaged model

c. Damage model

Figure 2.13. Strength spectra used for the modal spectral analyses

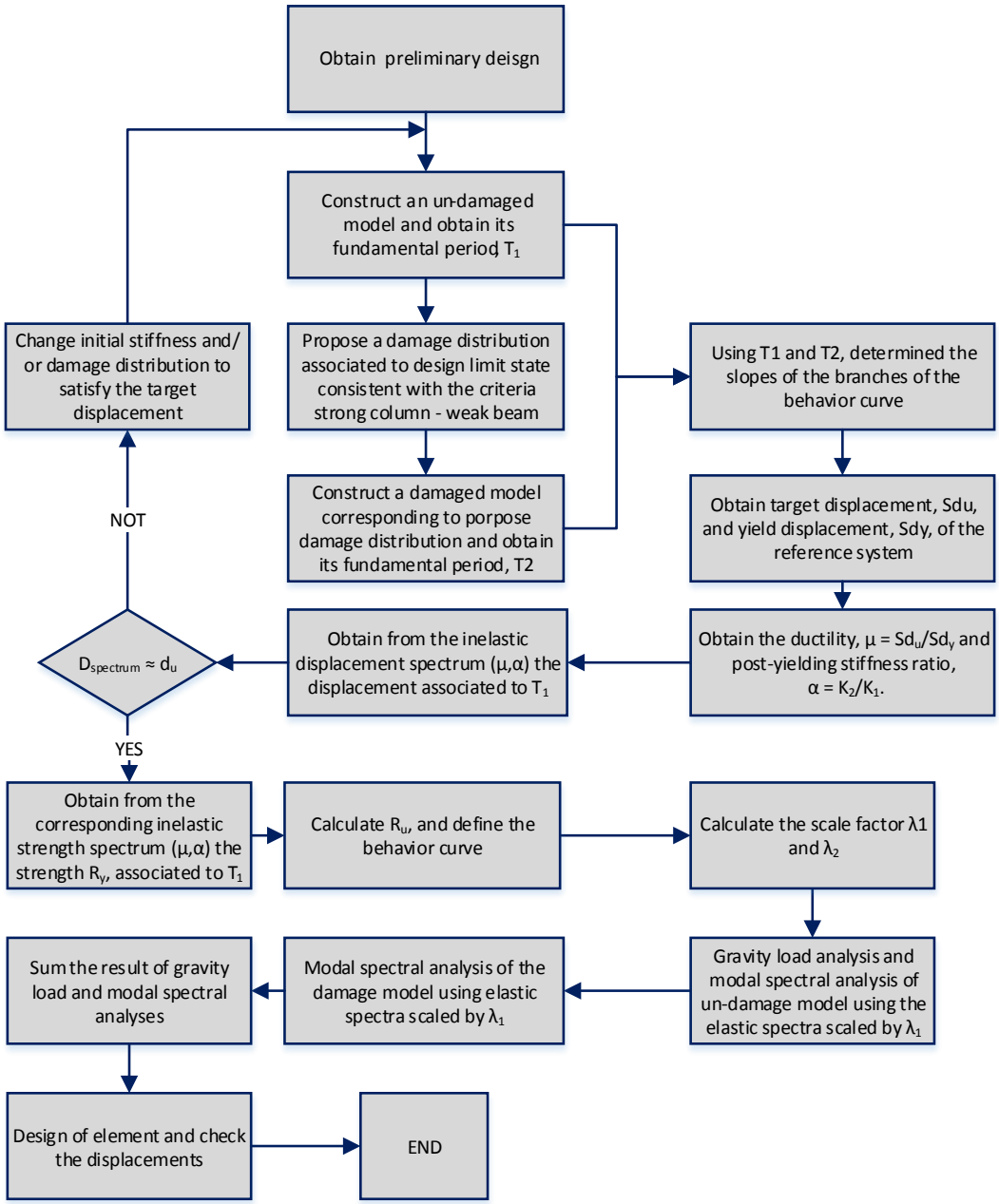

Figure 2.14. Flowchart of displacement based seismic design method with damage control. (Ayala, et al., 2012)

This approach allows PBD of irregular structures and to manage the local damage. It is formulated from basic approximations to concepts of structural dynamics used in design practice. Nevertheless, the method is sensible to the importance of proposing a realistic damage distribution and more rigorous relationship between stiffness of structural elements in order to have a good approximation. On the other hand, a comparison of spectral displacement and design displacement should be done in the process as a condition. That means that an iteration is involved in the process. Figure 2.11 shows the process of designing, where an iteration for the spectral displacement should converge with the ultimate displacement.

2.4.4 Performance – based plastic design of RC frames (Liao, 2010)

Performance-Based Plastic Design (PBPD) method has been recently developed to achieve enhanced performance of earthquake resistant structures. The design concept uses pre – selected target drift and yield mechanism as performance criteria. The design base shear for selected hazard level is determined by equating the work needed to push the structure monotonically up to the target drift to the corresponding energy demand of an equivalent SDOF oscillator.

By using the concept of energy balance applied to a pre-selected yield mechanism with proper strength and ductility, structures designed by the PBPD method can achieve a predictable structural performance under – strong earthquake ground motions. It is important to select a desirable yield mechanism and target drift as key performance limit states for given hazard levels right from the beginning of the design process. The distribution and degree of structural damage are greatly dependent on these two limit states.

An outline of the step-by-step Performance-Based Plastic Design (PBPD) procedure is given in the following. The details are then presented in the subsequent sections:

1. Select a desired yield mechanism and target drift for the structure for the design earthquake hazard.

2. Estimate the yielding drift (θ_y), the fundamental period (T), of the structure and determine an appropriate vertical distribution of design lateral forces.

3. Determine the elastic design spectral acceleration value S_a, by multiplying seismic response coefficient C_s, with R/I, where $R = 8$ and $I = 1$ in the design of RC SMF S_a was determined this way for two reasons:

   a. For long period the codes prescribe the minimum value of C_s but not for S_a;
   b. For consistency and fair comparison with the baseline frames.

4. Calculate the design base shear, V. In order to estimate the ductility reduction factor and the structural ductility factor, an inelastic seismic response of EP-SDOF is needed, such as idealized inelastic response spectra by Newmark-Hall (1985) used in this study.
5. Modify V for RC SMF as needed since the force-deformation behavior is different from the assumed EP behavior and P-Delta effect is not considered in the calculation of Vin Step 4.

6. Use plastic method to design the designated yielding members (DYM), such as beams in RC SMF. Members that are required to remain elastic (non-DYM), such as columns, are designed by a capacity design approach.

It was assumed in this study that the idealized inelastic spectra by Newmark and Hall for EP-SDOF systems are also valid for MDOF systems. This needs further study.

The modal shape of higher mode is significant for taller structures. P-Delta effect in the determination of required moment capacity of beams may be overestimated since the inclusion of P-Delta effect in this study was based on first mode shape (linear deformation pattern). Further refinement is needed for taller frames where higher modes can influence the deflected shape significantly.

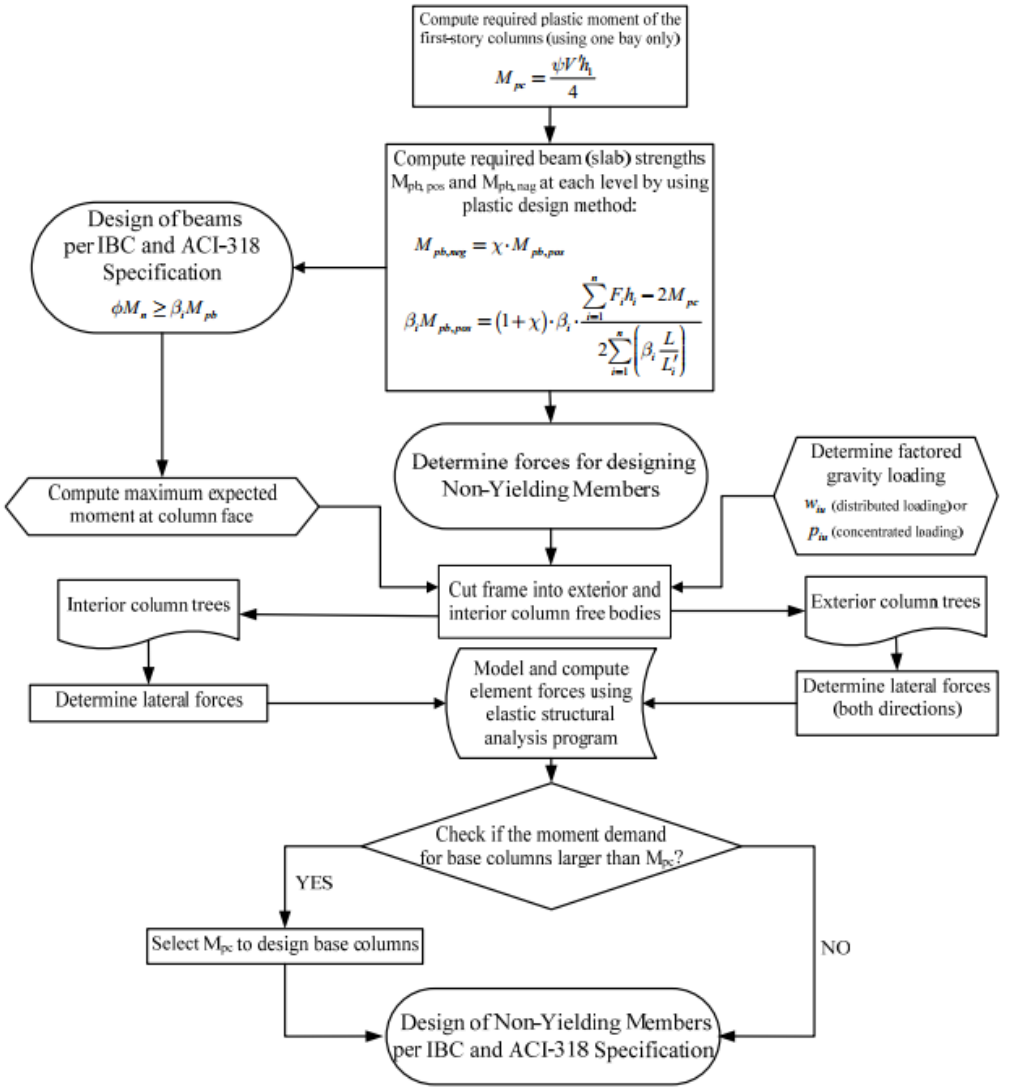

Figure 2.15. Performance-based plastic design flowchart for RC moment frames: member design (Liao, 2010)

2.4.5 Displacement-Based Method of Analysis for Regular Reinforced-Concrete Wall Buildings (Panagiotou & Restrepo, 2011)

This methodology consist on a displacement based (DB) approach for the analysis for performance based seismic design of regular RC wall buildings. The method considers two performance levels, immediate occupancy (IO) and life safety (LS). This method explicitly accounts for the combined effects of the inelastic first mode of response, kinematic system overstrength, and higher modes of response. Parametric analyses performed by (Panagiotou, 2008) suggest that in most wall buildings, including regular tall buildings, the effects of the higher modes of response are mostly dominated by the second translational mode. For the design of the building, the second mode is approximated by the following cubic polynomial:

$$\Phi_{2,i} = 2.4\left(\frac{h_i}{H}\right)^3 - 8.6\left(\frac{h_i}{H}\right)^2 + 5.2\frac{h_i}{H} \tag{2.37}$$

The second – mode modal weight $(W_{e,2})$, participation factor (Γ_2), and contribution factor. If the first-mode period and the structural system type are known, the second – mode period can be approximated. Thus, the second-mode base shear is

$$V_{b,2} = \frac{S_{a,2}}{g} W_{e,2} \tag{2.38}$$

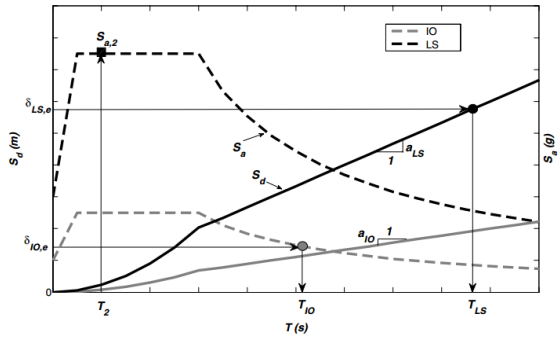

Figure 2.16. Design acceleration and displacement-response spectrum (Panagiotou & Restrepo, 2011)

The authors state that for most medium-rise buildings, there is no advantage in computing T_2 accurately. This is because T_2 often falls in the region of constant spectral acceleration. The second-mode base shear is distributed in lateral forces$\left(F_{2,i} \right)$ proportional to $W_i \cdot \Phi_{2,i}$. No base shear – force reduction is made in Eq. (2.38) for the inelastic response of the wall. It is assumed that the second response mode of the building is not significantly reduced by nonlinear response at the base of a wall. The method of analysis makes the following four assumptions:

1. The bending moment at the critical section at the base of the cantilever walls, where plastic hinges will ultimately develop, is attributable to the first mode of response only.

2. The wall is cracked in the whole height, and no tension stiffening exists in the reinforced-concrete walls.
3. The effect of overstrength, as defined in the following, is not accounted for to determine the required base bending moment strength of the walls.

4. The lateral deformations in the building are exclusively caused by the first mode. The second assumption results in a conservative design, particularly in regions of a low seismic hazard, in which the likelihood of significant cracking caused by ground shaking at IO is low. The fourth assumption limits the number of stories in a building to which the method proposed is suitable: as the number of floors increases, the participation of the higher modes of response increases to the extent that their contribution to lateral displacements and more importantly, to inter – story drifts, becomes non – negligible.

2.4.6 Direct displacement based seismic design (Priestley & Kowalsky, 2000)

In the case of direct displacement based seismic design method (DDBSD), the application involves the calculation of the design displacement Δ_d, an equivalent mass M_e, an effective height H_e, a ductility μ, and the yield displacement Δ_y of an equivalent single degree of freedom system. The effective period of the substitute structure T_e is found using the value of Δ_d in the displacement design spectrum associated to an equivalent viscous damping ratio, and from it, it is possible to find the equivalent stiffness, all of this data the base shear of the simplified system may be obtained as it is shown in Figure 2.17. This base shear will be distributed among all floors in proportion to their masses and assumed displacement. Once the force vector is calculated, the design forces of the elements are determined from a conventional linear static analysis of the structure subjected to the force vector obtained before. And finally the design of the structural elements is defined from a capacity design aimed to guarantee a safety mechanism due to seismic criteria.

Due to its apparent simplicity of this method has become it very attractive for seismic design in practice. However, its application has some limitations as its formulation is based on the validity of some questionable considerations like characterizing the behavior of a non – linear multi degree of freedom structures by the means of an equivalent linear viscous – elastic single degree of freedom systems, something that is not always appropriate on design consideration. Some other aspect as the distribution of forces by the shape of a single equivalent period similar to the first mode of vibration is an issue that in some full – scale test building demonstrate that some higher mode effect appears when inelastic behavior start.

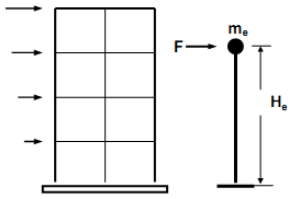

a. Substitute structure in SDOF

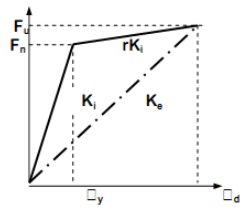

b. Effective stiffness

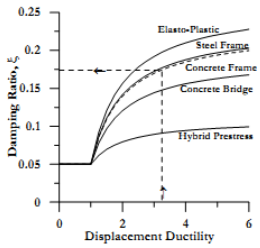

c. Effective damping vs ductility

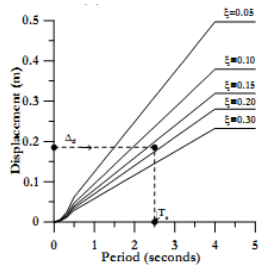

d. Design displacement spectra

Figure 2.17. Fundamentals steps of the Direct Displacement Based Design (Priestley & Kowalsky, 2000)

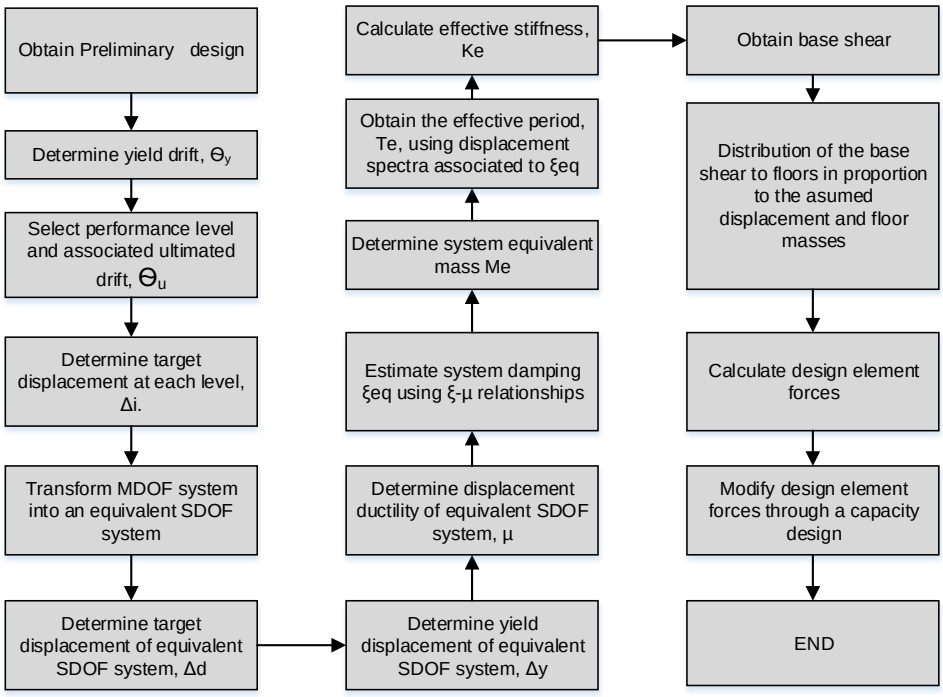

Figure 2.18. Flowchart of direct displacement seismic design propose by *(Priestley & Kowalsky, 2000)*

2.5 Full scale Experimental test in shear concrete wall with higher vibration mode effects

Higher vibration mode effects has been observed in many full scale experimental test, especially for medium rise building, for more than 2-3 story, as the following work presented in this section. Some proposal has been made in other to consider this effect in concrete walls, as in the work of Panagiotou (2008) and Panagiotou & Restrepo (2011). Other works highlighted the importance of making a proposal to consider higher modes effects in structural design phases as Luu, et al. (2014), Maniatakis et al. (2013), Ghorbani-renani (2010), Tremblay, et al. (2008) among many others.

2.5.1 Dual plastic hinge and displacement based design for shear walls

Panagiotou (2008) proposes the method of "Dual Plastic Hinge" for shear tall concrete walls. In this approach, plastic hinges are allowed to form in the wall base and near mid-height, while ensuring elastic response elsewhere. Bringing a reduction in the amount of longitudinal reinforcement and of transverse reinforcement in a significant portion of the walls. This concept is an approximation in order to reduce the effects of higher modes of response in high-rise building in shear walls as it is explained in Panagiotou & Restrepo (2009).

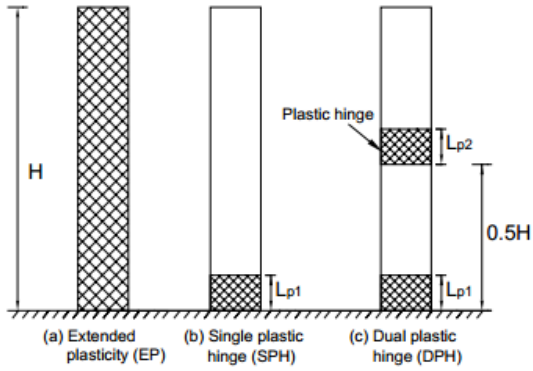

Figure 2.19.Three different cases of plasticity location in an Euler-Bernoulli cantilever.

Later, Panagiotou & Restrepo (2011) developed a displacement based method for regular RC wall buildings. It was applied to a full scale 7 story building sub-assembly tested at UC San Diego. The method relies in the following four assumptions: (1) the bending moment at the critical section at the base of the cantilever walls, where plastic hinges will ultimately develop, is attributable to the first mode of response only, (2) all walls are cracked, and no tension stiffening exists in the reinforced-concrete walls, (3) the effect of kinematic system overstrength, is not accounted for to determine the required base bending moment strength of the walls, (4) the lateral deformations in the building are solely caused by the first mode of response.

One important aspect is that it provides fixed polynomial expressions for both assumptions of first hinge dominated by the first mode and second hinge dominated by the second mode. For cantilever wall buildings, the shape of the first mode is approximated by the following polynomial expression

$$\Phi_{1,i} = \frac{1}{11}\left(\frac{h_i}{H}\right)^5 - \frac{10}{11}\left(\frac{h_i}{H}\right)^3 + \frac{20}{11}\left(\frac{h_i}{h}\right)^2 \tag{2.39}$$

The effects of the higher modes of response are largely dominated by the second translational mode. For the design of the building, the second mode is approximated by the following cubic polynomial:

$$\Phi_{2i} = 2.4\left(\frac{h_i}{H}\right)^3 - 8.6\left(\frac{h_i}{H}\right)^2 + 5.2\frac{h_i}{H} \tag{2.40}$$

2.5.2 Experimental test on shear walls specimen

In the work of Ghorbanirenani (2010), the first phase of the research included shaking table tests performed on two 9.0m tall models of 8-storey reinforced concrete shear walls designed in accordance with current Canadian code provisions. It was carried out on full-scale and 1:2.37 reduced scale wall (W1)

specimens to evaluate the seismic design provisions. A second series of experiments were conducted on two identical 1:2.33 scaled, 8-storey reinforced concrete shear wall (W2) specimens to investigate the effects of higher modes on the inelastic response of slender walls under high frequency ground motions.

To investigate the developing of damage for the different levels of intensity, one specimen was tested under incremented ground motion amplitudes ranging from 40% to 120% of the design level. For the second specimen, the first test was performed at 100% of the design level and the amplitude was increased stepwise in subsequent tests up to 200% of the design level.

In this work, the inelastic responses of a reinforced concrete wall is presented (Figure 2.20.a). A numerical model (Figure 2.20.b) was built using finite elements method and fiber element analysis. It should be noticed that for the numerical model, fiber element method was a good alternative in terms of computing time and it produced reasonable results in comparison to the finite element method, although, particular attention needs to be given to the selection of the damping ratios.

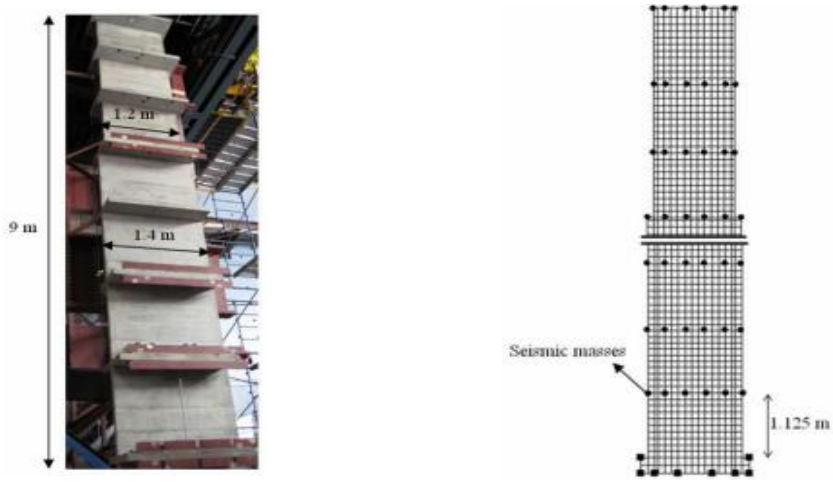

a) Model walls tested in the laboratory b) Finite Element model

Figure 2.20. Reinforced concrete wall model

The maximum base shear forces obtained from tests exceeded the wall design shear strength by the factor of 1.4. Figure 2.21 present the vertical distribution of

the horizontal accelerations along the height of Walls W1 and W2 at the time of maximum base shear under 100% earthquake. Seismic loads, acting on the walls directly correspond to the accelerations shown. The lateral force patterns, obtained from tests, show significant contributions from the second and third modes of vibration. In Figure 2.21 there is a comparison between the experimental tests, the analysis with Open Sees program (OS) and the analysis with VecTor2 (VT2) program.

Here, wall W2 is used to illustrate this dual hinge design procedure (Figure 2.22). In the dual-hinge concept, the wall is redesigned for plastic hinge at the sixth level, where it occurred in the original design. The design moment in that hinge region was taken equal to the value obtained from analysis and reduced. In Figure 2.22.c the moment demand along the wall height resulting from the dual-hinge concept is lower than the demand on the wall designed for hinging at the base only.

a) Wall (W1) b) Wall (W2)

Figure 2.21. Vertical distribution of horizontal accelerations under 100% Earthquake-

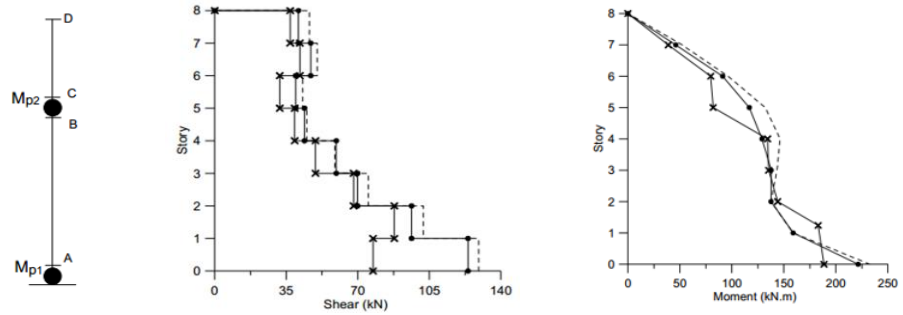

a) Location of hinges b) shear forces distribution along the wall height c) Moment distribution along the wall height

Figure 2.22.Analysis of wall based on the dual-hinge and modified single-hinge design approaches.

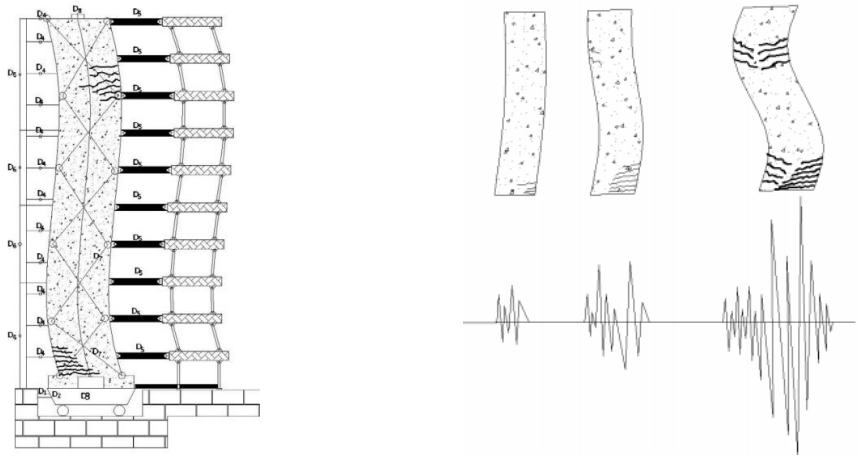

Figure 2.23. Scheme on the experimental investigation on higher mode effects (Ghorbanirenani, 2010)

One of the main conclusions of the research is that, by increasing the ground motion amplitudes, higher mode response of the walls was slightly more pronounced and resulted in higher drift. An example is shown in Figure 2.23, for particular a record from a zone with a high dominant frequency.

The works of Tremblay, et al. (2008), is part of the work explained above. It is part of a preliminary test program that was carried out to validate the use of reduced scale physical models to reproduce the inelastic cyclic flexural and shear responses of R/C wall. Time-history with ground motions for the region of Vancouver and Montreal were used. This record have high dominant frequency, which leads to relatively more significant higher mode response. The influence of the seismicity at the site on higher mode effects is illustrated for a 15-storey (each story height is 3 meters) reinforced concrete shear wall building located at two different sites in Canada: Vancouver, and Montreal. The analytical work is also used to highlight other parameters influencing the bending moment and shear demand on shear wall structures (see Figure 2.24).

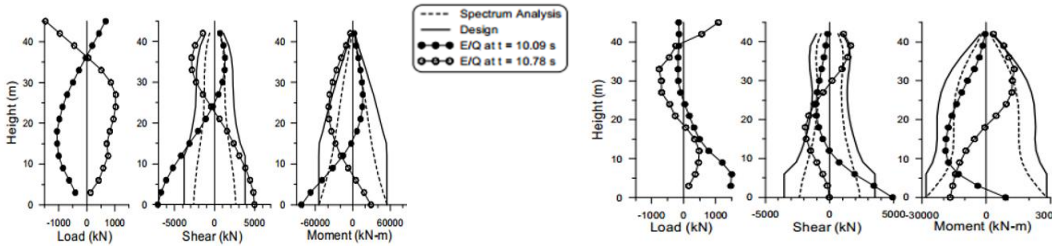

a) Vancouver record site b) Montreal record site

Figure 2.24. Vertical distribution of the inertial loads, shear forces and bending moments in the 15-storey walls.

The work of Luu, et al. (2014), is based on the same experimental and analytical tests described above. It is interesting to highlight the result in Figure 2.25. Where the typically design procedure is compared to the transient nonlinear behavior of the structure. It is evident that the effect results in the amplification of the base shear. The formation of the second hinge in the upper wall region is also explained following by redistribution of the shear forces, and a time lag between maximum base shear and maximum bending moment.

The Figure 2.25 shows the three analyses, the first (Figure 2.25.a), shows a typically linear modal spectral analysis, with its forces distribution along the wall height and the result of internal forces. Moreover, the second (Figure 2.25.b), shows the same linear analysis with the typical reduction of seismic force, with a single reduction factor for all vibration modes, it means that, the reduction of the final seismic force is linear. However, the third analysis (Figure 2.25.b), shows the real non – linear behavior in terms of the force distribution along the height, which the shape is totally different from the elastic analysis, and bigger as well, in comparison with the reduced by the typical reduction factor. The last observation, lead to focus on the importance of higher vibration modes effect.

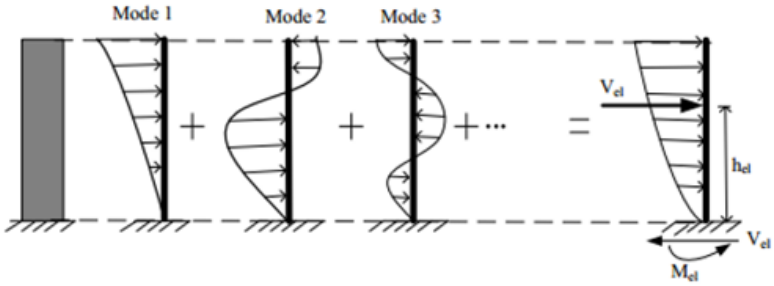

a. Linear modal response spectrum analysis

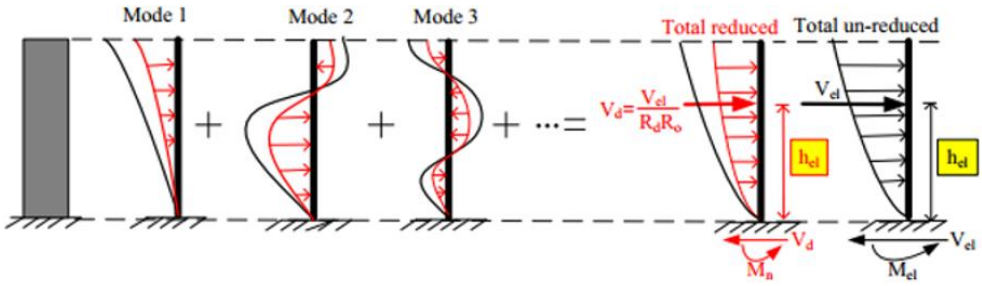

b. Linear modal response spectrum analysis considering nonlinearity

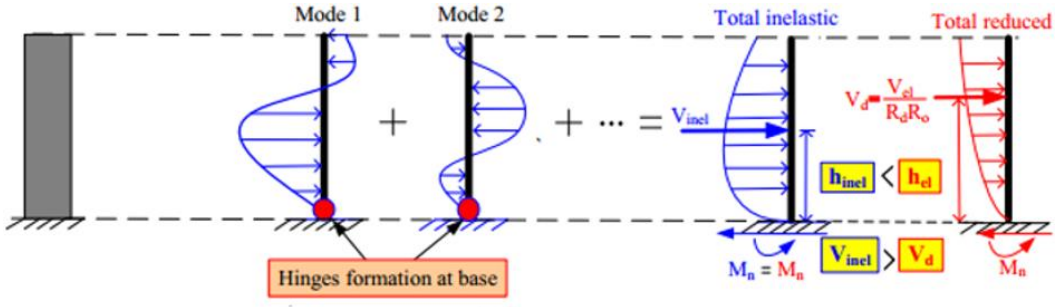

c. Observed nonlinear behavior

Figure 2.25. Analysis considering higher mode effects on structural wall response (Luu, et al., 2014)

This page is left intentionally blank

CHAPTER 3

EXTENSION OF THE DOUBLE LINEAR ANALYSIS METHOD TO SEISMIC LOADING

3.1 Introduction

Performance based seismic design (PBSD) process explicitly evaluates how a buildings is likely to perform given the potential hazard and design for a performance level. It starts with the selection of design criteria state in the form of one or more performance objectives. In general, performance objectives may be related to a certain level of damage, either structural or non-structural, associated to structural safety, economic losses or functionality. Most PBSD methodologies are based on modal dynamic spectral analysis (MDSA) through elastic design spectrum; although other are based on time history analysis.

In order to take into account the non – linear behavior of structures when MDSA is employed, a behavior factor (*q* or *R)* is typically listed in many standards codes in order to reduce the seismic demand. Those reduction factors consider sectional ductility and energy dissipation due to damage from cyclic loading in structures, as a global response, but depending on construction systems (reinforced concrete, prestressed concrete, steel structures, etc.).

Nevertheless, PBSD methodologies can find, through its own process, a more accurate alternative reduction factor, as is the case of DDBSD from the work of Priestley, et al. (2007) and others, such as Kappos & Stefanidou (2010), Ayala, et al (2012), Liao (2010). At present, direct methods only accounts for the first mode of vibration of the elastic structure, thus limiting its applicability in general situations. Methods for irregular structures are iterative. However, it is known that when damage occurs, e.g. cracking or local yielding, a variation of the stiffness is produced; hence, modal properties vary and affect the seismic demand and distribution of inertial forces. The differences with respect to the estimating based on the first elastic mode shape increase implies modification of the natural periods and the mass participation factor.

Figure 3.1 summarizes the study of Tremblay, et al. (2005) about the case of higher modes effect. They demonstrate problems where the main issue is clearly the load pattern more that is similar to second mode of vibration than the first. Hence, estimating load distributions from the elastic analysis and further application of a behavior factor produces unsafe design with incorrect distribution of resistance and ductility capacity.

In this chapter, the Double Linear Analysis method (DLA) will be extended to account for seismic loads. Further case studies analyses will be carried out in order to show that using a reduction factor, as standard codes recommend for seismic load reduction, is not, in general, the more convenient way to accounting inelastic seismic response as is shown Figure 3.2.

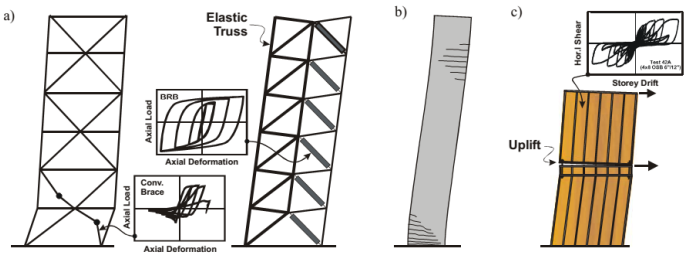

a) Seismic stability of braced steel frames; b) higher modes effects in slender R/C walls; and c) Seismic response of steel frame/wood panel walls.
Figure 3.1. Research topics for earthquake simulation testing and higher mode effect (Tremblay, et al., 2005)

Several laboratory tests on full – scale buildings have been carried out recently by Biondini, et al. (2012), Tremblay, et al. (2008) and (Panagiotou & Restrepo (2007). That reported discrepancies from the collapse mechanisms and the intended design. Even though, applying an up-to-date design procedure of standard codes by taking in consideration the seismic forces reduction factors and satisfying the concepts of strong column – weak beam.

In the methodology here proposed, means to account the above mentioned phenomena have been taken into consideration. The proposal provides an approach to evaluate them during the design process and control the collapse mechanism according to the chosen by the design strategies. In the following section, the proposed method is detailed.

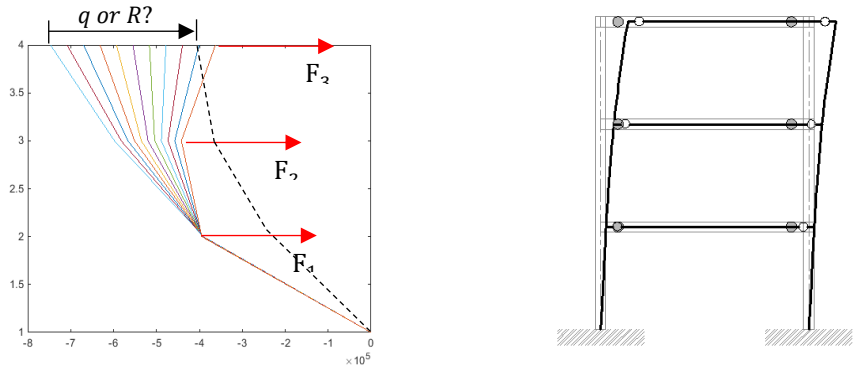

Figure 3.2. Variation of seismic load pattern due to local damage intentionally imposed in the “Double Linear Analysis” method (DLA)

3.2 Design methodology

This proposal methodology will be referred as "*Double Linear Analysis"* (DLA) method for performance based seismic design. This method is a design process of structures in order to resist certain loads considering the non – linear behavior for a global and local regions in the structure as an implicit way, the method also reports decision taking in a fast and transparent way. Designers will be able to decide working with a complete elastic structure, or a "damage" structure, by considering an intentional distribution of plastic hinges where designer need to reduce internal forces.

This method does not need an explicit non – linear analysis; however, if a non–linear analysis is performed on the structure designed according to this approach, one should obtain similar distribution of plastic hinges, internal forces and level of damage selected previously as a function of plastic ration capacity in proposed perfect hinges.

The methodology proposed is an extension of the "*Static non – linear design*" (SNLD) previously mentioned in chapter 2.4.1 proposed by Bairán, et al. (2011). Both methods are based on the superposition of two linear analysis on a reference elastic structure and an auxiliary structure. The main difference observed in the seismic design, with respect to static loading, is that the superposition is based on the final results of internal forces and deformation of two linear modal spectral analysis (MSDA), as shown in Figure 3.3. The two structural models used here referred as elastic structure (Figure 3.3.a), for the original model, and auxiliary structure for the second model (Figure 3.3.b).

The first structure is modeled as lineal elastic. It is subjected to both elastic gravitational and seismic forces. From it, the elastic internal forces and deformation can be obtained. Therefore, it corresponds to the same structural model used in current seismic design according to most codes. The auxiliary structural model is

similar to the previous one but includes a series of internal perfect hinges, which are distributed according to the designer decision. The points including the perfect hinges are the points where structural damage will be allowed in the design. Figure 3.4 shows the flowchart of the Double Linear Analysis method.

a) Elastic structure

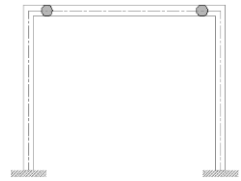

b) Auxiliary structure with perfect hinges

Figure 3.3. Type of structures in DLA

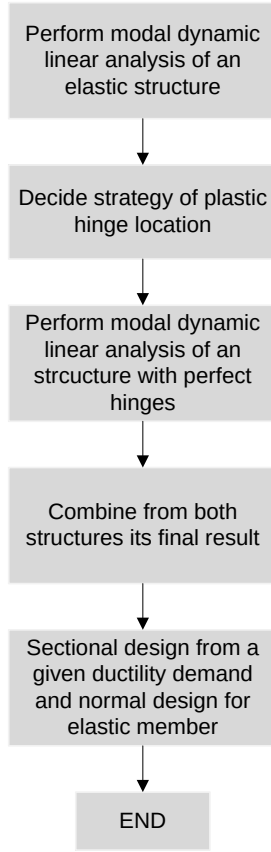

Figure 3.4. Flowchart for the “Double Linear Analysis” (DLA) for performance based seismic design

Seismic damage in structures does not only represent a hysteretic energy dissipation, but also, a different distribution shape of base shear along the height. The current method pretends to include the variation of the distribution of forces along the height of any structures that is changing due to the influence of higher modes during the damage process for a proposed level and damage distribution.

Most of the performance design methods studied in chapter 2.4 are based on iterative processes or, when direct methods are available, they are based on an equivalent structure and an equivalent period of vibration. This is suitable only for very regular structures, and does not allow to determine the effects of higher vibration modes. The DLA method accounts for higher vibration modes at the final state of an “inelastic” structure, local damage control, global behavior and different local hysteretic energy dissipation rule.

The general steps of DLA are direct, as is specified below:

1) Perform a linear MSDA on the reference elastic structure and obtain the elastic response.

2) Decide strategy of plastic hinge location based on the need of reduction of internal forces; based on reduction of base shear or evolution of local damage proposed in terms of plastic rotation in hinges. This defines the model of the auxiliary structure.

3) Perform a linear MSDA on the auxiliary structure with perfect hinge configuration.

4) Design the structure according to the superposition scheme and combination of internal forces depicted in chapter 3.3 of both structures and thus obtaining the final or intermediate structure design. Plastic rotation demand will control sectional design.

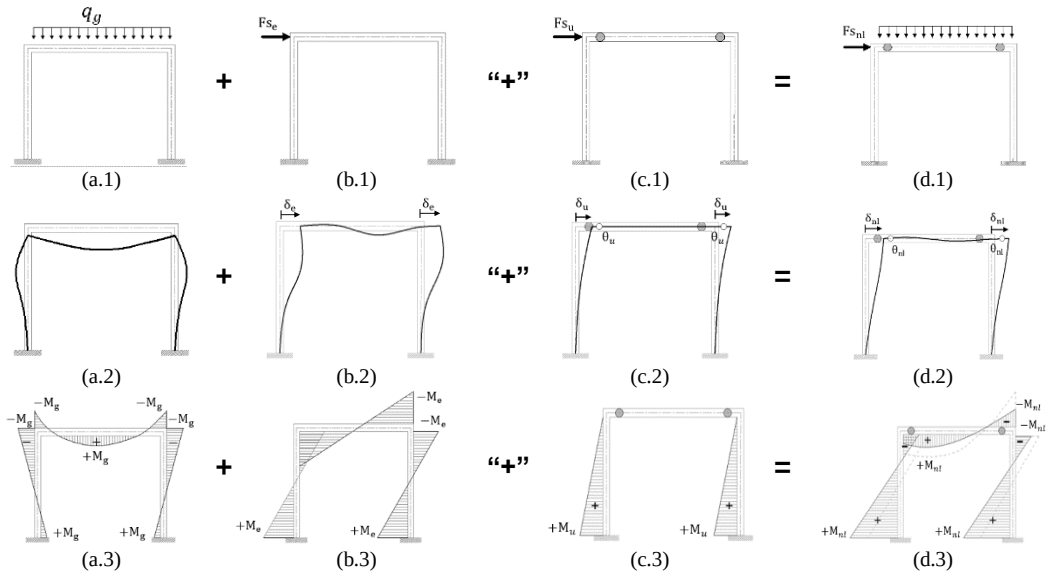

Figure 3.5. Final state estimation of Design steps for the DLA.
The symbol "+" stands for superposition combination

In Figure 3.5, the previous mentioned steps are presented. Figure 3.5 a1 to a3 and b1 to b3 represent the first step, consisting in performing a conventional MSDA of a structure loaded from an elastic design spectrum without any reduction factor of seismic forces, static loads are represent in columns "a". In this step, the elastic moments (M_e) and elastic displacements (δ_e) are calculated from the elastic seismic force (Fs_e) and gravitational load (q_g). Figure 3.5 c.1, c.2 and c.3 show the second and the third steps, respectively. They consist on a conventional MSDA of the auxiliary structure with perfect hinges, loaded with seismic spectrum forces (Fs_u), calculated with the modal properties of the auxiliary structure.

This seismic demand is clearly different in the two previous cases. In general, the auxiliary structure forces is lower than the one on the elastic reference structure, due to its higher flexibility and different modal properties. This analysis provides the largest possible deformation, according to the given distribution of hinges in terms of displacement (δ_u) and ductility demand (θ_p) at each hinge. For elements without hinges, a redistribution of internal forces will be observed. With the resulting combination shown in Figure 3.5 d.1, d.2 and d.3, structural design based on a given strength and ductility demand can be carried out.

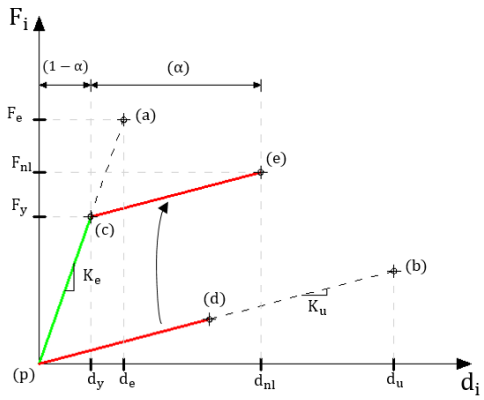

Figure 3.6. Superposition of Elastic and auxiliary structure in a force – displacement diagram in terms of damage parameter alpha (α)

In Figure 3.6, it is represented, from the points (p) to (a), the response of a linear analysis of the elastic structure with stiffness matrix $[K_e]$. After this, the designer should take a decision about the quantity and the location of damaging points, represented by perfect internal hinges in the auxiliary structure model. The decision of the distribution of hinges could be based on convenient levels of internal forces redistribution, reduction of base shear or a level of damage to be controlled as a function of plastic rotation in hinges, or a combination of both. In the same Figure 3.6, from point (p) to (b), the linear response behavior of the, more flexible, auxiliary structure with perfect hinges and stiffness matrix $[K_u]$ is shown. Curve (p)-(c)-(e) represent the combined response for a value of damage parameter, as will be introduced in the next section.

3.3 Combination of structures and damage control

After the analysis of the two elastic structures in previous section, the superposition of deformation and internal forces of both structure may be performed in order to obtain the non–linear response. For this goal, a combination factor (α) is proposed to combine both forces and displacements, as shown in Eq. (3.1) and (3.2), respectively. As will be shown latter, this factor controls the damage taken place in the structure; hence, providing a way to select its value objectively.

The α factor ranges from 0 to 1. For a totally plastic or damaged structure, α will be equal to 1. A fully undamaged structure will be obtained with $\alpha = 0$. The combination of internal forces and deformation is thus,

$$F_{nl}^{i} = F_{e}^{i} \cdot (1 - \alpha) \cdot \eta + F_{u}^{i} \cdot \alpha \cdot \eta \tag{3.1}$$

$$d_{nl}^{i} = d_{e}^{i} \cdot (1 - \alpha) \cdot \eta + d_{u}^{i} \cdot \alpha \cdot \eta \tag{3.2}$$

In this notation, F_{nl}^{i} and d_{nl}^{i} are the final results of the combined forces and displacement at the node i obtained in the two structural models from the multi modal spectrum analysis. Hence, F_{e}^{i} and d_{e}^{i} are the force and displacement of node i in the elastic structure respectively (step 1) and F_{u}^{i} and d_{u}^{i}, the ultimate possible forces and displacement coming from the auxiliary structure (step 3) at the same node i.

In Figure 3.6, it can be noticed that the force and displacement variation from point (p) to (d) is given by the second term in Eq. (3.1) and (3.2) for a particular value of the (α) factor. This term represents the plastic behavior of the combined structure and if it is placed in continuation of the elastic response, it will be the curve from point (c) to (e). The elastic part of the structure's behavior corresponds to the force and displacement variation from point (p) to (c). Thereby, superposition of both structures represents the final or combined structure.

Finally, the η factor in Eq. (3.1) and (3.2) is the damping correction factor that takes into account the energy dissipation by hysteretic damping in each hinges corresponding to a hysteretic loop model. The factor will be introduced in the next section.

3.4 Local and global damage control

As mentioned above, Eq. (3.1) and (3.2) control force and deformation combinations of elastic reference and auxiliary models of the structure; from their superposition the final demand of the inelastic structure is estimated. In the last step in this methodology, the final design of structure must be carried out by designing the steel reinforcement to satisfy the required strength and ductility demands, for the selected cross section sizes. To this end, the moment resistance demand is obtained as in Eq. (3.3) and the ductility demand is obtained from Eq. (3.4).

$$M_{nl}^{i} = M_{e}^{i} \cdot (1 - \alpha) \cdot \eta + M_{u}^{i} \cdot \alpha \cdot \eta \tag{3.3}$$

$$\theta_{nl}^{i} = \theta_{e}^{i} \cdot (1 - \alpha) \cdot \eta + \theta_{u}^{i} \cdot \alpha \cdot \eta \tag{3.4}$$

Where,

$$\theta_{e}^{i} = \frac{M_{e}^{i}}{E \cdot I} \frac{L_{p}}{6} \tag{3.5}$$

The Figure 3.7 shows a moment – rotation diagram evolution for a hinge i, in its final state, after the combination of structures for a particular value of combination factor (α). In this figure, point (a) is the reduced bending moment as a result of the yielding of plastic hinges and the redistribution of forces produced. However, the reduction of forces caused by the energy dissipation of hysteretic damping should still be added. After considering the effect of energy dissipation, the strength and plastic rotation demands are represented by point (b). The maximum reduction of bending moment would occur for a complete damage, hence, the maximum rotation possible in a hinge takes place. If this is the case, the strength demand in that hinge should be enough to resist gravity loads or static bending moment M_{st}, but will not have strength demand from seismic forces, as shown in point (c). In that case, internal forces will be redistributed in other elements that should resist all seismic forces.

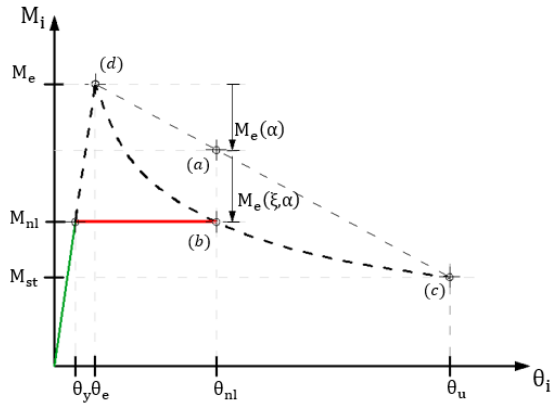

Figure 3.7. Moment – Rotation evolution diagram in hinge (i)

The energy dissipation correction factor (η) in Eq. (3.1) to (3.4) is defined in terms of the ductility demand in each local damaging point (hinge). Thus, is also dependent on the type of hysteresis loop of the component. The maximum ductility in the hinge (i) is then obtained as:

$$\mu_{max}^{(i)} = \frac{\theta_u^{(i)}}{\theta_e^{(i)}} \tag{3.6}$$

While the ductility demand can be computed as in Eq. (3.7), as a function of the α coefficient.

$$\mu^{(i)} = \frac{\theta_{nl}^{(i)}}{\theta_y^{(i)}} = \left[1 + \mu_{max}^{(i)} \cdot \frac{\alpha}{(1-\alpha)}\right] \tag{3.7}$$

Where the combined rotation $\theta_{nl}^{(i)}$ in the non-linear system is calculated as the Eq. (3.4), and the yield rotation $\theta_y^{(i)}$ is the first term of the Eq. (3.4) as below.

$$\theta_y^{(i)} = \theta_e^{(i)} \cdot (1-\alpha) \cdot \eta \tag{3.8}$$

The study from Dwairi et al. (2007) shows that the hysteretic damping component i can be calculated as:

$$\xi_{hyst}^{(i)} = \mathrm{C} \cdot \left(\frac{\mu^{(i)} - 1}{\mu^{(i)} \cdot \pi}\right) \tag{3.9}$$

Where the coefficient C depends on the shape of the hysteretic loop. This has a relationship on the theoretical area – based approach mentioned in chapter 2 for

the Elastic Perfectly Plastic (EPP) rule. The values of C can be taken from Table 2.2 in chapter 2.2.2. This design procedure requires relationship between rotation ductility and equivalent viscous damping. The total damping of the system is the sum of elastic and hysteretic damping:

$$\xi_{sys} = \xi_{el} + \xi_{eq} \tag{3.10}$$

The elastic damping can be considered as 5%. However, as ductility and strength demand in each component may be different, the equivalent damping is computed as the weighted average based on the energy dissipated by the different structural elements. That is,

$$\xi_{eq} = \frac{\sum_{i=1}^{n} \mathrm{M}_{nl}^{(i)} \cdot \theta_{nl}^{(i)} \cdot \xi_{hyst}^{(i)}}{\sum_{i=1}^{n} \mathrm{M}_{nl}^{(i)} \cdot \theta_{nl}^{(i)}} \tag{3.11}$$

The system determines the damping correction factor η. There are different models relating damping and η. Two main procedures can be applied: those that use inelastic spectra, and those using equivalent viscous damping. In this methodology, the second alternative is followed (equivalent viscous damping) to represent ductility and energy dissipation capacity, as it allows for a more direct compatibility with many design codes. In these sense, the η factor will be related to the equivalent damping through the Eq. (3.12) included in Eurocode-8 (2004).

$$\eta = \sqrt{\frac{0.10}{0.05 + \xi_{sys}}} \tag{3.12}$$

The final step of the method is to design the elements and plastic hinges for the computed strength and ductility demand. In this way, the structure should be able to perform as it was decided in the design process with the same cross section, as it is shown in Figure 3.5 c.3. Thus, it presents the damage proposed in terms of maximum rotation in plastic hinges as in Figure 3.8. For the element that should remain elastic, a capacity design should be made, for the strength demand computed in the analysis; and a convenient overstrength factor.

Plots of local and global ductility and strength demand evolution can be constructed using Eq. (3.1) to (3.4) by simply varying the factor α. Thus, it is possible to decide the value of α by looking for the local damage as plastic rotation desired or maximum displacement on top floor and, thereby, obtain a value of the behavior factor "q".

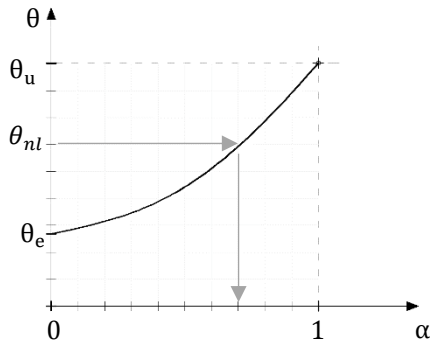

a) Plastic rotation evolution for the hinge i

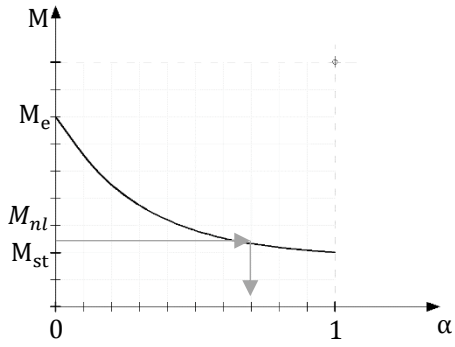

b) Bending moment evolution for the hinge i

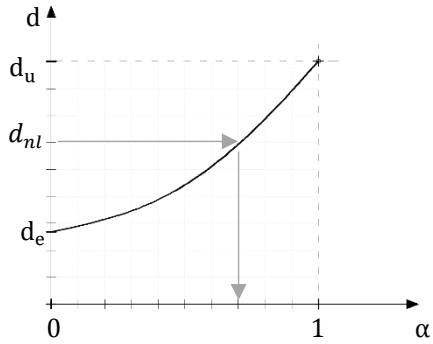

c) Displacement evolution for de node i

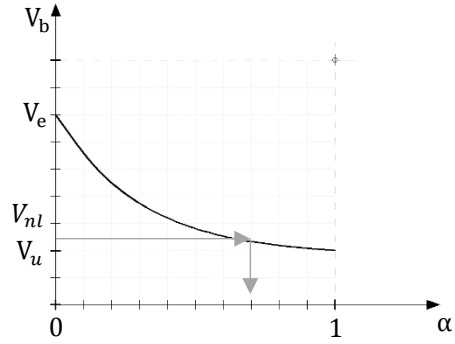

d) Total base shear evolution

Figure 3.8. Illustration of internal forces and deformation evolution by selecting a level of damage corresponding to an alpha (α) factor

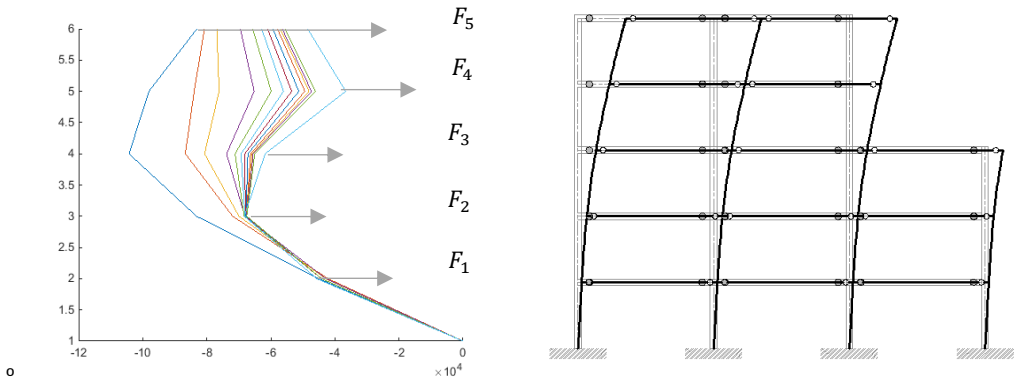

a. Evolution of seismic load pattern with α b. Building with all beams hinged

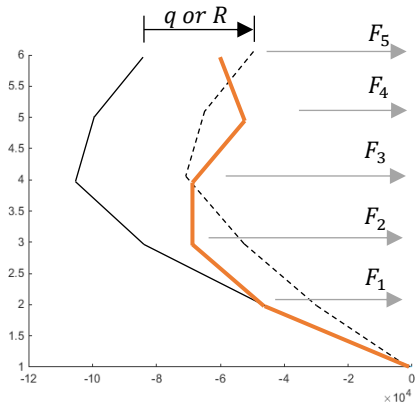

Figure 3.9. Comparison of inelastic seismic force for DLA and normal reduction q factor

Moreover, it is interesting to notice that, not only the reduction of base shear is produced by damage and yielding, but how seismic forces distribution varies along the height by changing the combination factor; as it is shown in Figure 3.9.a. Where the distribution of seismic forces for a 5 stories not so irregular building is shown when hinges in all beams are allowed. The dashed line that represents the typical homothetic reduction of the seismic forces, underestimating the forces in the lower and mid stories.

CHAPTER 4

NUMERICAL IMPLEMENTATION

4.1 Introduction

In order to develop de method presented in chapter 3, the REDIS2D and REDIS3D algorithms were developed as a matrix structural analysis. Those algorithm are extensions from the REDIS2D algorithm proposed (Bairán & Marí, 2010) in order to develop the method NLSD. In this chapter, it is developed the numerical algorithm in order to implement internal hinges in a 2D and 3D element. In the latter case, include directionality of perfect internal hinge behavior and the diaphragm behavior. These algorithms were extended to modal spectral dynamic analysis to implement finally tools and issue to develop the DLA methodology.

4.2 Structural matrix analysis

Frames structural analysis problem can be solved in matrix analysis approach. Two different methods can be used, the flexibility method and the stiffness method. The first, also referred to as the force or compatibility method, is essentially a generalization in matrix form of the classical deformation method. The latter method is derived from the classical slope-deflection method; and it is also referred as the displacement or equilibrium method. In this approach the unknowns are the joint displacement, which are determined first by solving the structure's equation of equilibrium (Kassimali, 1999).

The general formulation to account for distributed or concentrated loads acting on beam elements is

$$\{F\} = [K]\{d\} - \{F_o\} \tag{4.1}$$

Where F_o is a vector of fixed-end-reactions, expressed in terms of the global-coordinate components (Paz & Leigh, 2001). The fixed reactions are equal to the equivalent nodal forces, but with opposite sign.

The unknown nodal displacements and support reactions are calculated by partitioning the system stiffness equation, solving first for the unknowns displacements, and then calculating the unknown reactions. The nodal displacement, in local axes, are found as:

$$\{d_l\} = \{F_l\}[K_l]^{-1} \tag{4.2}$$

4.3 Internal hinges modeling

4.3.1 2D Element

An internal hinge in a beam element, cause a discontinuity in the slope. Moreover, the increment of bending moment is zero at the hinge. This required modifications to be applied to the stiffness matrix of continuous element. For a conventional stiffness method, no explicit compatibility equation is required, as the rotation (slope) on the left side of large should be equal to that on the right side. The conventional stiffness method to idealize an internal hinge could be used. To this aim one should separate beam segment (see Figure 4.1), formulate equilibrium equation and solve the unknowns.

Consider the cases of a 2D beam element with two nodal hinges, as shown in Figure 4.1, with global degrees of freedom as shown in Figure 4.2. At any internal hinge the bending moment is zero and the assembled matrix $[\mathrm{K_T}]$, with a size 14x14, corresponding to all nodal and hinges degree of freedom should be partitioned as below.

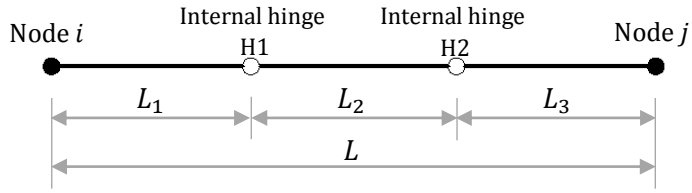

Figure 4.1 Idealized beam with two internal hinge

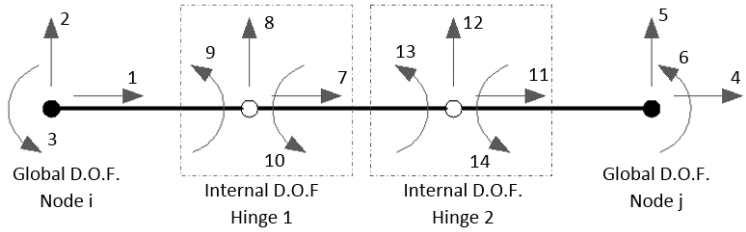

Figure 4.2. 2D beam element model with two internal hinge

$$K_T = \left[\begin{array}{cccccc:cccccccc}
\frac{AE}{L_1} & 0 & 0 & 0 & 0 & 0 & -\frac{AE}{L_1} & 0 & 0 & 0 & 0 & 0 & 0 & 0 \\
0 & \frac{12EI}{L_1^3} & \frac{6EI}{L_1^2} & 0 & 0 & 0 & 0 & -\frac{12EI}{L_1^3} & \frac{6EI}{L_1^2} & 0 & 0 & 0 & 0 & 0 \\
0 & \frac{6EI}{L_1^2} & \frac{4EI}{L_1} & 0 & 0 & 0 & 0 & -\frac{6EI}{L_1^2} & \frac{2EI}{L_1} & 0 & 0 & 0 & 0 & 0 \\
0 & 0 & 0 & \frac{AE}{L_3} & 0 & 0 & 0 & 0 & 0 & 0 & -\frac{AE}{L_3} & 0 & 0 & 0 \\
0 & 0 & 0 & 0 & \frac{12EI}{L_3^3} & -\frac{6EI}{L_3^2} & 0 & 0 & 0 & 0 & 0 & -\frac{12EI}{L_3^3} & 0 & -\frac{6EI}{L_3^2} \\
0 & 0 & 0 & 0 & -\frac{6EI}{L_3^2} & \frac{4EI}{L_3} & 0 & 0 & 0 & 0 & 0 & \frac{6EI}{L_3^2} & 0 & \frac{2EI}{L_3} \\
\hdashline
-\frac{AE}{L_1} & 0 & 0 & 0 & 0 & 0 & \frac{AE}{L_1}+\frac{AE}{L_2} & 0 & 0 & 0 & -\frac{AE}{L_2} & 0 & 0 & 0 \\
0 & -\frac{12EI}{L_1^3} & -\frac{6EI}{L_1^2} & 0 & 0 & 0 & 0 & \frac{12EI}{L_1^3}+\frac{12EI}{L_2^3} & -\frac{6EI}{L_1^2} & \frac{6EI}{L_2^2} & 0 & -\frac{12EI}{L_2^3} & \frac{6EI}{L_2^2} & 0 \\
0 & \frac{6EI}{L_1^2} & \frac{2EI}{L_1} & 0 & 0 & 0 & 0 & -\frac{6EI}{L_1^2} & \frac{4EI}{L_1} & 0 & 0 & 0 & 0 & 0 \\
0 & 0 & 0 & 0 & 0 & 0 & 0 & \frac{6EI}{L_2^2} & 0 & \frac{4EI}{L_2} & 0 & -\frac{6EI}{L_2^2} & \frac{2EI}{L_2} & 0 \\
0 & 0 & 0 & -\frac{AE}{L_3} & 0 & 0 & -\frac{AEI}{L_2} & 0 & 0 & 0 & \frac{AE}{L_2}+\frac{AE}{L_3} & 0 & 0 & 0 \\
0 & 0 & 0 & 0 & -\frac{12EI}{L_3^3} & \frac{6EI}{L_3^2} & 0 & -\frac{12EI}{L_2^3} & 0 & -\frac{6EI}{L_2^2} & 0 & \frac{12EI}{L_2^3}+\frac{12EI}{L_3^3} & -\frac{6EI}{L_2^2} & \frac{6EI}{L_3^2} \\
0 & 0 & 0 & 0 & 0 & 0 & 0 & \frac{6EI}{L_2^2} & 0 & \frac{2EI}{L_2} & 0 & -\frac{6EI}{L_2^2} & \frac{4EI}{L_2} & 0 \\
0 & 0 & 0 & 0 & -\frac{6EI}{L_3^2} & \frac{2EI}{L_3} & 0 & 0 & 0 & 0 & 0 & \frac{6EI}{L_3^2} & 0 & \frac{4EI}{L_3}
\end{array}\right] \tag{4.3}$$

In a compact notation the total stiffness matrix for an element with two internal hinge will be

$$K_T = \left[\begin{array}{c:c} \mathrm{K}_{gg} & \mathrm{K}_{gh} \\ \hdashline \mathrm{K}_{hg} & \mathrm{K}_{hh} \end{array}\right] \tag{4.4}$$

In order to eliminate the degrees of freedom (DOF) corresponding to internal hinge rotation associated with internal bending moment, it is proceed as follows:

$$\left\{\begin{array}{c} \mathrm{F}_g \\ \hdashline \mathrm{F}_h \end{array}\right\} = \left[\begin{array}{c:c} \mathrm{K}_{gg} & \mathrm{K}_{gh} \\ \hdashline \mathrm{K}_{hg} & \mathrm{K}_{hh} \end{array}\right] \cdot \left\{\begin{array}{c} \mathrm{d}_g \\ \hdashline \mathrm{d}_h \end{array}\right\} \tag{4.5}$$

In Eq. (4.5), d_g represents the d.o.f. of the element ends and d_h represents the d.o.f of the internal perfect hinge. Thus, is equivalent to:

$$\mathrm{F}_g = \mathrm{K}_{\mathrm{gg}} \cdot \mathrm{d}_g + \mathrm{K}_{\mathrm{gh}} \cdot \mathrm{d}_h \tag{4.6}$$

$$\mathrm{F}_h = \mathrm{K}_{\mathrm{hg}} \cdot \mathrm{d}_g + \mathrm{K}_{\mathrm{hh}} \cdot \mathrm{d}_h \tag{4.7}$$

Solving for $\mathrm{d_h}$ in the second term of Eq. (4.6), one gets

$$\mathrm{d}_h = \mathrm{K}_{hh}{}^{-1} \cdot (\mathrm{F}_h - \mathrm{K_{hg}} \cdot \mathrm{d}_g) \tag{4.8}$$

Substituting Eq. (4.8) in Eq. (4.7), it is obtained

$$\mathrm{F}_g = \left(\mathrm{K_{gg}} - \mathrm{K_{gh}} \cdot \mathrm{K}_{hh}{}^{-1} \cdot \mathrm{K_{hg}}\right) \cdot \mathrm{d}_g \; - \; \mathrm{K_{gh}} \cdot \mathrm{K}_{hh}{}^{-1} \cdot \mathrm{F}_h \tag{4.9}$$

Eq. (4.9) has the form of equation with concentrated or distributed load acting on beam elements by considering the following formulation for a general structure that is:

$$\mathrm{F} = \mathrm{K}_c \cdot \mathrm{d}_g - \mathrm{F_{eq}} \tag{4.10}$$

Therefore, the condensed stiffness matrix for the macro – element with two internal hinges will be

$$\mathrm{K_c} = \left(\mathrm{K}_{gg} - \mathrm{K}_{gh} \cdot \mathrm{K}_{hh}{}^{-1} \cdot \mathrm{K}_{hg}\right) \tag{4.11}$$

The equivalent nodal force vector is defined by

$$\mathrm{F_{eq}} = -\,\mathrm{K}_{gh} \cdot \mathrm{K}_{hh}{}^{-1} \cdot \mathrm{F}_h \tag{4.12}$$

Where $\mathrm{F_h}$ is the internal forces vector acting on the internal hinges,

$$\mathrm{F}_h = \begin{Bmatrix} F_{x_{h1}} \\ F_{y_{h1}} \\ M_{\theta_{h11}} \\ M_{\theta_{h12}} \\ F_{x_{h2}} \\ F_{y_{h2}} \\ M_{\theta_{h21}} \\ M_{\theta_{h22}} \end{Bmatrix} \tag{4.13}$$

Figure 4.3. Plastic rotation in $(\mathrm{M}-\theta)$, hinge i in a pure bending.

Figure 4.3 represent the case when the internal hinges models a plastic hinge in the element. Once internal forces and deformation at internal hinges are found in the macro – element, plastic rotation can be found as the difference of the rotation as in Eq (4.14) and Eq (4.15) and shown in Figure 4.4. For an element with only one internal hinge the same procedure must be followed.

$$\theta_{p1} = \theta_{h11} - \theta_{h12} \tag{4.14}$$

$$\theta_{p2} = \theta_{h21} - \theta_{h22} \tag{4.15}$$

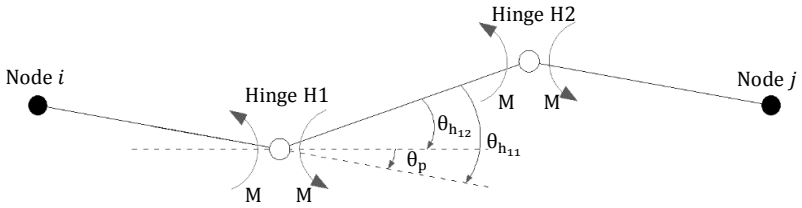

Figure 4.4. Illustration of plastic rotation in a beam model with two internal hinge

4.3.2 3D elements

An extension to three dimensional beams with one or two internal hinge is straight forward in the matrix form.

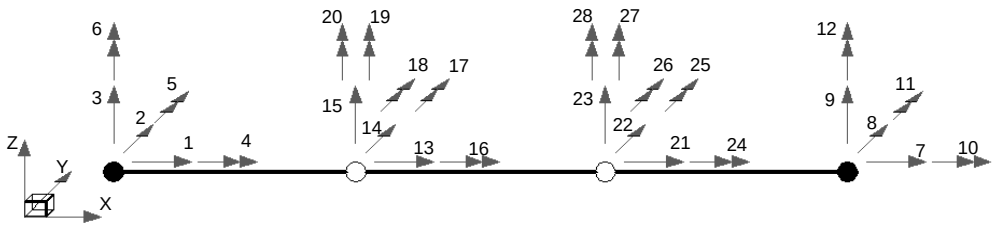

Figure 4.5. 3D beam model with two internal hinge

Similar to the previous section, in Figure 4.5 the internal degrees of freedom of 3D element with two internal hinges is presented. Eq. (4.16) shows the partitioned equation matrix for the 3D beam model corresponding to Figure 4.5. From here, the same procedure can be done in order to obtain the condensed matrix for an element, condense nodal forces and equivalent internal forces.

$$\begin{Bmatrix} F_{g_{[12x1]}} \\ \hline F_{h_{[16x1]}} \end{Bmatrix} = \begin{bmatrix} K_{gg_{[12x12]}} & K_{gh_{[12x16]}} \\ \hline K_{hg_{[16x12]}} & K_{hh_{[16x16]}} \end{bmatrix} \cdot \begin{Bmatrix} d_{g_{[12x1]}} \\ \hline d_{h_{[16x1]}} \end{Bmatrix} \tag{4.16}$$

4.4 Constrained degrees of freedom

4.4.1 Rigid Body

The deformation some structural components can be very small compared to the deformation the rest. Thus elements with a very small deformation enough to be neglected, they can be idealized as rigid bodies. (Cheng , 2001).

Two nodes on the rigid body are constrained, so that the deformation of a so called slave nodes can be represented by the deformation of the other, referred as master node. Deformation of all the constrained slave nodes will be depended on that of the master node. Hence, the degrees of freedom (DOF) of all the slave can be transferred to the master node. Therefore, the number of DOF in the structure is reduced, the size of the stiffness matrix will be reduced as well.

In the Figure 4.6, the notation X_{mj}, Y_{mj} and Z_{mj} are the coordinates of the relative position of the slave node with respect to its master nodes. The F_{sj} and M_{sj} are the forces and moments in the slave node, respectively. F_{mj} and M_{mj} are the forces and moments in the master node, respectively. The forces on the slave node can be substituted by static equivalent forces on the master node, as computed in the following equations:

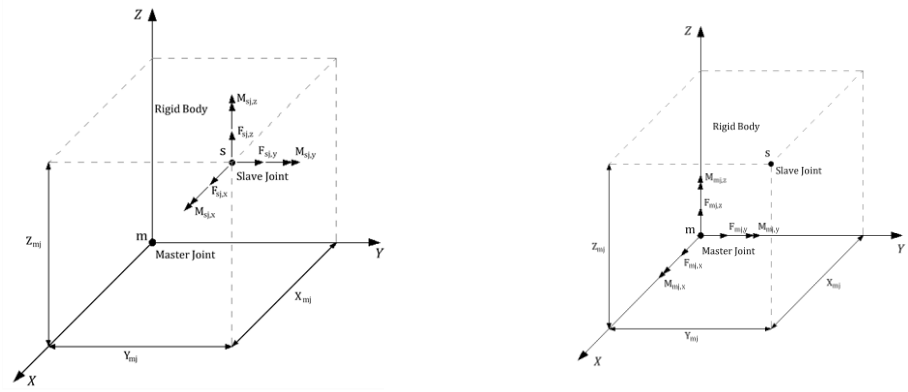

a) Before transformation b) After transformation

Figure 4.6. Rigid-body Constraint

$$\begin{bmatrix} F_{mj,x} \\ F_{mj,y} \\ F_{mj,z} \\ M_{mj,x} \\ M_{mj,y} \\ M_{mj,z} \end{bmatrix} = \begin{bmatrix} 1 & 0 & 0 & 0 & 0 & 0 \\ 0 & 1 & 0 & 0 & 0 & 0 \\ 0 & 0 & 1 & 0 & 0 & 0 \\ 0 & -Z_{mj} & Y_{mj} & 1 & 0 & 0 \\ Z_{mj} & 0 & -X_{mj} & 0 & 1 & 0 \\ -Y_{mj} & X_{mj} & 0 & 0 & 0 & 1 \end{bmatrix} \begin{bmatrix} F_{sj,x} \\ F_{sj,y} \\ F_{sj,z} \\ M_{sj,x} \\ M_{sj,y} \\ M_{sj,z} \end{bmatrix} \tag{4.17}$$

In matrix notation,

$$\{F_{mj}\} = [C_j]\{F_{sj}\} \tag{4.18}$$

Where the matrix $[C_j]$ is a constraint matrix, coordinates in the matrix are those referred in the Figure 4.6. Similarly, a transformation could be used for the displacements of corresponding degrees of freedom. Resulting that the displacement of a salve node located at a X_{mj}, Y_{mj} and Z_{mj} from the master node is:

$$\{u_{sj}\} = [C_j]^T \{U_{mj}\} \tag{4.19}$$

Where $\{u_{mj}\}$ represents displacement of the master node, and $\{u_{sj}\}$ represents displacement of the slave node. In this Thesis a planar constraint is need to model floor diaphragms. The constraint for this particular case, is explained in the following.

4.4.2 Floor diaphragm constraints

A floor slab in a building is very stiff in its plane, but very flexible out of its plane. Therefore, the in–plane deformations in the floor system are small compared to the inter–story horizontal displacements. Thus, a *planar constraint* can be used to model the floor slab's diaphragm as a 2D rigid body. The in – plane displacements of the diaphragm can be expressed in terms of two displacement, $u_x^{m(i)}$ and $u_y^{m(i)}$, and a rotation about z – axis $u_{\theta z}^{m(i)}$ (see notation in Figure 4.7.b).

Figure 4.7 shows a slab with a slave node with its corresponding six degrees of freedom and the same slab after matrix transformation due to constraints. The number of degrees of freedom are reduced, and the master node has now the sum of forces of all the slave node, the diaphragm displacements and the rotation about z – axis.

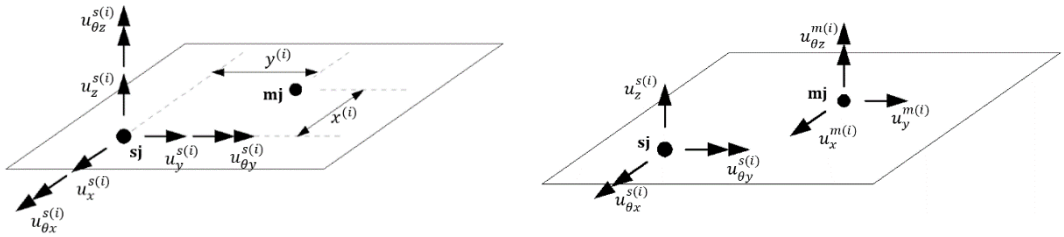

a) Typical joint "i" on floor system in x – y plane

b) Constrained system

Figure 4.7. Rigid diaphragm approximation model

In the case of static loading, the location of the master node mj can be arbitrarily selected in the plane of the slab. However, for dynamic loading, it is recommended to locate the master node at the center of mass of the weights that are assigned to the slave joints. As the result of this rigid diaphragm approximation, the following compatibility equations must be satisfied for joints attached to the diaphragm:

$$u_x^{s(i)} = u_x^{s(i)} - y^{(i)} \cdot u_{\theta z}^{m(i)} \tag{4.20}$$

$$u_y^{s(i)} = u_y^{s(i)} + x^{(i)} \cdot u_{\theta z}^{m(i)} \tag{4.21}$$

The rotation $u_{\theta z}^{s(i)}$ may or may not be constrained to the rigid body rotation of the diaphragm. This decision must be based on how beams and columns are physically connected to the floor system. That is, if the connection implies fixing of torsional moments of columns to the slab or transversal bending moment of beams, this can be considered the cases of monolithic construction. In that case, the following constraint is used:

$$u_{\theta z}^{s(i)} = u_{\theta z}^{m(i)} \tag{4.22}$$

In matrix form, the displacement transformation is as Eq. (4.23) and if rotation in $u_{\theta z}^{s(i)}$ is not used will be as Eq. (4.25):

$$\begin{Bmatrix} u_x^{s(i)} \\ u_y^{s(i)} \\ u_{\theta z}^{s(i)} \\ \end{Bmatrix} = \begin{bmatrix} 1 & 0 & -y^{(i)} \\ 0 & 1 & x^{(i)} \\ 0 & 0 & 1 \end{bmatrix} \begin{Bmatrix} u_x^{m(i)} \\ u_y^{m(i)} \\ u_{\theta z}^{m(i)} \\ \end{Bmatrix} \tag{4.23}$$

$$\begin{Bmatrix} u_x^{s(i)} \\ u_y^{s(i)} \end{Bmatrix} = \begin{bmatrix} 1 & 0 & -y^{(i)} \\ 0 & 1 & x^{(i)} \end{bmatrix} \begin{Bmatrix} u_x^{m(i)} \\ u_y^{m(i)} \end{Bmatrix} \tag{4.24}$$

In matrix notation,

$$\{u^s\} = [C_j] \cdot \{u^m\} \tag{4.25}$$

Where $\{u^s\}$, is the displacement of the slave node due to the transformation of the constraint matrix $[C_j]$, and $\{u^m\}$ is the displacement of the master node.

4.4.3 Multipoint constraint computational modeling

In general, in a numerical model of a real structure, a master node can have associated more than two slave nodes with six degree of freedom, for a 3D model. The force in the master node correspond to summation of the internal forces acting

on all slave nodes in the constrained matrix degrees of freedom ($F_x^{s(i)}, F_y^{s(i)}, M_z^{s(i)}$) (see Figure 4.8.b.). Therefore, the other three free degrees of freedom in the slave node are independent of the master node's influence ($F_z^{s(i)}, M_x^{s(i)}, M_y^{s(i)}$). Hence, the stiffness matrix will be reduced by the same *constrained matrix* $[C_j]$. The *constrained forces* vector corresponding to the *constrained stiffness matrix* will be:

$$\begin{bmatrix} F^{ms(1)} \\ F^{ms(2)} \\ F^{ms(3)} \\ F^{ms(4)} \\ F^{mj(1)} \end{bmatrix} = \left[\begin{array}{cccc} \mathrm{C_f} & 0 & 0 & 0 \\ 0 & \mathrm{C_f} & 0 & 0 \\ 0 & 0 & \mathrm{C_f} & 0 \\ 0 & 0 & 0 & \mathrm{C_f} \\ \mathrm{CC} & \mathrm{CC} & \mathrm{CC} & \mathrm{CC} \end{array}\right] \begin{bmatrix} F^{s(1)} \\ F^{s(2)} \\ F^{s(3)} \\ F^{s(4)} \end{bmatrix} \tag{4.26}$$

In matrix notation,

$$\{F^c\} = [C_j] \cdot \{F^s\} \tag{4.27}$$

In Eq. (4.27) the vector F^c will be the constrained forces vector, F^s the vector of forces each slave nodes. $F^{ms(i)}$ is the vector of forces in the master node that is statically equivalent to the forces applied in the slave node. The matrix $[\mathrm{CC}]$ is the *constrained matrix* that relates the slave nodes internal forces with the master node and the matrix $[\mathrm{C_f}]$ represents the independent degrees of freedom of slave node.

$$\mathrm{CC} = \begin{bmatrix} 1 & 0 & 0 & 0 & 0 & 0 \\ 0 & 1 & 0 & 0 & 0 & 0 \\ -y_{mj}^{(i)} & x_{mj}^{(i)} & 0 & 0 & 0 & 1 \end{bmatrix} \tag{4.28}$$

$$\mathrm{C_f} = \begin{bmatrix} 0 & 0 & 1 & 0 & 0 & 0 \\ 0 & 0 & 0 & 1 & 0 & 0 \\ 0 & 0 & 0 & 0 & 1 & 0 \end{bmatrix} \tag{4.29}$$

$$F^{ms(i)} = \begin{Bmatrix} F_z^{ms(i)} \\ F_{\theta x}^{ms(i)} \\ F_{\theta y}^{ms(i)} \end{Bmatrix} \tag{4.30}$$

$$F^{mj(i)} = \begin{Bmatrix} F_x^{m(i)} \\ F_y^{m(i)} \\ F_{\theta z}^{m(i)} \end{Bmatrix} \tag{4.31}$$

$$F^{s(i)} = \begin{Bmatrix} F_x^{s(i)} \\ F_y^{s(i)} \\ F_z^{s(i)} \\ F_{\theta x}^{s(i)} \\ F_{\theta y}^{s(i)} \\ F_{\theta z}^{s(i)} \end{Bmatrix} \tag{4.32}$$

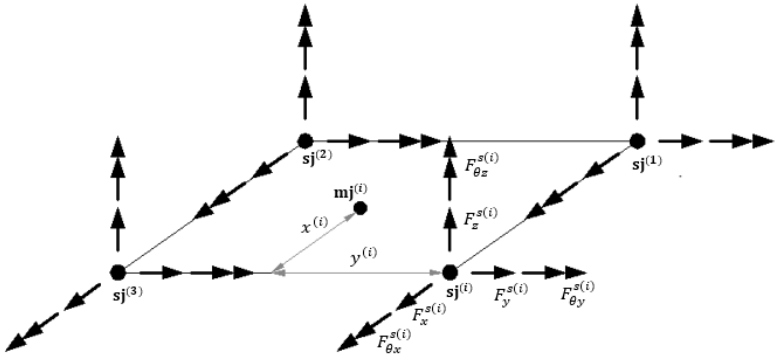

a) Typically floor system without constraint

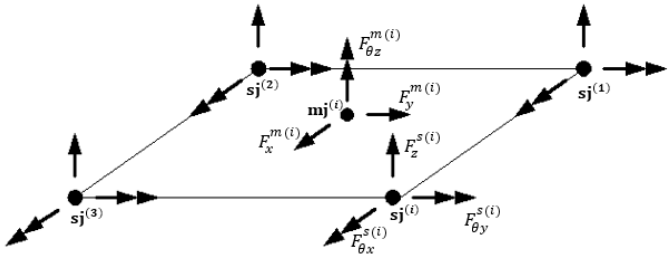

b) Constrained floor system after transformation

Figure 4.8. Diaphragm model

In the constraint matrix $[\mathrm{CC}]$, the notation $x_{mj}^{(i)}$ and $y_{mj}^{(i)}$ are the distance in the plane between master node $m_j{}^{(i)}$ of its corresponding diaphragm and slave node $s_j{}^{(i)}$. They can be computed by the difference between the in plane coordinate of the master node minus the slave node.

$$x_{mj}^{(i)} = (x^{(m)} - x^{(i)}) \tag{4.33}$$

$$y_{mj}^{(i)} = (y^{(m)} - y^{(i)}) \tag{4.34}$$

As it was mentioned before, the stiffness matrix is reduced to a *constrained stiffness matrix*, and it can be computed by Eq. (4.35):

$$[K_c] = \left[C_j\right] \cdot [K_e] \cdot \left[C_j\right]^T \tag{4.35}$$

Finally, the *constrained displacement* vector $\{u^m\}$ and the total displacement vector $\{u^s\}$ at the slave node, due to the influence of the master node of its corresponding diaphragm, is:

$$\{u^m\} = [K_c]^{-1} \cdot \{F^m\} \tag{4.36}$$

$$\{u^s\} = \left[C_j\right]^T \cdot \{u^m\} \tag{4.37}$$

As mentioned in 4.4.2, the master node will be located in the center of masses of the diaphragm. Which can be computed as:

$$\underline{x}^{(m)} = \frac{\sum_{i=1}^{i} \underline{x}^{(i)} M_{x^{(i)}}}{\sum_{i=1}^{i} M_{x^{(i)}}} \tag{4.38}$$

Where $\underline{x}^{(i)}$ is the coordinate vector of the masses $M_{x^{(i)}}$ belonging to the floor diaphragm.

4.5 Structural dynamics

Time dependent response of an undamped system in free vibration is governed by the equation of motion. The frequency and vibration mode of the system is given by the, so called, characteristic equation, presented in chapter 2. In a multi-degree of freedom problem, nodes without masses in some DOF may exist, this provokes singularities in the mass matrix. For this reason, the mass and stiffness matrices must be condensed. The following section shows the static condensation method.

4.5.1 Static condensation method

The static condensation method is used to eliminate the degrees of freedom that have no assigned mass, in order to conduct the dynamic analysis. First, one should identify those degrees of freedom to be condensed and those that are not, for instance, by looking at the mass assigned in the degree of freedom. The algorithm for this method, starts by assigning a value, e.g. unit, for the values to be condensed and those to be independent, as in Eq. (4.41) and Eq. (4.42), respectively, taking as example the mass and stiffness matrix as in Eq. (4.39) and Eq. (4.40).

$$\mathrm{K} = \begin{bmatrix} k_{11} & \cdots & k_{15} \\ \vdots & \ddots & \vdots \\ k_{51} & \cdots & k_{55} \end{bmatrix} \tag{4.39}$$

$$\mathrm{M} = \begin{bmatrix} 0 & & & & \\ & m_2 & & & \\ & & m_3 & & \\ & & & m_4 & \\ & & & & 0 \end{bmatrix} \tag{4.40}$$

$$\mathrm{MC} = \begin{bmatrix} 1 & 0 & 0 & 0 & 0 \\ 0 & 0 & 0 & 0 & 1 \end{bmatrix} \tag{4.41}$$

$$\mathrm{MI} = \begin{bmatrix} 0 & 1 & 0 & 0 & 0 \\ 0 & 0 & 1 & 0 & 0 \\ 0 & 0 & 0 & 1 & 0 \end{bmatrix} \tag{4.42}$$

The partitioned condensed and independent matrices are computed by:

$$[\mathrm{KCC}] = [\mathrm{MC}] \cdot [\mathrm{K}] \cdot [\mathrm{MC}]^{\mathrm{T}} \tag{4.43}$$

$$[\mathrm{KCI}] = [\mathrm{MC}] \cdot [\mathrm{K}] \cdot [\mathrm{MI}]^{\mathrm{T}} \tag{4.44}$$

$$[\mathrm{KIC}] = [\mathrm{MI}] \cdot [\mathrm{K}] \cdot [\mathrm{MC}]^{\mathrm{T}} \tag{4.45}$$

$$[\mathrm{KII}] = [\mathrm{MI}] \cdot [\mathrm{K}] \cdot [\mathrm{MI}]^{\mathrm{T}} \tag{4.46}$$

The reduced condensed matrix is finally obtain as follows:

$$[\mathrm{K_c}] = [\mathrm{KI}] - [\mathrm{KIC}] \cdot [\mathrm{KCC}]^{-1} \cdot [\mathrm{KCI}] \tag{4.47}$$

In order to work with the same independent degrees of freedom, the mass matrix is reduced as well by,

$$[\mathrm{M_c}] = [\mathrm{MI}] \cdot [\mathrm{M}] \cdot [\mathrm{MI}]^{\mathrm{T}} \tag{4.48}$$

4.5.2 Modal Analysis

In the proposed design method, the seismic analysis problem is solved by means of the modal spectral dynamic analysis. To carry out this methodology, the characteristic equation, as in Eq. (4.49), must be solved and modal properties of the structures is analyzed.

$$\left([\mathrm{K}]-\omega^2\cdot[\mathrm{M}]\right)\{a\} \tag{4.49}$$

The roots ω^2 of this equation provides the eigenvalues of the system, and the square root of the natural frequencies ω_i. Thus, it is possible to solve for the unknown vectors $\{a_i\}$ in terms of relative values. These vectors are the eigenvector and represent the vibration modes. As the solution are the eigenvectors, they are represented in relative magnitude, i.e., normalized for practical magnitude. Several normalization criteria are possible. Here the eigenvector are normalized as:

$$\phi_{ij}=\frac{a_{ij}}{\sqrt{\{a_j\}^{\mathrm{T}}[\mathrm{M}]\{a_j\}}} \tag{4.50}$$

The directional eigenvector in “x” can be obtain by:

$$\left[\phi_{ij,x}\right]=\begin{bmatrix}1&0&0&0&0&0\\0&0&0&1&0&0\end{bmatrix}\cdot\begin{bmatrix}\phi_{11,x}&\phi_{12,x}&\phi_{13,x}&\phi_{14,x}&\phi_{15,x}&\phi_{16,x}\\\phi_{21,y}&\phi_{22,y}&\phi_{23,y}&\phi_{24,y}&\phi_{25,y}&\phi_{26,y}\\\phi_{31,\theta}&\phi_{32,\theta}&\phi_{33,\theta}&\phi_{34,\theta}&\phi_{35,\theta}&\phi_{36,\theta}\\\phi_{41,x}&\phi_{42,x}&\phi_{43,x}&\phi_{44,x}&\phi_{45,x}&\phi_{46,x}\\\phi_{51,y}&\phi_{52,y}&\phi_{53,y}&\phi_{54,y}&\phi_{55,y}&\phi_{56,y}\\\phi_{61,\theta}&\phi_{62,\theta}&\phi_{63,\theta}&\phi_{64,\theta}&\phi_{65,\theta}&\phi_{66,\theta}\end{bmatrix} \tag{4.51}$$

Where, J_x is a directional reduction matrix, in matrix notation is:

$$\left[\phi_{ij,x}\right]=\left[J_x\right]\cdot\left[\phi_{ij}\right] \tag{4.52}$$

For “y” direction, J_y is as below, directions matrix J in other direction is obtained in the same manner.

$$\left[J_y\right]=\begin{bmatrix}0 & 1 & 0 & 0 & 0 & 0\\ 0 & 0 & 0 & 0 & 1 & 0\end{bmatrix} \tag{4.53}$$

For a normalized eigenvector, the mass participation factor is computed as:

$$\Gamma_i = -\left[\phi_j\right]^T \cdot \left[M\right] \cdot \{1\} \tag{4.54}$$

In order to obtain displacement and forces in all degrees of freedoms (DOF), the previously condensed DOF should be recovered. Hence, the condensed modal displacement is obtained as:

$$\left[\phi_{\mathrm{j,cond}}\right] = -\left[\mathrm{KCC}\right]^{-1} \cdot \left[\mathrm{KCI}\right] \cdot \left[\phi_j\right] \tag{4.55}$$

And the total modal displacement for each mode is computed by:

$$\left[\phi_{\mathrm{j,tot}}\right] = \left[\mathrm{MC}\right]^T \cdot \left[\phi_{\mathrm{j,cond}}\right] + \left[\mathrm{MI}\right]^T \cdot \left[\phi_j\right] \tag{4.56}$$

4.5.3 Modal Spectral analysis

Modal spectral analysis is used to determine the maximum earthquake response by means of the response spectrum. For seismic design using a design spectrum, spectral acceleration should be obtained for each natural vibration mode of the structures. Thus, nodal forces for each mode can be computed as:

$$\left\{f_{\mathrm{j}}\right\} = \left[\mathrm{M}\right] \cdot \left[\phi_{\mathrm{j}}\right] \cdot \left[\Gamma_j\right] \cdot \left[Sa_j\right] \cdot g \tag{4.57}$$

The modal base shear is obtained as:

$$\left\{Vb_{\mathrm{j}}\right\} = \left\{f_j\right\}^T \cdot \{1\} \tag{4.58}$$

All the internal forces (shear force, bending moment, axial force, etc.) due to each modal response "R_j" are combined, in this proposal, by the method (SRSS) for well separated natural frequencies. In the DLA method, the auxiliary structure presents the plastic rotation in each internal perfect hinge. When the modal spectral analysis is carried out, the plastic rotation from each modal response must be combined by the combination method, in that cases SRSS method.

$$R = \sqrt{\sum_{j=1}^{n} \left\{ R_j^2 \right\}} \tag{4.59}$$

In order to obtain directional modal forces, base shear, and internal forces response by modal combination, directional matrix should be used as in Eq. (4.51).

CHAPTER 5

EFFECTS OF HIGHER VIBRATION MODES

5.1 Introduction

In current seismic design process, the modal spectral analysis provides an overview of the importance of the first mode of vibration, typically regarded as the fundamental one. Based on elastic properties, higher vibration modes can be neglected. Nevertheless, when inelastic behavior occurs, the contribution of different mode shapes may be more important.

The current seismic design practice is to estimate the structures response based on elastic models, but, for economic reasons, buildings are not designed to remain elastic under the design earthquake. Instead, yielding is normally allowed to form at the end of beams or base of walls under such severe ground shakings. Although, the plastic rotation in the hinge zone must be within an acceptable limit and the length of the element outside the hinge zone is expected to remain elastic.

The response spectrum analysis (RSA), which accounts for multi-mode effects, is commonly used in the seismic design of buildings. In the RSA procedure, the elastic responses of each vibration modes are first determined from the response spectrum at 5% damping ratio. Then, the total elastic response is combined by either the SRSS or the CQC method. Finally, seismic load is affected by a response modification factor (“R” or “q”) that accounts for the system overstrength and inelastic effects.

The most common practice is to assume the same reduction factor for all modes, without changing the load distribution and, in some cases, applying an equally overstrength factor to all elements to remain elastic. Although, there is a strong evidence that inelasticity affects higher modes of vibration unequally. In some case, only one mode is considered.

Recently, extensive research by Biondini et al. (2012), Ghorbanirenani (2011), Tremblay et al. (2008), Panagiotou & Restrepo (2007) and Tremblay, et al. (2005) have been carried out on the effects of higher modes through laboratory experiments for low and medium rise concrete building. A plastic analysis was carried out in Moehle (2015) in order to highlight the problem of the concept of weak beam – strong columns related to higher modes in inelasticity process. Those research has been conducted regarding higher-mode effects on the response of multi degree-of-freedom (MDOF) systems. In some of these researches, certain proposals or approximations are made attempting to avoid this problem.

In this chapter, the work of Moehle (2015) and Biondini, et al. (2012) are analyzed, and the performance based seismic design method proposed in Chapter 3 is used as an assessment methodology of the effects of higher vibration modes.

5.2 Plastic and collapse mechanism for a 12-storey regular building

In Moehle (2015) it is stated that, when a building sways during an earthquake, the distribution of damage over height depends on the distribution of lateral drift. In a case where a building have weak columns, drift tends to be concentrated in one or few stories, and may exceed the drift capacity of the columns. If columns provide a stiff and strong spine over a building height, drift will be more uniformly distributed, and localized damage will be reduced (see Figure 5.1).

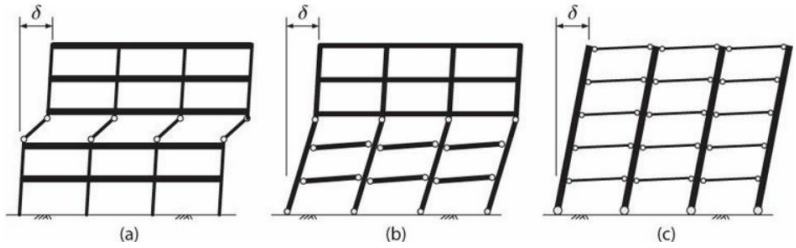

Figure 5.1. Idealized beam-yielding mechanisms: (a) story mechanism; (b) intermediate mechanism; (c) beam mechanism.

Another aspect is that, in order to achieve a complete mechanism involving hinges in all stories as in Figure 5.1 (c), columns moment strength several times larger than the beam moment strengths may be required, which may result uneconomical. Therefore, some yielding of the columns has to be anticipated especially at the base of the column in the first story.

Moehle (2015) also analyzed a 12-storey building (see Figure 5.2). Here the failure mechanism developed was studied with a “strong column – weak beam” overstrength ratio of 1.2, as it is required in ACI 318 (2014). It is observed in the Figure 5.2, that some columns are yielding and the mechanism is formed in the 6th floor, even though it had been designed following the “strong columns – weak beam” design philosophy.

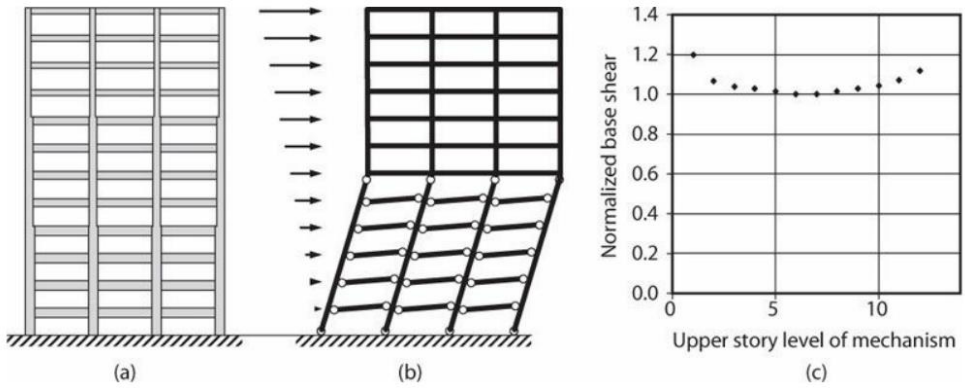

Figure 5.2. Calculated plastic mechanism for a 12-story frame. (Moehle, 2015)

Even if beam overstrength was negligible, which generally is not the case, column yielding along the building height was unavoidable unless the columns were made much stronger than the beams. That is, the overstrength factor is largest then 1.2.

This conclusion was demonstrated using a limit analysis of a frame under lateral loading, as follows. Let us consider the frame shown in Figure 5.2(a). An Imposed virtual displacement was applied in a kinematically acceptable yield mechanism, such as the one shown in Figure 5.2(b). For this example, it was considered only virtual mechanisms extending from the base to some upper level. A virtual work is done by the external forces, acting through virtual lateral displacements, and by internal moments, acting through the hinge virtual rotations.

The correct solution is the one corresponding to the minimum base shear. For this example, it was found that, the correct solution is a mechanism extending from the base through level 6 Figure 5.2(c), when the overstrength factor of 1.2 was used.

Although the correct mechanism was found to extend up to level 6, it can be seen in Figure 5.2(c) that other mechanisms were nearly as critical. It was stated that slight changes in relative strengths within the frame could result in different mechanism.

Thus, it is explicitly interpreted that "*It should be expected that yield mechanisms during earthquake ground shaking will vary from one time to another because the lateral load profile continuously changing with time" […].* An issue that the methodology proposed in Chapter 3 is expected to take into account.

In the next section a parametric analysis is presented. Three buildings with similar layout as the one in Figure 5.2 are analyzed. The difference between the three are the columns stiffness (columns size). The objective, is to compare the results when designing with the DLA method and the observed in Figure 5.2. The DLA is used in order to analyze the "strong column – weak beam" performance through the overstrength factor, obtained from the DLA method. Those analyzes are part of a numerical validation comparing with the plastic analysis done in Figure 5.2. A fourth case with similar building is analyzed. However, in this case the mechanism proposed is that beams yield from first to sixth story and yielding of top columns in the sixth floor. The aim of this proposal is to impose a columns failure in middle height.

5.2.1 Assessment with the "Double Linear Analysis" (DLA) of higher mode effects for a twelve story building.

The example presented in the previous sections is considered as benchmark, as it has a simple geometry, fully regular, and it is a relatively tall structure. Although there is not a detailed information described as the cross section, story height, gravitational loads and seismic hazard.

Nevertheless, a variation of cross section strength is considered. By analyzing the model with the "Double linear analysis" (DLA) described in Chapter 3, it is shown that the beam hinges formed in a high floor due to a biggest force in this a high floor produced by higher modes effect. After reproducing the original case-study, a parametric analysis is carried out.

This first case corresponds to square columns of 150, 130 and 100 cms from level 1 to 4, level 5 to 8 and level 9 to 12 respectively; the second case are columns of 130, 110, 90 cm and the third case columns of 100, 90, 80 cm. Beams are all equal to 40x60 cm. The building is subjected to a gravity load of 35 KN/m and a seismic hazard correspond to a design spectrum from EC8 (2004) type 1, ductility factor $q = 1$, soil type B and a pga = 0.25g, (see Figure 5.3).

For the first three cases, the DLA method is used to design a beam yielding mechanism in whole height, that is means all beam completely damage for the seismic action. Load pattern in all cases is compared from an elastic and inelastic structure. The “strong column – weak beam” overstrength factor (Ω) is compared in order to appreciate the difference distribution of strength demand along the height of the structure.

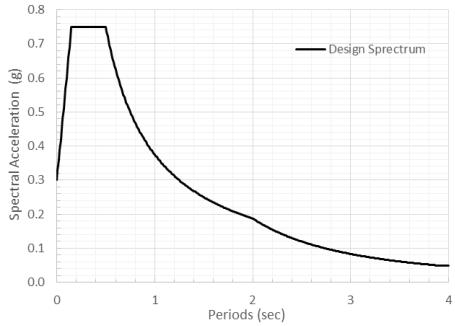

Figure 5.3. Design Spectrum

5.2.1.1 Case 1

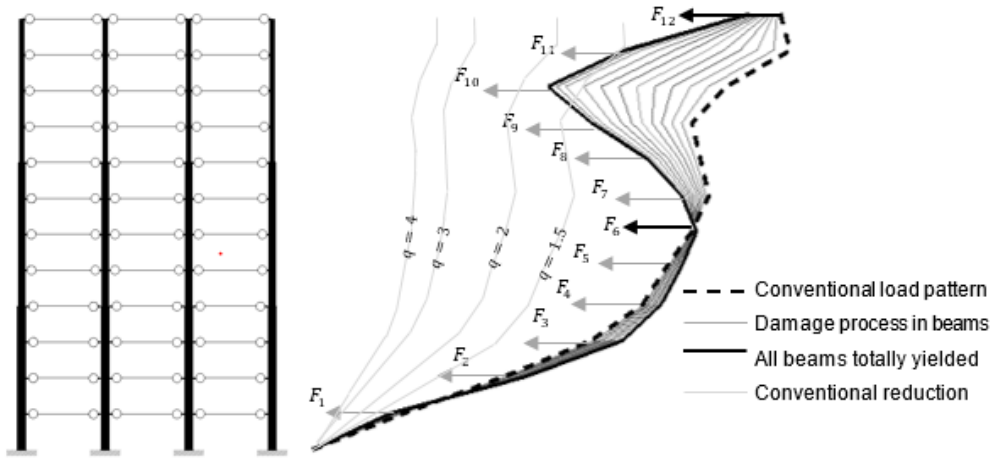

Figure 5.4. Conventional load pattern in comparison with the obtained from the "Double Linear Analysis"

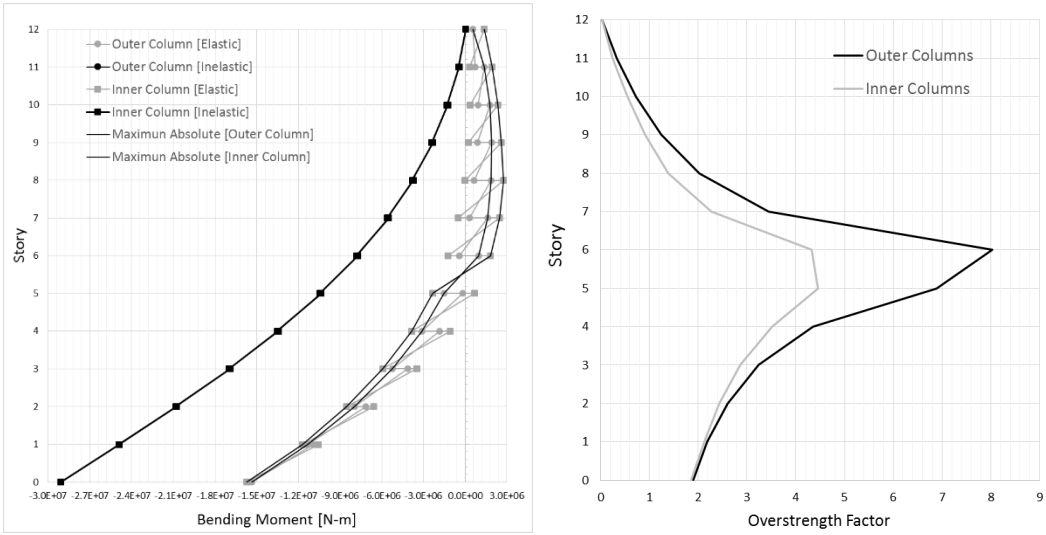

a. Bending moment for columns b. Overstrength required in column by floor

Figure 5.5. Overstrength required of columns with the double linear analysis for the a criteria of "strong column – weak beam"

5.2.1.2 Case 2

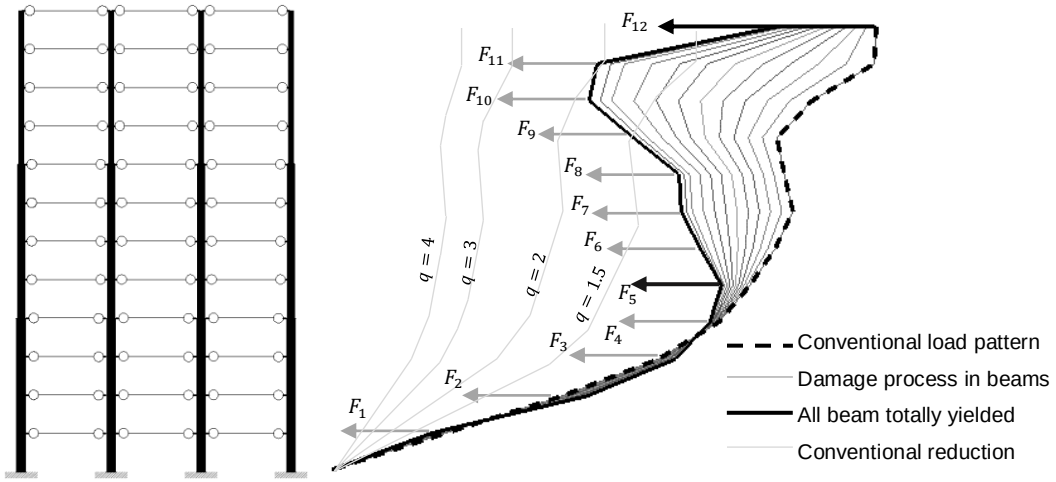

Figure 5.6. Conventional load pattern in comparison with the obtained from the "Double Linear Analysis"

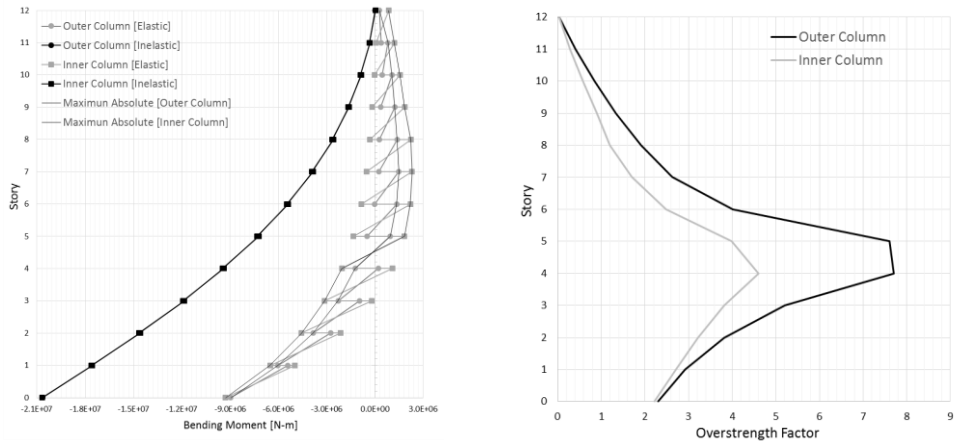

a. Bending moment for columns b. Overstrength required in column by floor

Figure 5.7. Overstrength required of columns with the double linear analysis for the concept of "strong column – weak beams" for the case 2.

5.2.1.3 Case 3

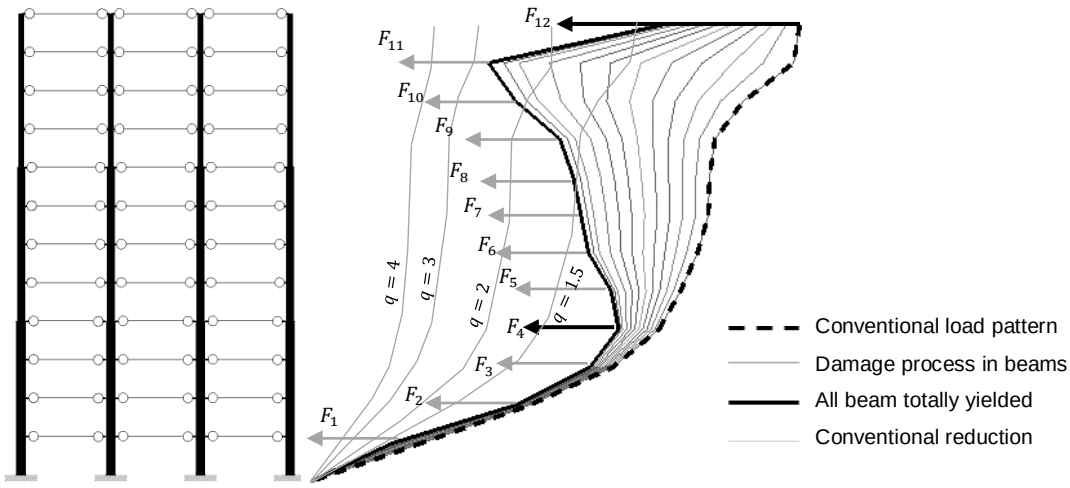

Figure 5.8. Conventional load pattern in comparison with the obtained from the "Double Linear Analysis"

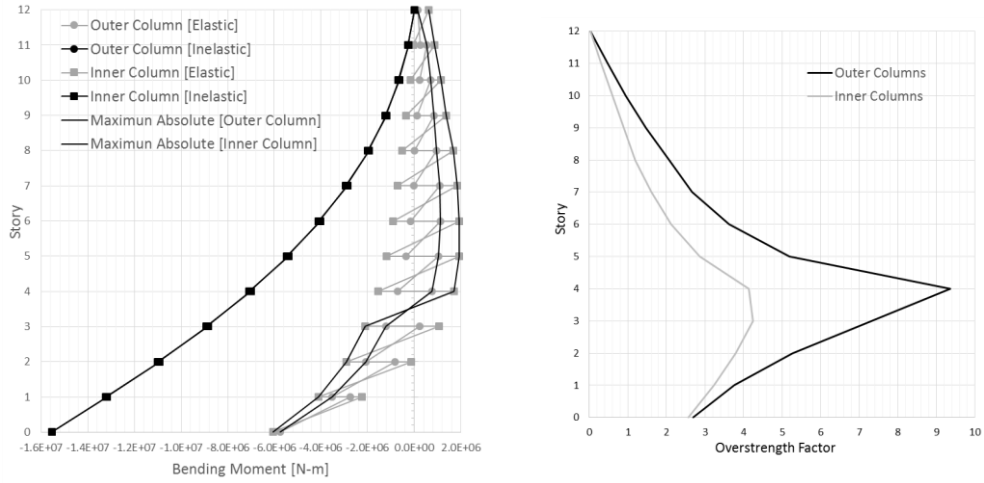

a. Bending moment for columns b. Overstrength required in column by floor

Figure 5.9. Overstrength required of columns with the double linear analysis for the concept of "strong column – weak beams" for the case 3.

5.2.1.4 Case 4

The effect of varying the strengths of columns and beams using a limit analysis approach is shown in Figure 5.10. It shows a case where the overstrength ratios, where α_{os} is ranging from 0.8 to 4.0. For $\alpha_{os} = 0.8\ or\ 1.0$, the critical mechanism is a soft story in the sixth floor. As α_{os} increases above 1.2, the base shear strength increases and the controlling yield mechanism corresponding to the minimum base shear for that value of α extends higher into the structure. For the case of $\alpha_{os} = 4$, Moehle (2015) obtained yielding in the columns in the sixth floor. However, a full beam mechanism is never achieved.

For the sake of comparison, in the following, DLA is going to be used to study the maximum overstrength factor needed for a similar collapse mechanism (Figure 5.11.a). The maximum overstrength factor obtained with the DLA is 3.6. If the curve in Figure 5.10 is interpolated to a value of $\alpha_{os} = 3$, or, to others curves the minimum value will be for the fifth floor or higher floor. Meantime, the DLA prediction is compared to the limit plastic analysis of Moehle. It is worth noting, as it can be seen in Figure 5.11.c, that the overstrength factor is not uniform in all stories. Nevertheless, for conventional seismic design, a single overstrength factor is considered. This issue can lead to never achieving the full "strong column – weak beam" collapse mechanism. This leads, in many cases, to column yielding in an upper story.

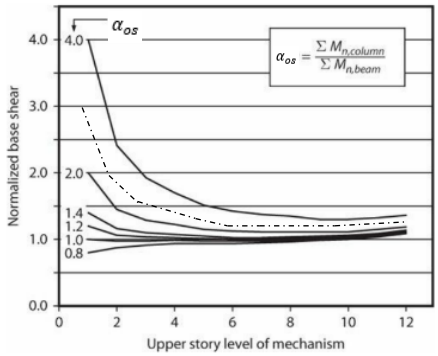

Figure 5.10. Yield mechanism solution for frame designed with different ratios of columns to beam strengths. The base shear is normalized to the value for $\alpha_{os} = 0.2$. (Moehle, 2015)

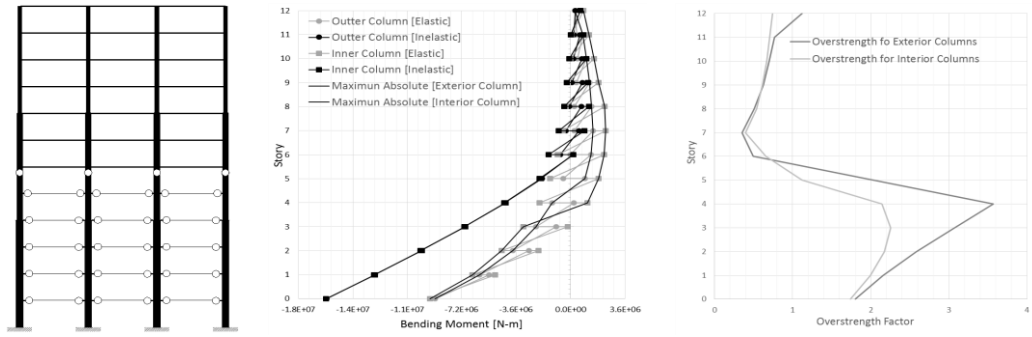

a) Mechanism proposed

b) Bending moments in columns

c) Overstrength factor necessary along the height

Figure 5.11. Overstrength factor assessment for a mechanism in the sixth floor

5.2.2 Discussion

In Figure 5.4, Figure 5.6 and Figure 5.8, there were presented conventional load patterns obtained with an elastic modal dynamic spectral analysis (MDSA) for 12-story building. This first load pattern, shown in dash line, is compared to a load pattern from a MDSA of a second structure assuming all beams yielded (with perfect hinges). These two load patterns are compared, and discussion about the different characteristic of the design shear force are discussed in the following.

5.2.2.1 Relationship of the force reduction factor to the shape of load distribution

The criterion of “strong column – weak beam” suggests that all beams should be yielded before a mechanism is formed. After all beams are yielded, columns at the base story should present plastic hinges. However, in Figure 5.4, Figure 5.6 and Figure 5.8, it was demonstrated that, when all beams yield in the column connections, the load pattern will vary, resembling more to a system where columns act as a cantilever. In Figure 5.4, Figure 5.6 and Figure 5.8 it can be observed that, in between those two load patterns, there will be other patterns that should appears in the process of damage of all beams until have a complete damage.

Although, the reduction factor q is uniformly applied in standards codes, the method of Double Linear Analysis for Performance Based Seismic Design (DLA) shows that this load pattern can vary much when all beams are damaged. Being more similar to the second mode of vibration with local maximum values, in the top floor and 1/2 - 1/3 height approximately.

In the Figure 5.4, Figure 5.6 and Figure 5.8 it was shown, in light continuous line that, the load pattern for a conventional MDSA but applying the reduction factor $q = 4,\ q = 3,\ q = 2\ and\ q = 1.5$. It is evident that the difference between the load pattern with all beam damage in comparison with the elastic reduced by a single factor.

5.2.2.2 Strong column – weak beam overstrength factor

By comparing the bending moments on the beams and columns in a joint, obtained from the DLA, it can be observed that the bending moment vary after considering the beam yielded. Therefore, the required overstrength factor of the columns can be computed in order for not yielding in the columns of that joint.

The three cases are represented in Figure 5.5.b, Figure 5.7.b and Figure 5.9.b, respectively. The evaluation is done with the elastic moment of interior columns and other case with exterior columns with the respectively moment at the same joint with all beam completely damaged. It can be observed in Figure 5.5.a, Figure 5.7.a and Figure 5.9.a, which the maximum overstrength factor in all cases investigated is located at about 1/3 of height of the building. The maximum overstrength factor decreases to zero at the top floor, where there is no need bending moment for the auxiliary structure, when $\alpha = 1$. However, in practice the overstrength factor should be larger than 1. Analyzing the Figure 5.5.b, Figure 5.7.b and Figure 5.9.b, it can be concluded that overstrength factor are not needed from columns 9 to 12 almost in all cases. Although, some minimum overstrength should be considered to account for the stochastic variability of the beam and column strength. Nevertheless, the minimum overstrength factor is needed in almost 1/3 of the height. Hence, providing

a constant value is not economical. Furthermore, from middle height to base floor the overstrength factor is decreasing not to zero but between 2 and 2.5, which is reasonably consider in some standards code as the overstrength factor should be 1.2 or 1.35.

A similar result it is highlighted in the work of (Franchin & Pinto, 2012), where, the deformation inter-story drift is compared in each floor for a normal MSDA capacity design and the peak inter-story drift profile for five return periods for a non-linear time-history analysis. In the modified design method proposed in (Franchin , et al., 2016), the news constraint ensure that Columns-Beams-Capacity design ratios (CBCRs) is larger than 1.2 at all nodes but for the base of ground floor columns.

5.2.2.3 Sensitivity analysis of DLA results

Another relevant aspect for this analysis is that, the building studied in (Moehle, 2015) was analyzed changing the size of columns as it was mentioned earlier. The first remark is that, the lateral behavior is practically the same in terms of shape deformations; however, it is observed that if the structure is less stiff, the base shear is reduced more than for a stiffer structure.

Another important observation is related with the overstrength factor. In all cases the maximum load is higher than elastic seismic forces in the middle height of the structure. In the case 1, the maximum overstrength factor is in the sixth floor while by reducing the column's stiffness the peak overstrength factor occurs on lower floor. In case 2 the maximum overstrength factor is in the 5-4 story and in case 3 is clearly in the 4 story. Note that the case 1 coincides with the example in the work of Moehle (2015).

Therefore, in the case 1 (see Figure 5.4 and Figure 5.5) the maximum demand of overstrength factor is also in the sixth floor, with a much higher value than the required in standards codes, but coinciding with the results of Moehle (2015).

5.2.2.4 Recommendation for the “strong column – weak beam” capacity design criterion

Currents seismic standards codes requires designing frames structures with the criterion of “strong columns –weak beam”. This requires that, in a joint, the sum of moments of columns should be larger than the sum of the moment of beams connected to this joints by a certain overstrength factor. The multiplying factor varies in different codes, from 1.2 in UBC code to 1.35 in EC8. In any case, the intended objective is to avoid plastic hinges in columns, by assuming that if the beam yields first in any joint the column would not experiment an increment of amount demand. The intention is to exploit all sectional ductility capacity of plastic hinges in beams.

This assumption mentioned above, should be a first step in a capacity design to ensure that all beam will yielded in plastic hinges. A second step should emphasize a second state after beams are yielded, in which columns are acting as a cantilever. Here, bending moments can be much bigger than the supposed elastic state and beams are presented a very low bending moment or zero. Along the height of columns acting as a cantilever, the overstrength factor is different in each story and much higher than the increasing factor to meet the concept of “strong column – weak beam” as it was mentioned above. This can be observed in Figure 5.5.b, Figure 5.7.b and Figure 5.9.b.

5.3 Assessment for a Pseudo-dynamic test on a full scale prototype

5.3.1 Description of the case study

In the work of Biondini et al. (2012) a numerical investigation was carried out on a full-scale prototype of a multi-storey precast structure (see Figure 5.12). The main objective of the research was to analyze the performance of different types of precast connections. A pseudo-dynamic tests was carried out on the different structural schemes shown in Figure 5.13. The forces on each actuator was initially estimated based on the base shear distribution of the design seismic forces from a modal spectral analysis. However, after that, a non – linear time – history analysis was carry out and showed that the maximum floor forces expected was much higher and exceed the actuators capacity as it is shown in Figure 5.15.b to Figure 5.17.b. Hence, the prototype was forced to reduce one span and the final model was as it is shown the final configuration in Figure 5.12.

The results of the non – linear analyses highlighted the importance of the higher vibration modes, which were considered the responsible of higher forces, in some cases in mid-floors. For all the numerical cases studied with this prototype, it is shown that the response spectrum modal analysis allows a reliable estimation of the storey displacements (see Figure 5.15.a to Figure 5.17.a), whereas it may lead to a significant underestimation of the maximum story forces, as it is shown in

Table 5.1. Here, it is shown the comparison of peak floor forces and floors displacements of a modal analysis and a non – linear time – history analysis.

Table 5.1. Story forces and displacements evaluated through modal analysis and non – linear time – history analysis for the prototype Model 2, 3 and 4 for viscous damping ($\xi_v = 0\%$)

		Displacement (cm)		Peak story forces (KN)	
	Storey	Modal	Time-History	Modal	Time-History
Model 2	III	19.86	16.48	195	722
	II	10.72	9.81	233	1047
	I	3.32	4.12	234	1384
Model 3	III	11.1	10.44	250	738
	II	8.34	7.16	231	747
	I	3.14	3.17	223	1143
Model 4	III	3.79	5.60	410	875
	II	2.99	4.38	395	1100
	I	1.51	2.4	265	982

Figure 5.12. The structural prototype.

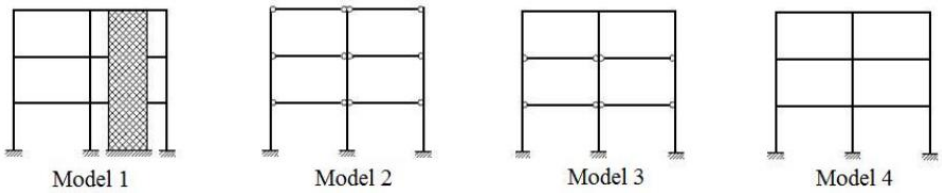

Figure 5.13. Schemes of the structural prototype.

The seismic input action was the East-West component of the modified Tolmezzo accelerogram (see Figure 5.14.a), with a total duration of 12 second. The corresponding scaled response spectrum matches very well the Eurocode-8 (2004) design spectrum for a soil class B, (see Figure 5.14.b). The maximum amplitude of the accelerogram is scaled due to the soil factor to 0.3g.

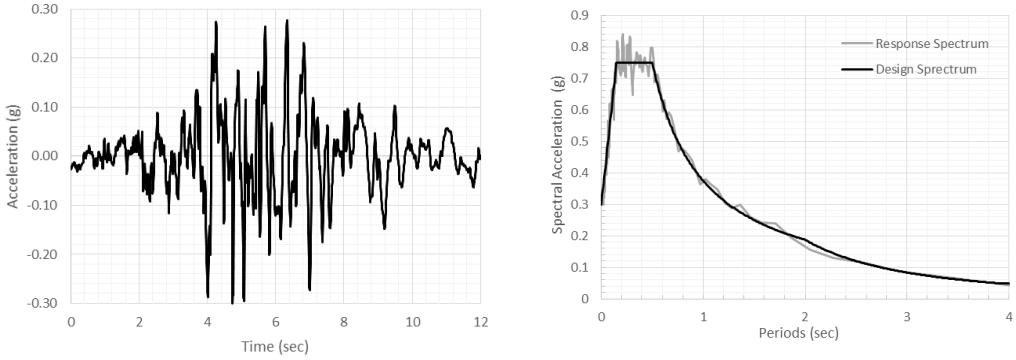

a) Tolmezzo Accelerogram b) Scale response spectrum Modified

Figure 5.14. Seismic input action

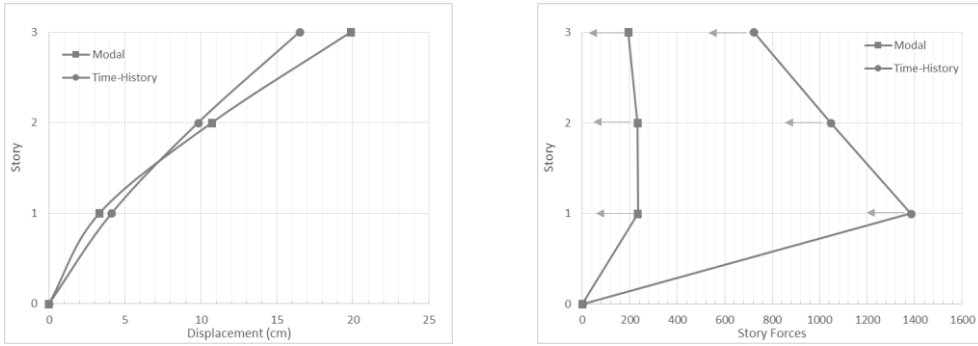

a) Story displacement b) Story forces

Figure 5.15. Comparison of modal and time-history analysis for Model 2 for $\xi_v = 0\%$

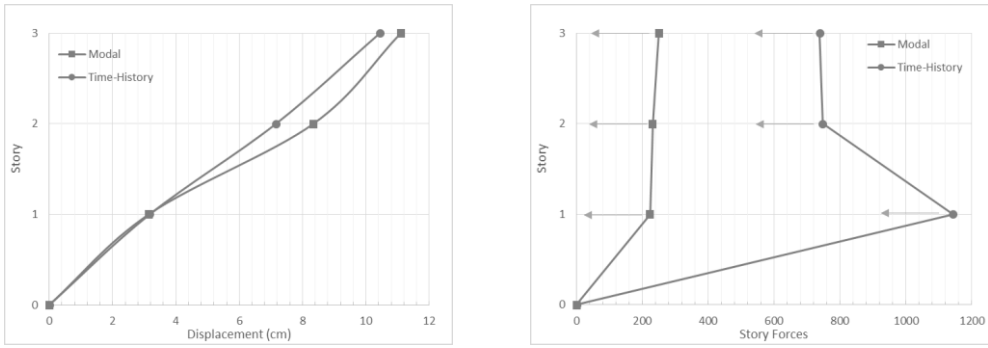

a) Story displacement b) Story forces

Figure 5.16. Comparison of modal and time-history analysis for Model 3 for $\xi_v = 0\%$

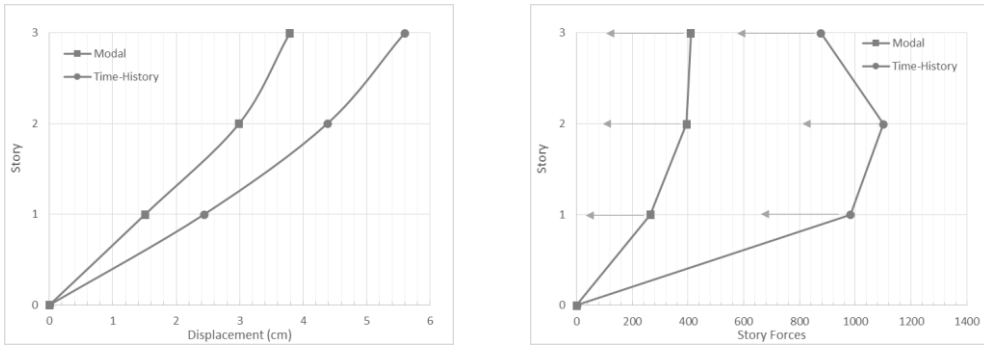

a) Story displacement b) Story forces

Figure 5.17. Comparison of modal and time-history analysis for Model 4 for $\xi_v = 0\%$

5.3.2 Assessment of Model 2 by means of the DLA method

The model 2 (Figure 5.15) has been numerically tested by a time-history non-linear analysis (THNLA) for different viscous damping implementing the Rayleigh proportional damping. In the pseudo-dynamic test the viscous damping is neglected. This consideration is made assuming that, while full-scale test is done, hysteretic behavior is present, but not viscous damping. However, the modal spectral analysis was carried out for a 5% of viscous damping to design the full-scale prototype, the behavior factor q corresponding is 3.

The DLA method was used as an assessment method. A blind prediction was done in order to propose a mechanism that satisfies the same load pattern for the THNLA results. As the THNLA, three viscous damping were proposed ($\xi_v = 0\%$, $\xi_v = 2\%$, $\xi_v = 5\%$); however, for the DLA, theses ξ_v were used for MSDA for a scaled response spectrum corresponding to the same signal used in THNLA (Tolomezzo earthquake), see Figure 5.18. Figure 5.18 shows the three response spectrum compared with the design spectrum.

The first test with the DLA method proposed for a certain distribution of hinges resulted in a different configuration of distribution of peak story forces (load pattern) in comparison to an elastic modal dynamic spectral analysis (MDSA).

Other tests (varying the local damage) were done in order to seek for a similar load pattern found in the THNLA (see Figure 5.19). For practical proposes, the same scheme of local damage proposed with the DLA for one case study is used to vary the viscous damping. Finally, it was possible to find the load pattern obtained from the THNLA (see Figure 5.19.b, Figure 5.19.d. Figure 5.19.f).

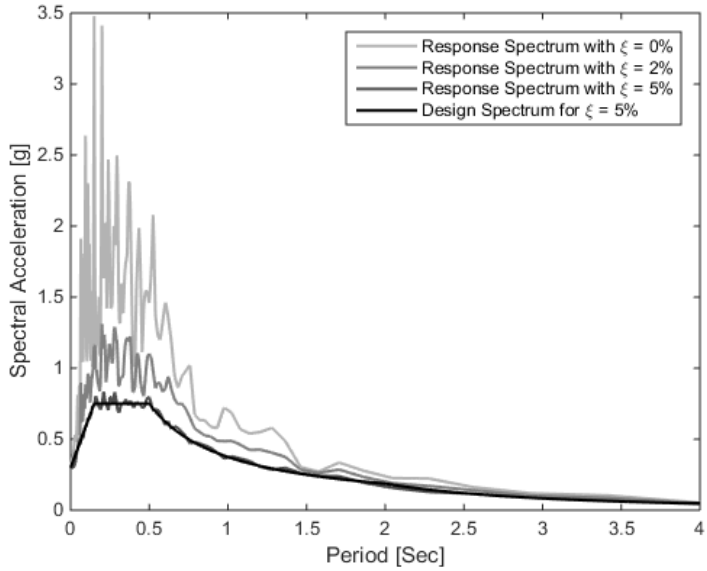

Figure 5.18. Series of Response spectrum corresponding to the scaled Tolomezzo earthquake.

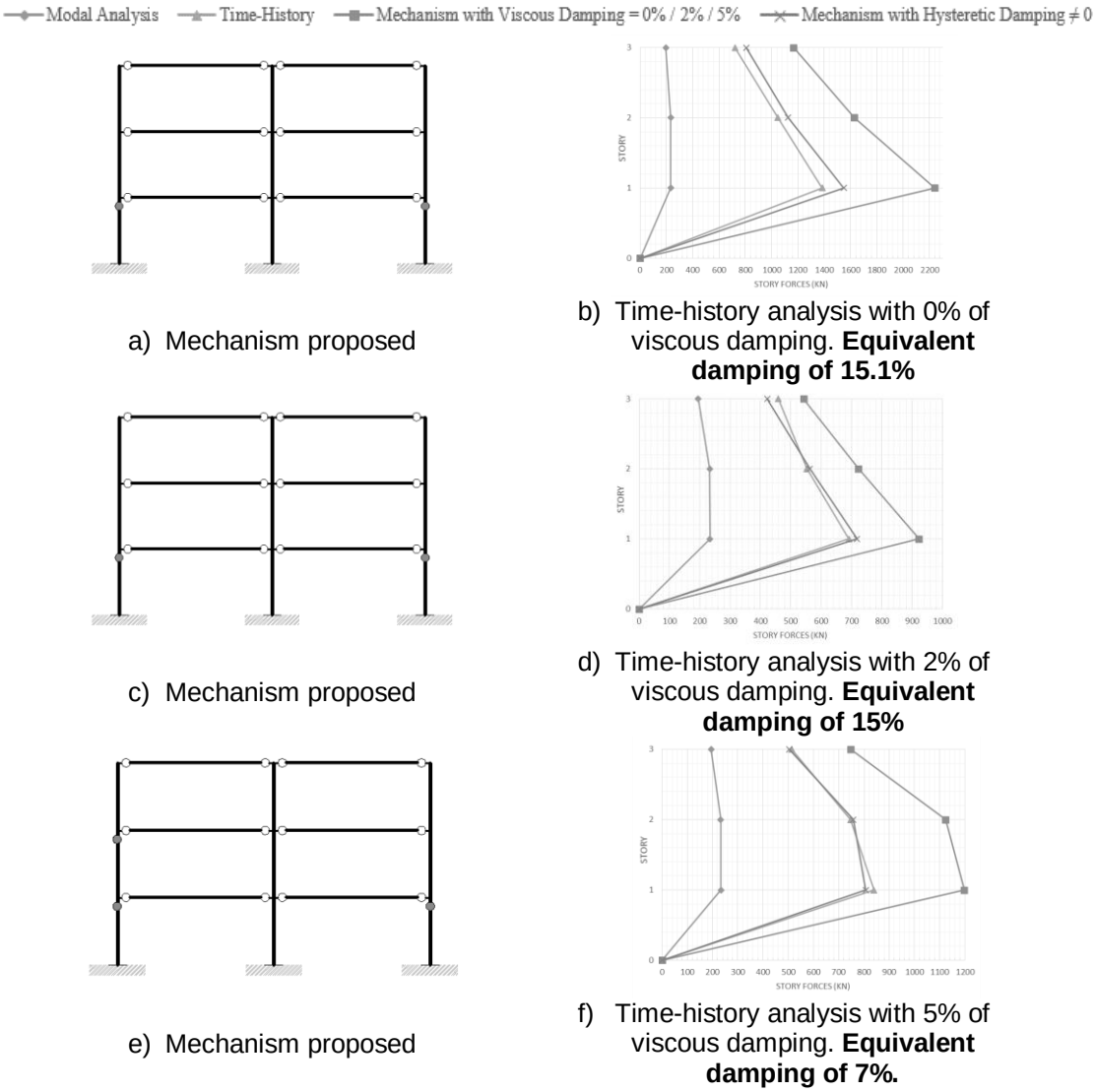

a) Mechanism proposed

b) Time-history analysis with 0% of viscous damping. **Equivalent damping of 15.1%**

c) Mechanism proposed

d) Time-history analysis with 2% of viscous damping. **Equivalent damping of 15%**

e) Mechanism proposed

f) Time-history analysis with 5% of viscous damping. **Equivalent damping of 7%.**

Figure 5.19. Comparison of modal analysis, non-linear time-history analysis and the DLA with and without equivalent damping for Model 2

The Figure 5.19 is summarized in the Table 5.2, where the conventional MDSA used for the design of the prototype is compared with the time – history analysis peak stories forces with the shown viscous Rayleigh damping, then, it is compared with the DLA method using a MDSA for the same viscous damping (ξ_v) values finding the same load pattern distribution. Finally, for these last result, a wide range

of equivalent damping (ξ_{eq}) values were proposed. The hysteretic rule used was a Takeda fat law. A damping correction factor (η) could be computed from an equivalent damping. Thus, a wide range of equivalent damping are proposed in order to find the best that fits with the peak stories forces from THNLA, as it is shown in Table 5.3.

Table 5.2. Comparison of the time – history analysis story forces [KN] with DLA with different viscous damping but with a hysteretic damping and with the modal analysis with the 5% of viscous damping

	Story	Modal ξ_v =5%	Time-History ξ_v =0%	DLA ξ_{eq} = 15%	DLA ξ_v =0%
	III	195	**722**	**825.2**	1167
Model 2	II	233	**1047**	**1151.2**	1628
	I	234	**1384**	**1583.9**	2240
	Story	Modal ξ_v =5%	Time-History ξ_v =2%	DLA ξ_{eq} = 15%	DLA ξ_v =2%
	III	195	**514**	**503.7**	747
Model 2	II	233	**747**	**757.3**	1123
	I	234	**839**	**807.2**	1197
	Story	Modal ξ_v =5%	Time-History ξ_v =5%	DLA ξ_{eq} = 7%	DLA ξ_v =5%
	III	195	**459**	**422.3**	542
Model 2	II	233	**553**	**562.9**	723
	I	234	**691**	**717.8**	922

Table 5.3. Reduction of load pattern [KN] for three story due to a wide range of equivalent damping values $\boldsymbol{\xi_{eq}}$ for a time-history analysis with 0% of viscous damping

$\boldsymbol{\xi_{eq}}$		0.05	0.100	0.130	**0.150**	0.170	0.190	0.210	0.230	0.250
$\boldsymbol{\eta}$		1	0.816	0.745	**0.707**	0.674	0.645	0.620	0.598	0.577
Story	**III**	1167.00	952.9	869.8	**825.2**	786.8	753.3	723.7	697.4	673.8
	II	1628.00	1329.3	1213.4	**1151.2**	1097.6	1050.9	1009.6	972.9	939.9
	I	2240.00	1829.0	1669.6	**1583.9**	1510.2	1445.9	1389.2	1338.7	1293.3

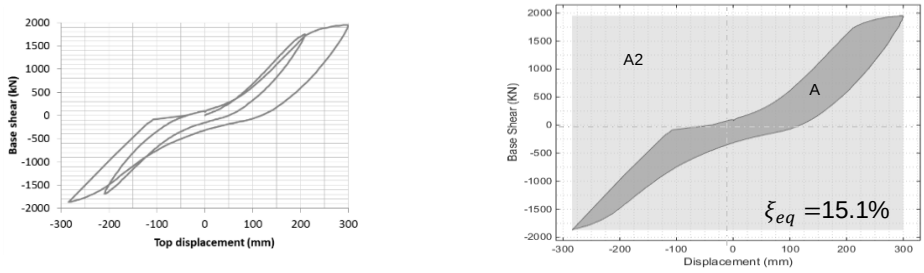

a. Complete cyclic response test b. Biggest loop for a cycle

Figure 5.20. Cyclic test for the full scale prototype for the model 2

Table 5.3, shows the responses for a wide range of equivalent damping, it can be seen that an equivalent damping corresponds to a good estimation of story forces distribution. However, for $\xi_v = 0\%$, a $\xi_{eq} = 21\%$ fits the story peak story forces from time-history analysis. Nevertheless, analyzing the cyclic test in Figure 5.20, the energy dissipate is, for an equivalent damping of 15%, despite this, the story forces for the DLA for $\xi_v = 0\%$ with 15% of equivalent damping is still a good accuracy compared for the peak forces of THNLA (Figure 5.19.b).

One of the reason of this different load pattern and higher forces is the effect of higher mode of vibration. Leading to a distribution of plastic hinge different than expected for the designed prototype. The scheme of local damage was correctly predicted with a blind prediction for many proposal of local damage, selecting the one that fit the load pattern from non-linear time-history, by using the method of the DLA. Hence, another indicator that 15% of equivalent damping is adequate is because of the maximum base shear in the cyclic analysis, in the Figure 5.20 is 1948 KN. Assuming that the second mode of vibration is predominat, one of the story forces should have opposite sign. In Table 5.3, for an equivalent damping of 15%, the 3rd story is considered negative (see Figure 5.21). This force distribution sums a base shear of 1909.9 KN. The assumption of a stories forces as a negative value can be perfectly adopted due to the modal combination where the SRSS method the sign is lost with the square exponent.

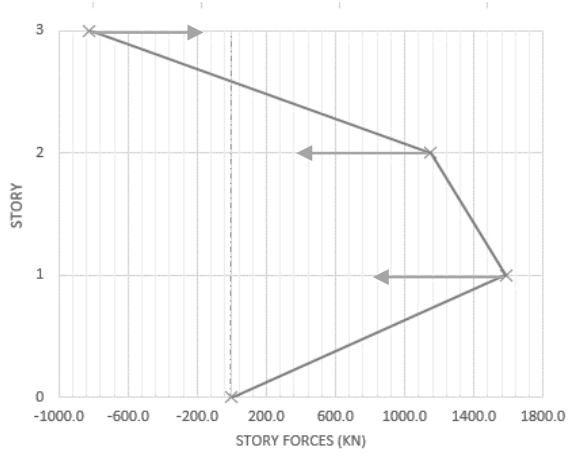

Figure 5.21. Floor forces with sign assumption for model 2. An equivalent damping of 15% for a mechanism with hinges at the top of first floor's column.

A visual inspection on the full scale prototype at the end of the test campaign was done by the referred authors. The aim is to give a general description of the damage in structural members. For instance, the cracking pattern has not been represented by following the exact pattern of each member, but patterns have been simplified in order to represent the common status of all similar members. Some damage are presented in Figure 5.22, in particular damage at the second story, where it was unexpected according to the original design.

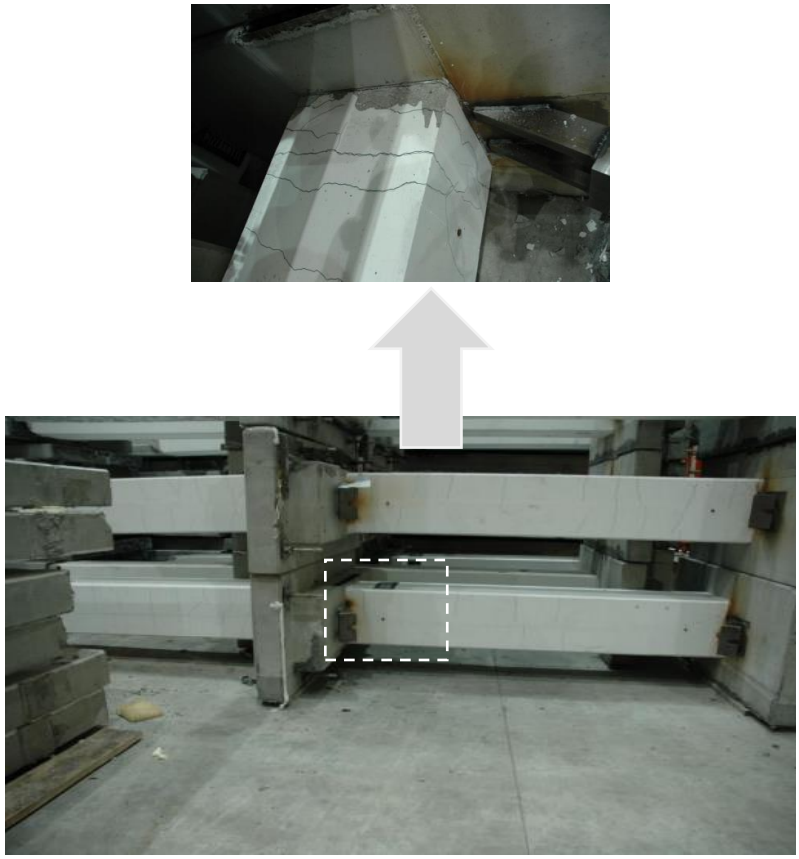

Figure 5.22. Column crack pattern
(Negro, et al., 2012)

5.3.3 Assessment of model 3 and 4 (monolithic prototype)

Similarly to model 2, a non-linear time-history analyses were made in order to look for the forces necessary in the actuators for the pseudo-dynamic test for the model 3 and 4. The model 4 is a monolithic structure as it is shown in Figure 5.23.c. The analysis is performed in the same manner as in the previous section, in order to find an equivalent damping that occurred in the time-history analysis for the real structure.

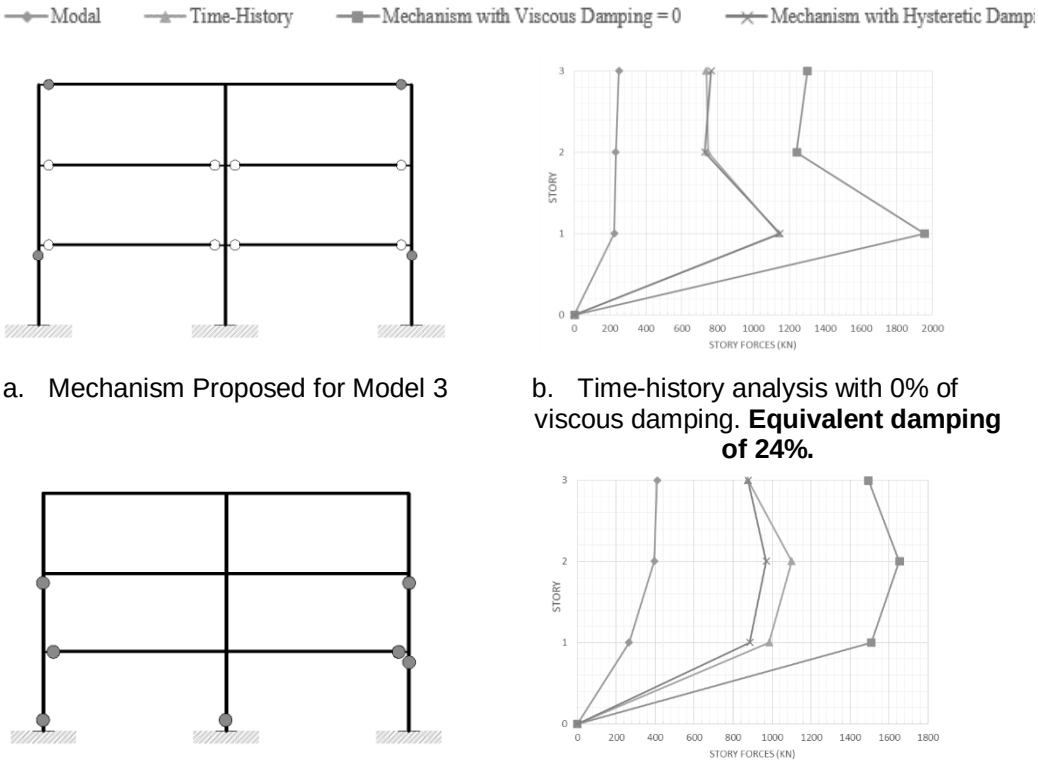

a. Mechanism Proposed for Model 3

b. Time-history analysis with 0% of viscous damping. **Equivalent damping of 24%.**

c. Mechanism Proposed for Model 4

d. Time-history analysis with 0% of viscous damping. **Equivalent damping of 24%**.

Figure 5.23. Comparison of the result with time-history analysis and the DLA for Model 3 y Model 4.

Table 5.4. Reduction of load pattern [KN] due to a wide range of equivalent damping values ξ_{eq} belonging to a time-history analysis with 0% of viscous damping for the Model 3

ξ_{eq}		0.05	0.10	0.13	0.16	0.19	0.21	**0.24**	0.27
η		1.000	0.816	0.745	0.690	0.645	0.620	**0.587**	0.559
Story	III	1301.40	1062.6	970.0	898.1	840.1	807.1	**764.2**	727.5
	II	1241.40	1013.6	925.3	856.6	801.3	769.9	**729.0**	694.0
	I	1956.50	1597.5	1458.3	1350.1	1262.9	1213.4	**1148.9**	1093.7

Table 5.5. Reduction of load pattern [KN] due to a wide range of equivalent damping values ξ_{eq} belonging to a time-history analysis with 0% of viscous damping for the Model 4

ξ_{eq}		0.05	0.10	0.13	0.16	0.19	0.21	**0.24**	0.27
η		1.000	0.816	0.745	0.690	0.645	0.620	**0.587**	0.559
Story	**III**	1493.50	1219.4	1113.2	1030.6	964.1	926.2	**877.0**	834.9
	II	1652.30	1349.1	1231.6	1140.2	1066.6	1024.7	**970.3**	923.7
	I	1507.80	1231.1	1123.8	1040.5	973.3	935.1	**885.4**	842.9

On the model 3 and 4, there were two different mechanism proposed for each case in order to find the same stories forces as in the non-linear time-history, respectively. A cycle test of the full-scale prototype for all configuration was done, as it is shown in Figure 5.20 and Figure 5.24; a visual inspection was performed (see Figure 5.22). The global damage, after all cycle test, is referenced in the Figure 5.25. This figure, helped to decide the best mechanism for the model 3 and 4, (see Figure 5.23.a and Figure 5.23.c).

For the cycle test of model 4, the biggest hysteretic loop correspond to an $\xi_{eq} = 24\%$. If this equivalent damping is used for the DLA, it fits very well in comparison with floor forces for the time-history analysis, as it is shown in Table 5.5. Moreover, an equivalent damping of 19% fit even better.

The proposal of damage with the method of the DLA is reasonably good, as it reproduced the local damages by experimental test.

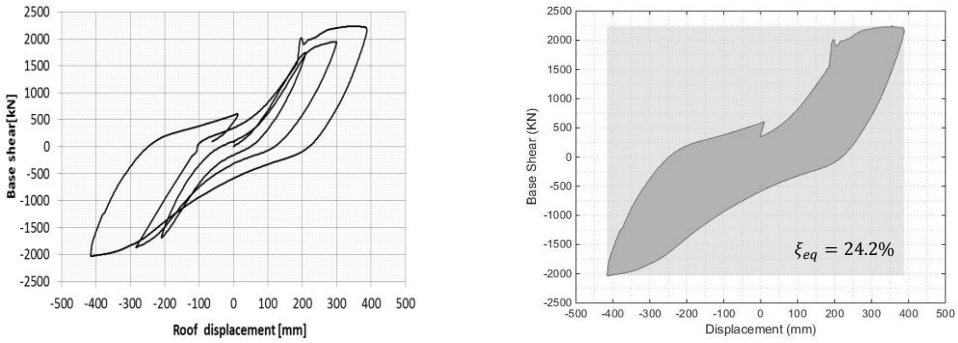

a) Complete cyclic response test b) Biggest loop for a cycle

Figure 5.24. Cyclic test for the full scale prototype for the model 4

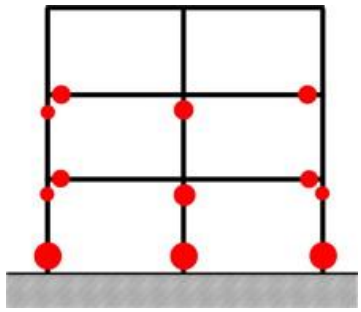

Figure 5.25. Typical damage and plastic hinging formation after the cyclic test

5.3.4 Discussion

In this section, it was studied the importance of the influence of higher modes effect on experimental test. The method of the DLA was used as an assessment method for a numerical example in literature, and for full – scale experimental test for a three story precast building. Others full – scale experimental test for concrete walls are presented in chapter 2. In Chapter 3, it was demonstrated that the higher modes gain importance when damage start to happen. The first occurrence of damage appear with the first mode of vibration as the predominant mass participation factor. Nevertheless, as it was explained, when damage occurs, the structures becomes more flexible, the importance of first mode of vibration decreases and higher vibration modes gain weight in mass participation factor.

The example of Luu, et al. (2014) presented in section 2.5.1 in chapter 2 is demonstrated similar conclusions (see Figure 3.9) as the DLA methodology exposed in chapter 3. In Figure 3.9, the result of the experimental test, and the elastic analysis using the reduction factor "*q*" for seismic force in order to account for inelastic behavior is compared. A conclusion is that load pattern shape should not be homotetically reduced along the height. As it was stated in previous sections, the load pattern changes along the damage process. This leads to different configuration of internal forces. In some cases, for mid height and tall buildings, similar values for bottom inelastic forces and elastic forces are observed, although, it might differ for other floors, as in work of Moehle (2015), (see Figure 5.4, Figure 5.6 and Figure 5.9). For this reason the base shear in many cases is bigger than expected when using a reduction factor, as in the case of the work of Biondini, et al. (2012). On the other hand, for 3D models and irregular structures it is a complex issue, as the deformed shape can change in different direction even different from vibration modes shapes, the phenomenon depends on the damage location, this will be discussed in Chapter 6.

Some different proposal exist in order to account for an approximation of the higher modes effects. Many full scale experimental test, especially for those medium rise building (more than 2-3 story), are made some proposal in other to consider this effect in concrete walls as in the work of Panagiotou (2008) and Panagiotou & Restrepo (2011). Other works highlighted the importance of making a proposal to consider higher modes effects in structural design phases as Luu, et al. (2014), Maniatakis et al. (2013), Ghorbani-renani (2010), Tremblay, et al. (2008), among many others.

CHAPTER 6

VALIDATION EXAMPLES

6.1 Introduction

In this chapter, five structure are designed with the DLA method in order to show the applicability of the approach to different performance objectives and types of irregularities. Each example is also used as a validation of the method as the performance of the designed cases. They are also assessed by means of both pushover (PO) and non-linear time-history analysis (NLTH) computed by the software SAP2000.

The first example consists on a simple regular 3-story building, while the irregularities and complexity is increased in the following cases. Finally, a 3D building showing torsional horizontal coupling is also investigated.

All structures were first pre-sized for gravity load and an estimating of seismic demand according to EC8 (2004). In all the examples the total gravitational load is accounting for the live and dead load, the 40% and 60% respectively. The mechanical properties of materials used are $f'_{ck} = 30$ MPa, modulus of elasticity $E_c = 30$ GPA. For Steel reinforcement properties, the yield stress $f_{yk} = 500$ MPa and modulus of elasticity $E_s = 200$ GPA. The seismic demand, considered for all cases, is the design spectrum from the EC8, with a PGA = 0.30g, type 1 and a type C soil. The hysteresis rule assumed is rectangular, i.e. with unloading equals to the elastic stiffness bilinear. The seismic input action used is the record accelerogram from L'Aquila earthquake (Figure 6.1.d) scaled to the design spectrum (Figure 6.1.b). The scaling method implemented is as it is proposed by (Bermudez, et al., 2012). In this type of scaling it is considered that all mode of vibration in the scaled response spectrum should be fit as best as possible. This assumption comes from the fact that, inelastic structures present important contribution of higher modes of vibration. The reason that the response spectrum from L'Aquila earthquake fits so well along all spectral acceleration, as it is shown in Figure 6.1.b., is the scaling process following along the ranges of frequencies in the response spectrum (Figure 6.1.c) filtered from the earthquake record (Figure 6.1.b). This methodology is developed in (Bermudez, et al., 2012).

The second validation procedure consists on comparing against an incremental non-linear static analysis (Pushover). It should be highlighted that the load pattern is taken as the one obtained in the DLA design. The pushover analysis is sensitive to load distribution of load along the height, highlight in many works as in Javadein & Taghinezhad (2007), Jingjiang, et al. (2003), Khoshnoudian, et al. (2011) among others. A similar concept as the DLA method regarding the load pattern is proposed by Antoiou & Pinho (2004), as the adaptive pushover; where, the load pattern is changing step by step by updating the damage stiffness. In this chapter, the load pattern used is the maximum load corresponding to the level of damage proposed in the design according to the performance objective.

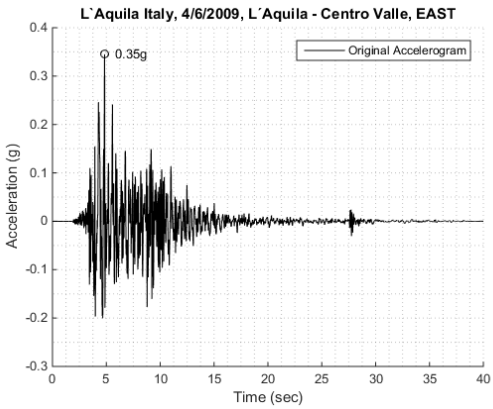

a. Original Accelerogram

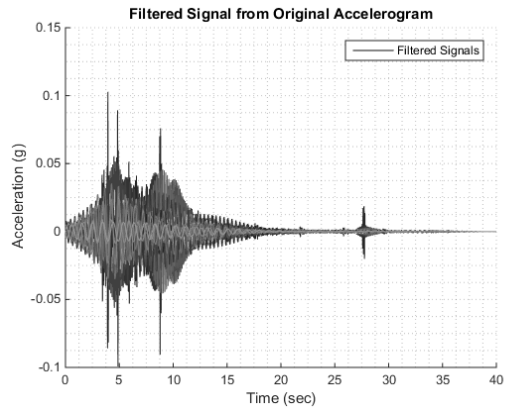

b. Filtered signals

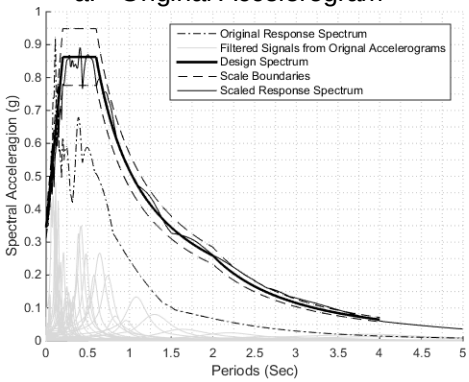

c. Scaled response spectrum

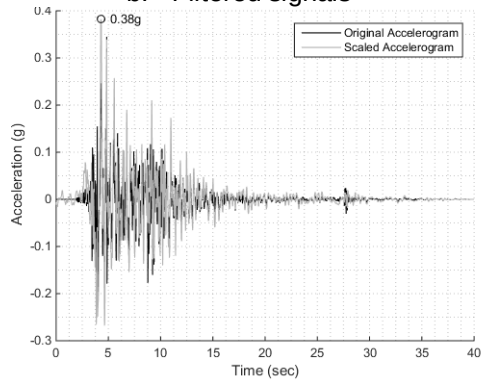

d. Scaled accelerogram

Figure 6.1. L'Aquila earthquake record scaled to design spectrum from (Eurocode-8, 2004)

6.2 3-Storey regular building [Example 1]

This first example shows a regular low-rise 3-storey building. The aim, is to show the accuracy of the method and the information that could be achieved using the DLA method. The structure is subjected to a gravity load of 56 KN/m. In this case, the α factor is taken as 0.5. This value is selected by fixing a maximum rotation in all hinges at 1.5e-2 rad, as it is shown in Figure 6.4.b. This corresponds to the case of limiting the maximum local damage to reproduce cracking and small residual deformation. At the same time, trying to keep an inelastic displacement slightly higher than elastic. On the other hand, the distribution of hinges were located in all end-beams. The intention is to meet the weak beam – strong columns criterion. That assumption highlights the effect of higher modes. In Figure 6.4.a, it is shown the evolution of the absolute maximum lateral story forces obtained by the DLA compared with the typically used in conventional design process, which is reduced by a behavior factor ("q" or "R"). The geometry of the structure is detailed in Table 6.1. Modal properties for elastic and auxiliary structures are shown in Table 6.2.

Table 6.1. Geometry of elements sections of elastic (E) and auxiliary structure (A)

Element		Edge	Story	Width [mm]	Height [mm]	Length [mm]
Column	C1	A - B	1-3	400	400	3500
Beam	V1	A - B	1-3	400	600	8000

Table 6.2. Modal properties of elastic (E) and auxiliary structure (A)

Mode	Period [sec.]		Mass participation factor [%]	
	(E)	(A)	(E)	(A)
1	0.672	2.584	87.00	72.49
2	0.215	0.398	10.52	21.67
3	0.129	0.148	02.47	05.83

This first example aims to show the accuracy of the method and, the amount of information obtained latter analyze of both structures (elastic and auxiliary), by superposing final behavior of both structures. Several figures can be constructed to support the decision of selecting the value of α factor; such as, the evolution of all internal forces, base shear, plastic rotation demand, hysteretic energy

dissipation, equivalent damping, sectional ductility demand, and evolution of the damping correction factor (see Figure 6.2 to Figure 6.5 and Figure 6.8).

In this example, two considerations are taken as starting point for the structural design with the DAL method. The first, the criterion of strong column – weak beam has to be reached; therefore, the distribution of hinges were placed in all beam ends. Secondly, the damage in those hinges need to be controlled. For that reason, with the evolution of rotation on hinges (Figure 6.4.b), the value α could be select as equal to 0.5. For this value, it was observed (Figure 6.4) that the maximum plastic rotation as 1.5e-2 rad. Finally, the fact that, damage is allowed, higher vibration modes gain importance. Figure 6.3.a shows the evolution of maximum absolute floor-forces, it can be noticed how evolves from the elastic shape. One can notice different magnitude in the story forces than the obtained by applying the force reduction factor (q) uniformly.

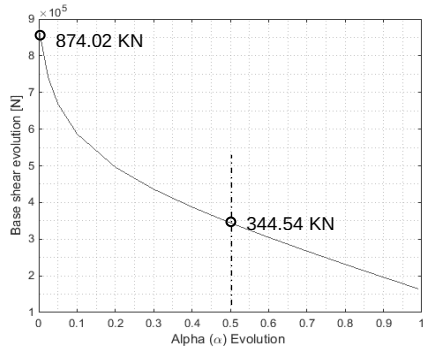

Figure 6.2. Base shear evolution for a wide range of α factor.

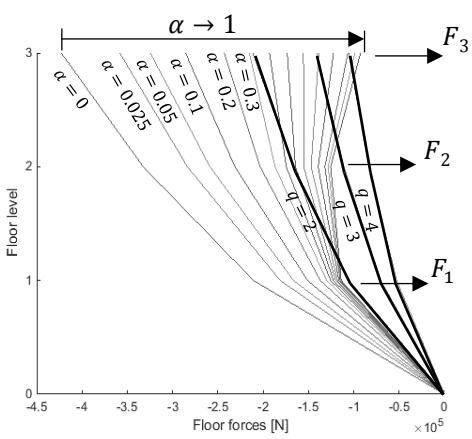

a. Load pattern evolution with damage

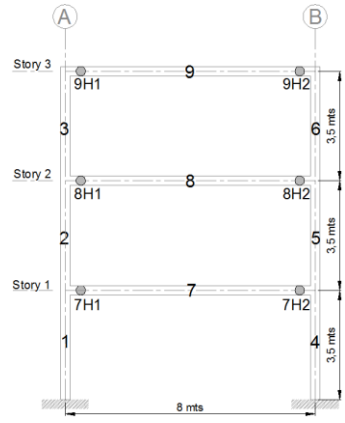

b. Structure with hinges configuration

Figure 6.3. Hinges configuration and load pattern evolution for a wide range of α factor

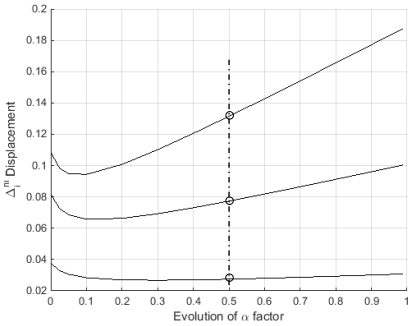

a. Displacement evolution

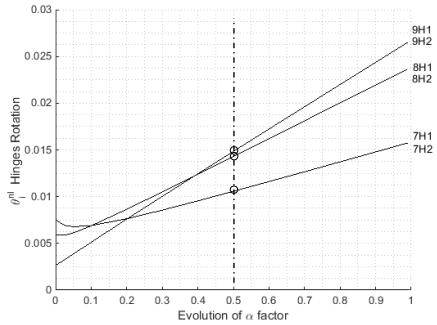

b. Rotation evolution

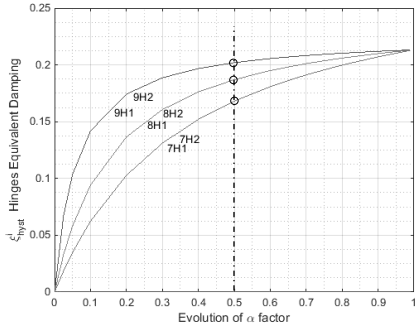

c. Hysteretic damping evolution by hinge

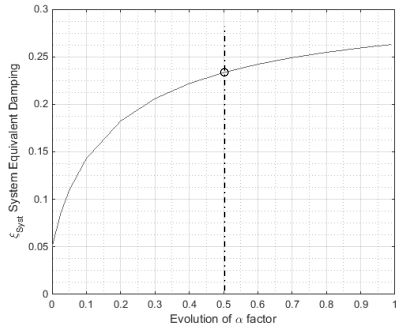

d. Equivalent damping evolution

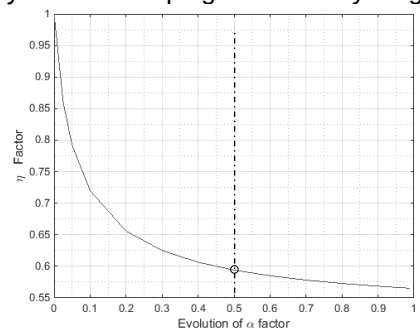

e. Damping correction factor evolution

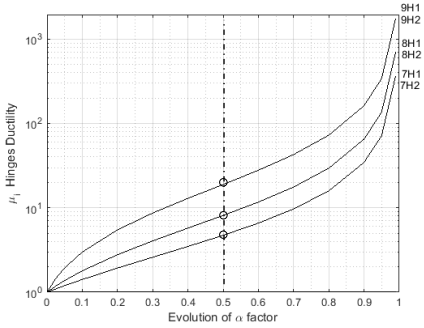

f. Ductility rotation evolution

Figure 6.4. Analysis with the DLA. Combination for a wide range of alpha factor

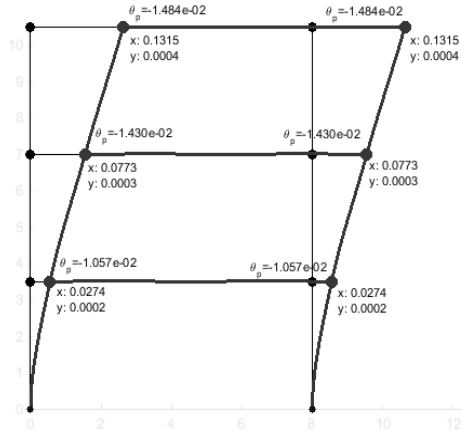

a. Maximum displacement

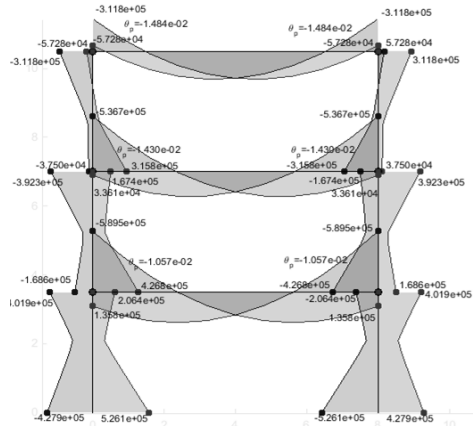

b. Maximum bending moment

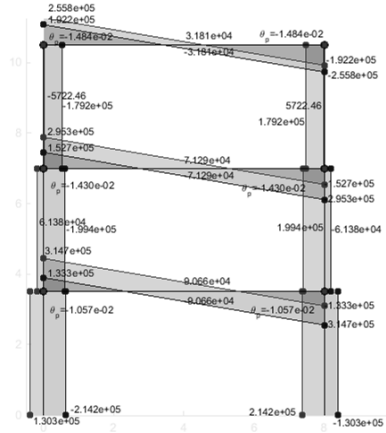

c. Maximum shear forces

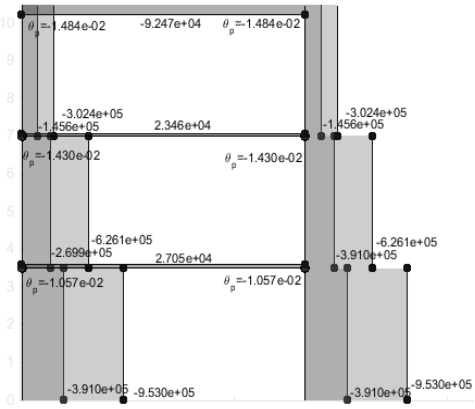

d. Maximum axial forces

Figure 6.5 Representation of maximum internal forces after combination with DLA method

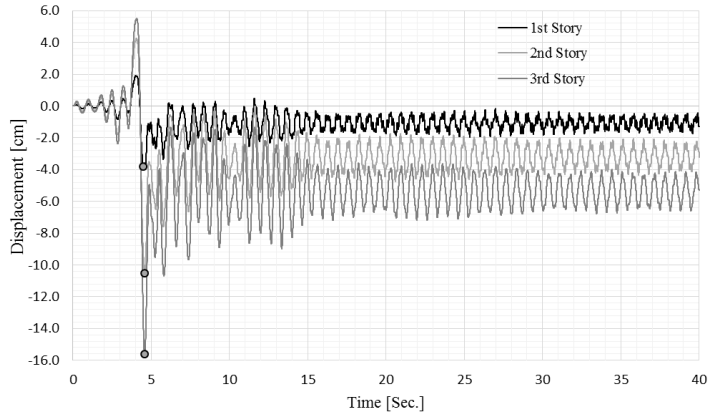

Figure 6.6. Non – linear time – history of displacements floors

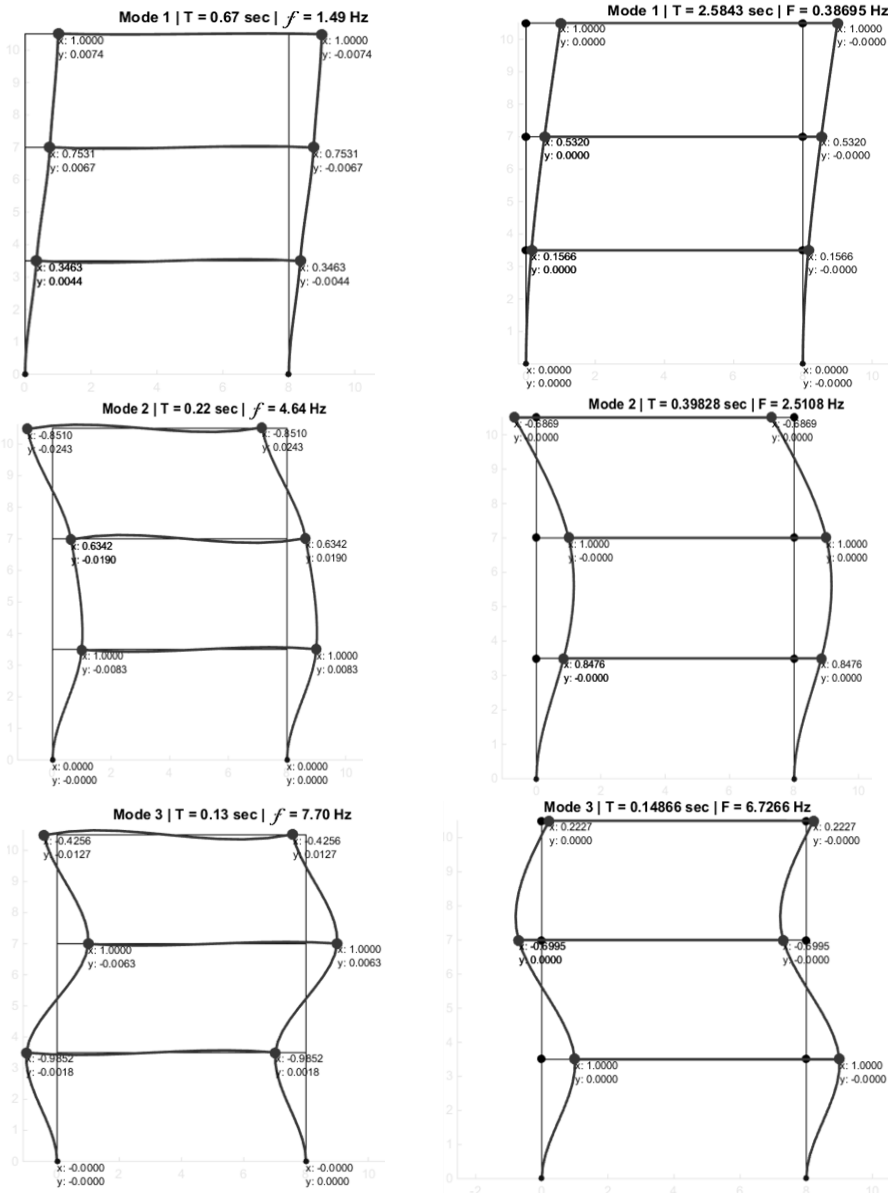

a. Elastic structure b. Auxiliary structure

Figure 6.7. Comparison of vibration modes of elastic and auxiliary structure

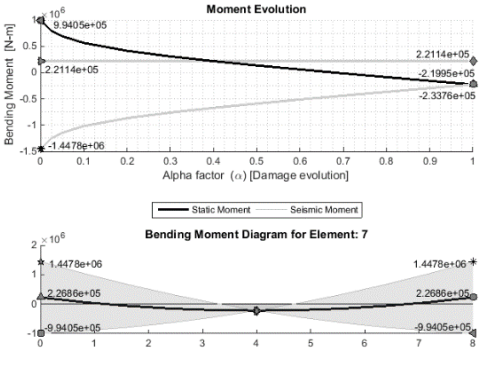

a. Element 7

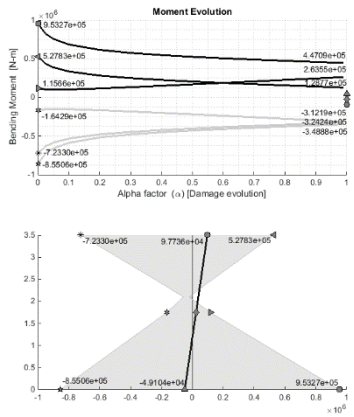

b. Element 1

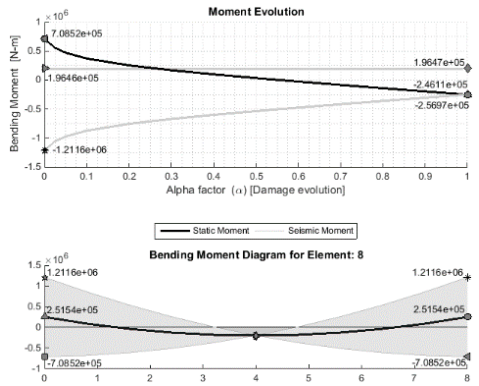

c. Element 8

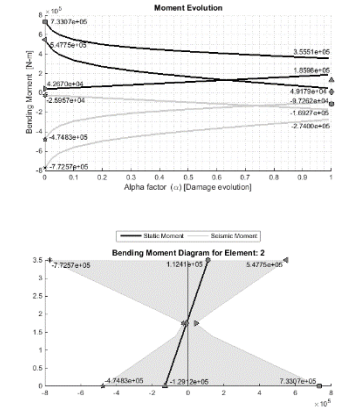

d. Element 2

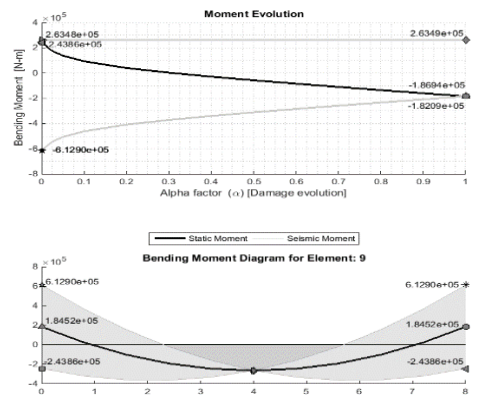

e. Element 9

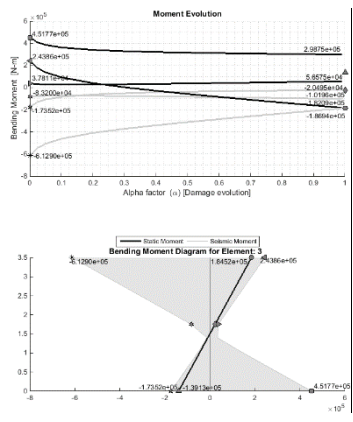

f. Element 3

Figure 6.8. Evolution of seismic bending moment compared with static moment

Table 6.3. Maximum displacement [cm] for non-linear time – history analysis (NLTH) and non-linear static analysis (PO), compared with the prediction using the DLA design

Story	1st	2nd	3rd
PO	4.21	9.62	13.20
NLTH	3.82	10.53	15.63
DLA	2.74	7.73	13.15

Table 6.4. Ductility demand (θ_d) [rad] from non-linear time–history analysis (NLTH) and non-linear static analysis (PO), compared to the DLA design

Hinge ID	7H1	7H2	8H1	8H2	9H1	9H2
PO	1.250e-2	1.140e-2	1.150e-2	9.764e-3	-	8.424e-3
NLTH	1.080e-2	1.310e-2	1.340e-2	**1.760e-2**	1.460e-2	9.138e-3
DLA	1.057e-2	1.057e-2	1.430e-2	1.430e-2	1.484e-2	1.484e-2
Hinge ID	1H1	2H1	3H1	4H1	5H1	6H1
PO	3.052e-3	-	-	4.603e-3	-	-
NLTH	3.428e-3	4.254e-3	-	1.855e-3	-	-
DLA	-	-	-	-	-	-

Table 6.5. Maximum bending moment [KN/m] in plastic hinge for non-linear time – history analysis (NLTH) and non-linear static analysis (PO), compared with the prediction using the DLA design

Hinge ID	7H1	7H2	8H1	8H2	9H1	9H2
PO	125.70	593.90	21.69	537.63	195.62	288.49
NLTH	596.77	594.38	529.69	537.63	314.88	309.55
DLA	589.50	589.50	536.70	536.70	311.80	311.80
Hinge ID	1H1	2H1	3H1	4H1	5H1	6H1
PO	526.76	56.21	100.82	527.08	380.25	119.96
NLTH	526.84	427.54	365.26	526.51	365.26	312.01
DLA	526.10	426.80	375.01	526.10	426.80	375.01

Table 6.3 to Table 6.7 compare the internal forces obtained from the NLTH, PO and the predicted with the DLA method. Figure 6.9 and Figure 6.10 demonstrate the good approximation on base shear resulting the NLTH and PO compared to the DLA design. On other hand, columns were designed to remain elastic; although, in the NLTH and PO analysis show small rotations on columns (Table 6.4). However, these plastic rotation may be considered as minor damage. Furthermore, as the PO and NLTH analyses show (Figure 6.10) that the DLA methodology is capable to capture the effect of higher vibration mode, simulating, in that manner, an adaptive pushover, but for design cases.

Table 6.6. Maximum shear forces [KN] in plastic hinge for non-linear time – history analysis (NLTH) and non-linear static analysis (PO), compared with the DLA design

Hinge ID	**7H1**	**7H2**	**8H1**	**8H2**	**9H1**	**9H2**
PO	131.01	316.98	151.25	296.74	162.25	285.75
NLTH	315.74	315.69	296.23	268.22	312.96	278.15
DLA	314.70	314.70	295.30	295.30	255.80	255.80
Hinge ID	**1H1**	**2H1**	**3H1**	**4H1**	**5H1**	**6H1**
PO	170.35	51.06	23.69	218.56	234.44	122.91
NLTH	256.02	247.10	153.48	240.71	238.39	167.85
DLA	214.20	199.40	179.20	214.20	199.40	179.20

Table 6.7. Maximum axial forces [KN] in plastic hinge for non-linear time – history analysis (NLTH) and non-linear static analysis (PO), compared with the DLA design

Hinge ID	**7H1**	**7H2**	**8H1**	**8H2**	**9H1**	**9H2**
PO	67.58	67.58	42.85	42.85	49.68	49.68
NLTH	77.41	77.41	72.17	72.17	93.51	93.51
DLA	27.05	27.05	23.46	23.46	92.47	92.47
Hinge ID	**1H1**	**2H1**	**3H1**	**4H1**	**5H1**	**6H1**
PO	444.52	313.50	162.25	899.47	532.49	285.74
NLTH	928.03	616.99	317.89	927.37	613.73	303.13
DLA	953.00	626.10	302.40	953.00	626.10	302.40

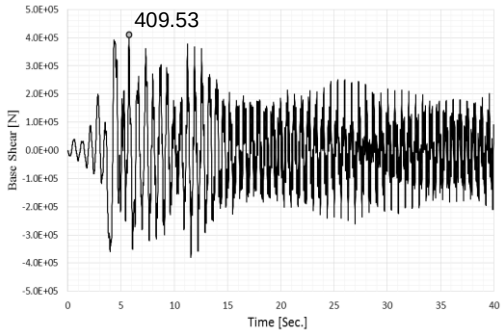

Figure 6.9. Non – linear time – history of the base shear

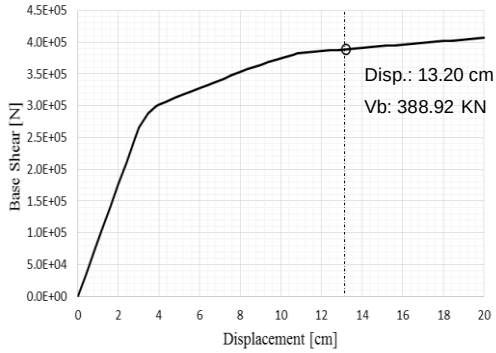

Figure 6.10. Non-linear incremental static (Pushover) curve

6.3 2-Storey irregular building [Example 2]

The example 2 consists on an irregular 2-storey building subjected to a gravity load of 61.25 KN/m together with the seismic action. Two different configuration of hinges are considered in order to evaluate capacity of the DLA for different performance objectives. The first, is the capability to select hinges where redistribution of internal force wants to occur. In this case, hinges were located in elements 9 and 12 in order to redistribute bending moment. The aim of this example is to obtain similar internal forces from central beams negative bending moment from beams sides. According to this criteria the selected α was taken as equal to 0.30.

The second case, the performance objectives was not to exceed a plastic rotation of 1.5e-2 rad in the irregular structure. The geometry of the structure is detailed in Table 6.8 and sketched in Figure 6.11 modal properties for elastic and auxiliary cases are shown in Table 6.9.

Table 6.8. Geometry of elements sections of elastic (E) and auxiliary structure (A)

Element		Edge	Story	Width [mm]	Height [mm]	Length [mm]
Column	C1	A-B-C-D	1-2	400	400	3500
Beam	V1	A to B	1-2	350	500	3000
Beam	V1	B to C	1-2	350	500	6000
Beam	V1	C to D	1-2	350	500	2000

Table 6.9. Modal properties of elastic (E) and auxiliary structure case 1 (A1) and case 2 (A2)

Mode	Period [sec.]			Mass participation factor [%]		
	(E)	(A1)	(A2)	(E)	(A1)	(A2)
1	0.351	0.466	1.037	87.76	89.13	75.58
2	0.138	0.142	0.187	12.22	10.86	24.41
3	0.042	0.043	0.043	5.7e-4	1.4e-3	1.1e-19
4	0.037	0.037	0.037	6.9e-3	2e-4	1.8e-17

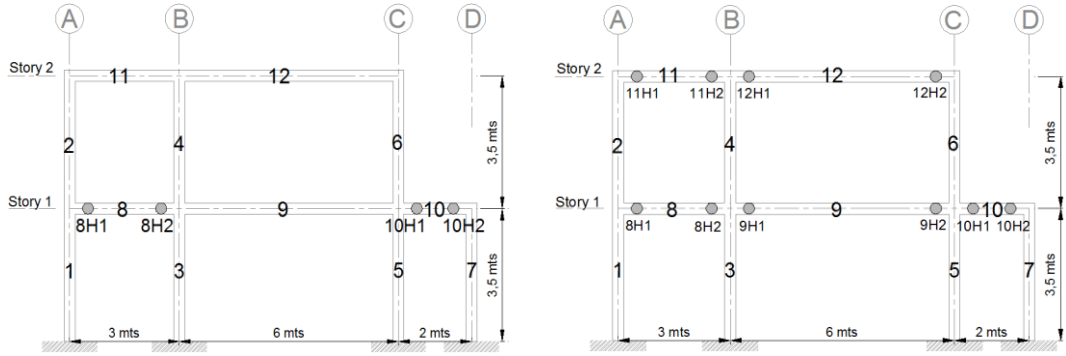

a. Case 1 – bending moment redistribution b. Case 2 – All beams yielded

Figure 6.11. Structure layout for both cases

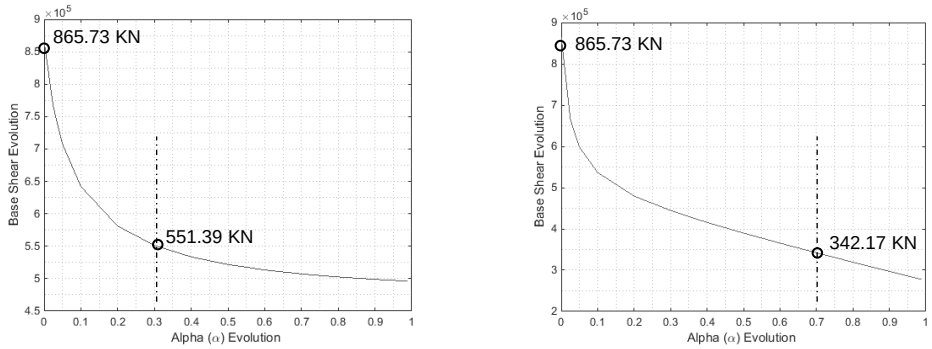

a. Base shear evolution [Case 1] b. Base shear evolution [Case 2]

Figure 6.12. Base shear evolution for a wide range of α factor.

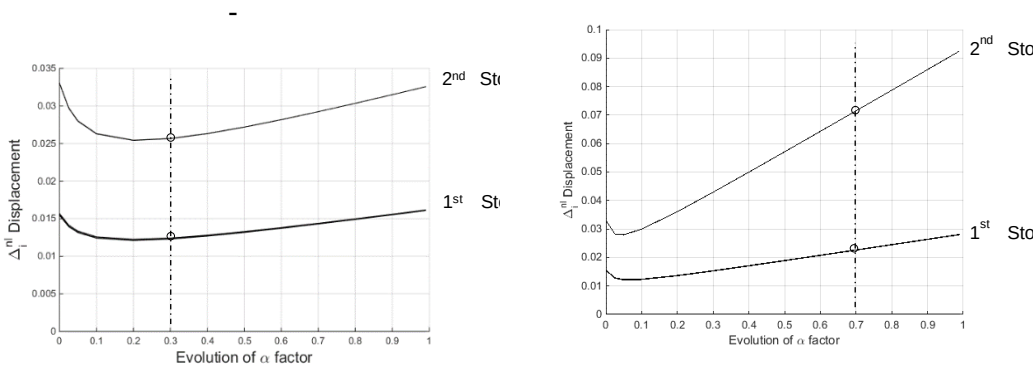

a. Displacement evolution [Case 1] b. Displacement evolution [Case 2]

Figure 6.13. Base shear evolution for a wide range of α factor.

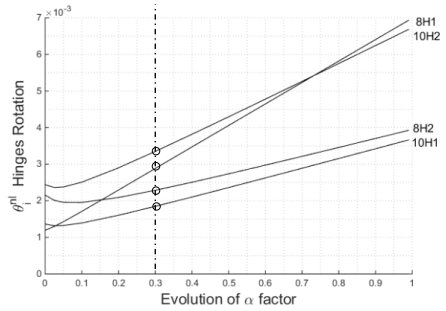

a. Rotation evolution [Case 1]

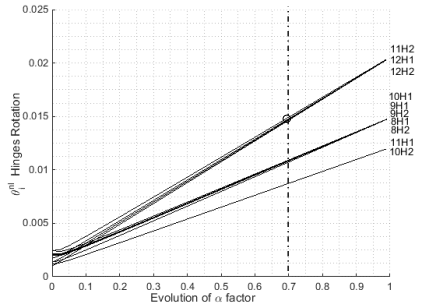

b. Rotation evolution [Case 2]

Figure 6.14. Rotation evolution for a wide range of α factor.

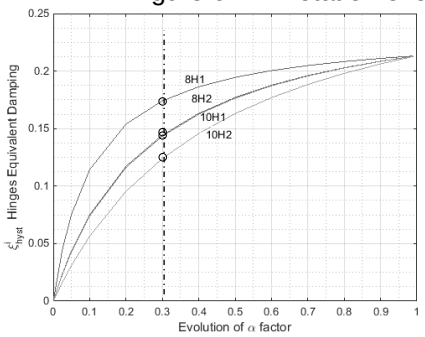

a. Hysteretic damping evolution [Case 1]

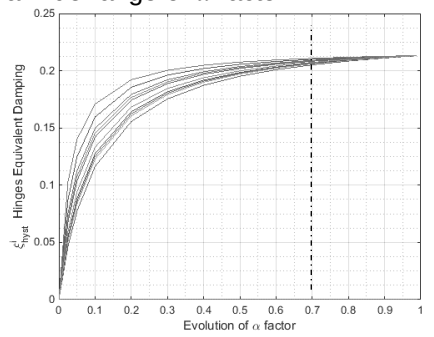

b. Hysteretic damping evolution [Case 2]

Figure 6.15. Hysteretic damping evolution in hinges

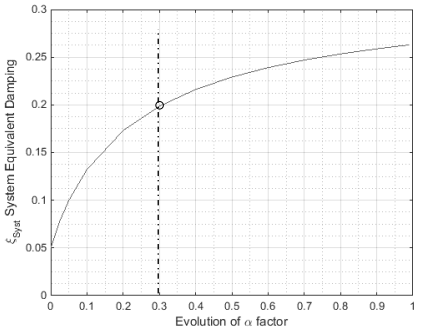

a. Hysteretic damping evolution [Case 1]

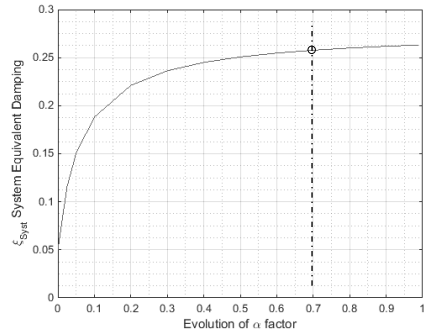

b. Hysteretic damping evolution [Case 2]

Figure 6.16. Equivalent damping in structures

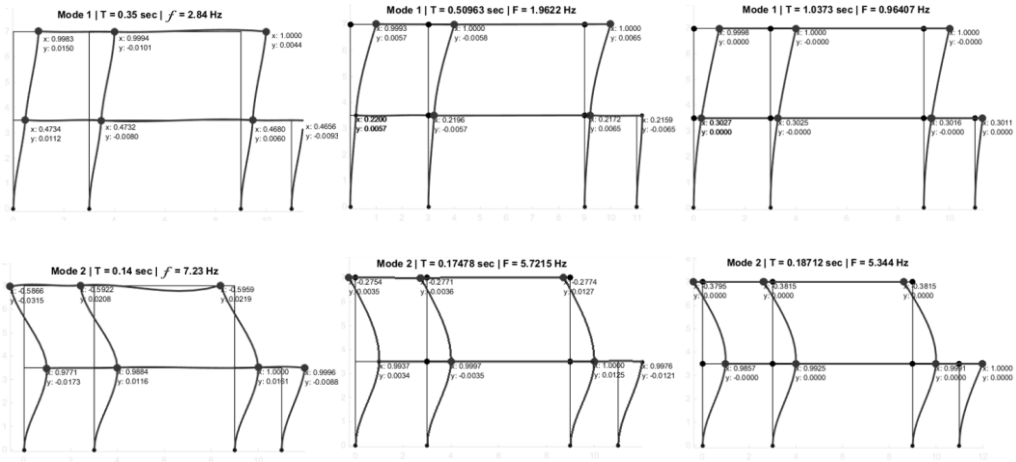

a. Elastic structure b. Auxiliary structure Case 1 c. Auxiliary structure Case 2

Figure 6.17. Comparison of vibration modes of elastic and auxiliary structure

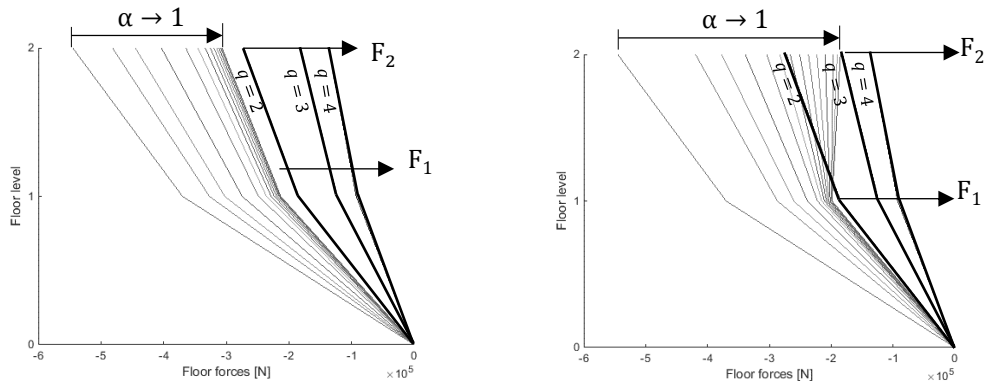

a. Maximum story forces evolution [Case 1] b. Maximum story forces evolution [Case 2]

Figure 6.18. Evolution of maximum story forces

Table 6.10. Maximum displacement [cm] for NLTH and PO, compared with DLA [Case 1]

Story	1st	2nd
PO	1.24	2.52
NLTH	1.90	3.79
DLA	1.24	2.57

Table 6.11. Ductility demand (θ_d) [rad] from NLTH and PO compared to the DLA design [Case 1]

Hinge ID	**8H1**	**8H2**	**9H1**	**9H2**	**10H1**	**10H2**
PO	2.28e-3	1.33e-3	-	-	1.08e-3	2.31e-3
NLTH	**3.71e-3**	**1.72e-3**	1.55e-3	2.58e-3	**3.67e-3**	**2.52e-3**
DLA	**3.35e-3**	**2.28e-3**	-	-	**1.84e-3**	**2.88e-3**
Hinge ID	**11H1**	**11H2**	**12H1**	**12H2**	**1H1**	**2H1**
PO	-	-	-	-	-	-
NLTH	2.08e-3	2.28e-3	2.05e-3	3.27e-3	2.14e-3	2.98e-3
DLA	-	-	-	-	-	-
Hinge ID	**3H1**	**4H1**	**5H1**	**6H1**	**7H1**	
PO	-	-	-	6.24e-4	-	
NLTH	1.97e-3	5.98e-4	1.23e-3	2.08e-3	1.75e-3	
DLA	-	-	-	-	-	

Table 6.12. Maximum bending moment [KN/m] in plastic hinge for NLTH and PO, compared with the prediction using the DLA design [Case 1]

Hinge ID	**8H1**	**8H2**	**9H1**	**9H2**	**10H1**	**10H2**
PO	208.69	287.22	65.58	372.67	130.21	179.54
NLTH	264.66	287.79	403.92	378.19	266.31	179.99
DLA	266.7	290.5	410.7	401.0	268.5	180.1
Hinge ID	**11H1**	**11H2**	**12H1**	**12H2**	**1H1**	**2H1**
PO	171.20	259.52	48.316	273.80	254.19	88.00
NLTH	217.01	264.5	311.86	287.19	264.97	121.70
DLA	218.61	267.3	315.1	294.2	264.6	148.6
Hinge ID	**3H1**	**4H1**	**5H1**	**6H1**	**7H1**	
PO	291.69	162.84	327.77	235.21	283.67	
NLTH	322.08	319.78	328.81	232.14	283.07	
DLA	321.80	253.10	326.60	263.80	282.80	

The first case, two the beam's end are hinged, the factor α selected is 0.3. Note that, the reduction of the magnitude of forces is larger due to redistribution than energy dissipation. Table 6.11 and Figure 6.20.a shows the PO curve for which the structure presents limited yielding deformation. Moreover, Figure 6.18.a shows that, for those low quantity of active hinges and small rotations, higher vibration modes are negligible. This previous mentioned phenomenon differs from the second case (Figure 6.18.b) where all beams are hinged and present considerable damage.

Table 6.13. Maximum displacement [cm] for NLTH and PO, compared with the DLA design [Case 2]

Story	1st	2nd
PO	2.64	7.12
NLTH	2.19	6.87
DLA	2.27	7.15

Table 6.14. Ductility demand (θ_d) [rad] from NLTH and PO compared to DLA [Case 2]

Hinge ID	8H1	8H2	9H1	9H2	10H1	10H2
PO	1.080e-2	1.040e-2	8.277e-3	1.150e-2	1.080e-2	9.783e-3
NLTH	1.010e-2	1.040e-2	1.130e-2	7.263e-3	9.402e-3	8.382e-3
DLA	1.092e-2	1.087e-2	1.086e-2	1.083e-2	1.073e-2	8.738e-3
Hinge ID	**11H1**	**11H2**	**12H1**	**12H2**	**1H1**	**2H1**
PO	1.300e-2	1.111e-2	8.650e-3	1.390e-2	1.45e-3	
NLTH	1.410e-2	1.190e-2	1.280e-2	1.270e-2	-	-
DLA	1.470e-2	1.465e-2	1.477e-2	1.493e-2	-	-
Hinge ID	**3H1**	**4H1**	**5H1**	**6H1**	**7H1**	
PO	-	-	-	-	-	
NLTH	-	-	-	-	-	
DLA	-	-	-	-	-	

Table 6.15. Maximum bending moment [KN/m] in plastic hinge for NLTH and PO, compared with the prediction using the DLA design [Case 2]

Hinge ID	8H1	8H2	9H1	9H2	10H1	10H2
PO	61.11	161.75	8.77	209.76	1.45	73.64
NLTH	122.50	161.84	209.36	210.54	146.66	74.24
DLA	121.1	161.8	208.6	208.6	143.8	73.40
Hinge ID	**11H1**	**11H2**	**12H1**	**12H2**	**1H1**	**2H1**
PO	28.44	148.90	9.35	153.25	315.55	101.73
NLTH	73.28	148.96	215.86	154.07	308.51	202.73
DLA	72.01	148.88	215.8	152.40	316.9	216.9
Hinge ID	**3H1**	**4H1**	**5H1**	**6H1**	**7H1**	
PO	331.51	174.60	331.83	212.40	389.19	
NLTH	316.20	279.88	320.22	188.73	371.67	
DLA	331.32	274.82	331.62	275.30	390.20	

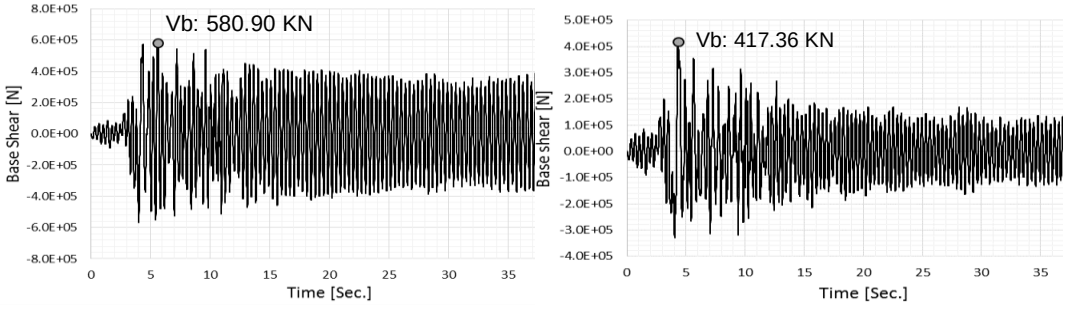

a. Case 1 b. Case 2

Figure 6.19. Non – linear time – history of base shear

The second case, the criterion of strong column – weak beam is met while considerable damage is allowed on the beams. As the PO curve shows (Figure 6.20.b), the structure exhibits important yielding. In spite of extensive damage, the method succeeded in avoiding yielding of the columns (Table 6.14)

In both design cases the capability of the method to account for inelastic behavior is demonstrated. Internal forces and base shear on NLTH and PO result are compared and a good approximation is achieved by the DLA design method.

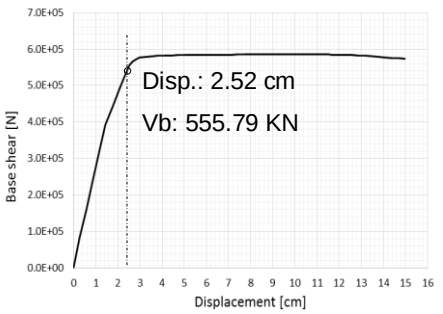

a. Base shear vs top floor displacement [case 1]

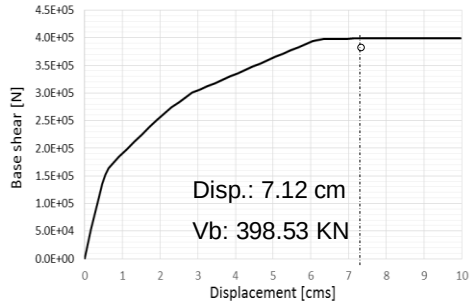

b. Base shear vs top floor displacement [case 2]

Figure 6.20. Non-linear incremental static (Pushover) curve

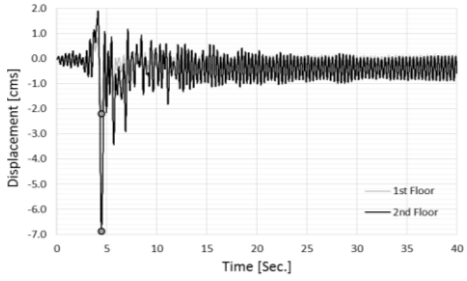

a. Case 1

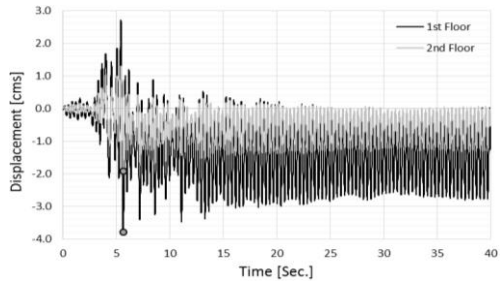

b. Case 2

Figure 6.21. Non – linear time – history of displacement

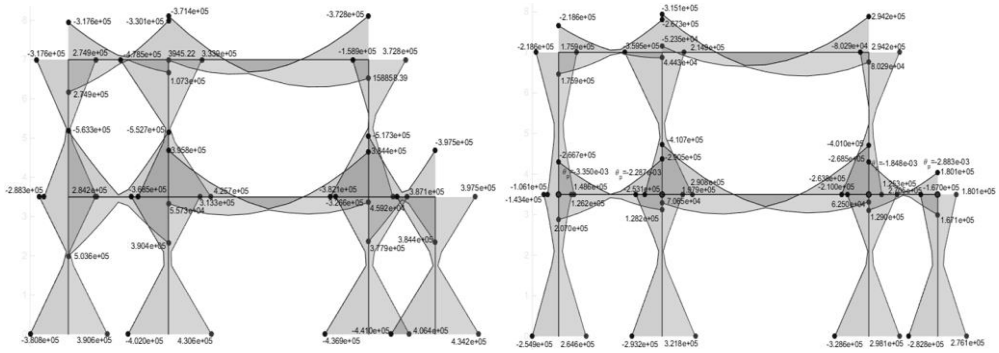

a. Elastic maximum bending moment b. Case 1 – Inelastic maximum bending moment

Figure 6.22. Comparison of bending moment diagrams for the elastic and Inelastic structures in case 1

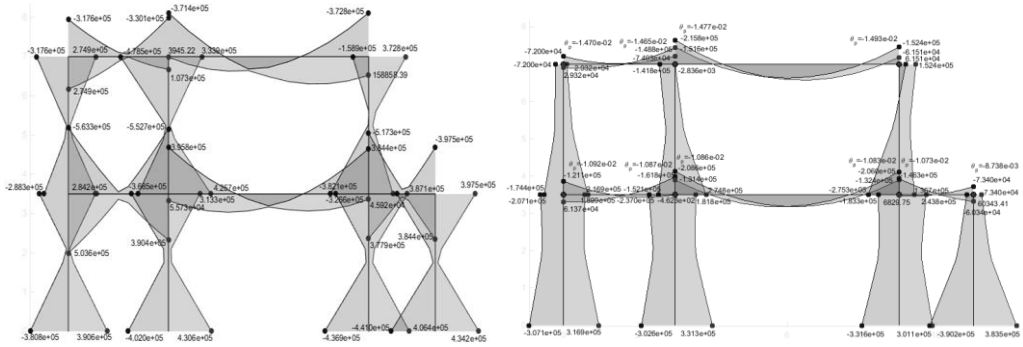

c. Elastic maximum bending moment d. Case 2 – Inelastic maximum bending moment

Figure 6.23. Comparison of bending moment diagrams for the elastic and Inelastic structures in case 2

6.4 7–Storey irregular building [Example 3]

This example consists on an irregular 7-storey building subjected to a gravity load of 61.25 KN/m together with the seismic action. The structural layout and height of this example are chosen in order to evaluate the importance of higher vibration modes and the design method accuracy for irregular structures. The geometry of the structure is detailed in Table 6.16. Modal properties are shown in Table 6.17.

The plastic mechanism proposed is that all beams are damaged, in order to have an approximation of the criterion of "strong column – weak beam". Columns are designed to remain elastic. In Figure 6.24.c to Figure 6.24.f, there are some of the parameter to take in to account for the selection of the damage factor (α) are shown. In this case α is taken as 0.5. The selection of the damage factor value, was selected on the analysis of the floor displacement evolution according to the DLA. The top displacement for this cases is similar to the elastic ones, while the base shear is reduced from 2584KN to 1254 KN. This is possible because of the variation of the evolution of period and the increment of participation factor of vibration mode 2 and 3.

Table 6.16. Geometry of elements sections of elastic (E) and auxiliary structure (A)

Element		Edge	Story	Width [mm]	Height [mm]	Length [mm]
Column	C1	A-B-C-D	5-7	600	600	3500
Column	C2	A-B-C	1-4	800	800	3500
Column	C3	D	1-4	500	500	3500
Beam	V1	-	1-7	350	500	7000

Table 6.17. Modal properties of elastic (E) and auxiliary structure (A)

Mode	Periods [sec.]		Mass participation factor [%]	
	(E)	(A)	(E)	(A)
1	1.11	3.15	71.94	59.73
2	0.39	0.72	12.83	20.03
3	0.19	0.27	6.38	9.72
4	0.13	0.15	3.37	4.22

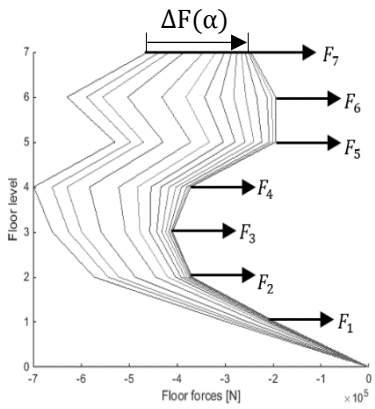

a. Maximum absolute floor – forces evolution with the mechanism proposed

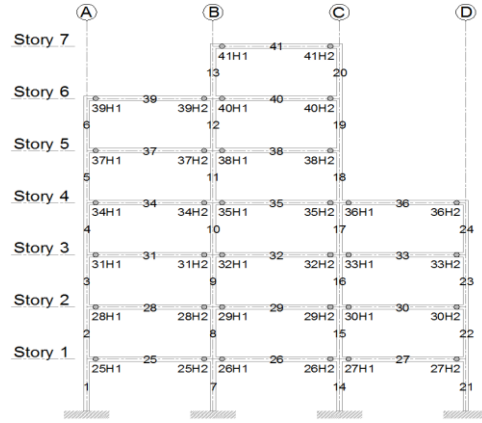

b. Mechanism proposed, all beams hinged

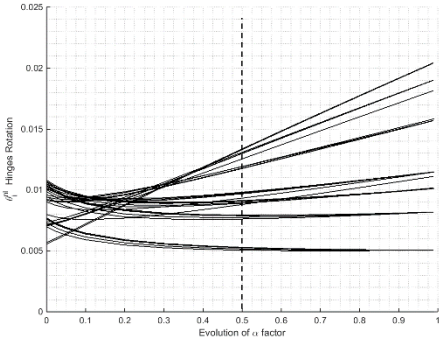

c. All hinges plastic rotation evolution

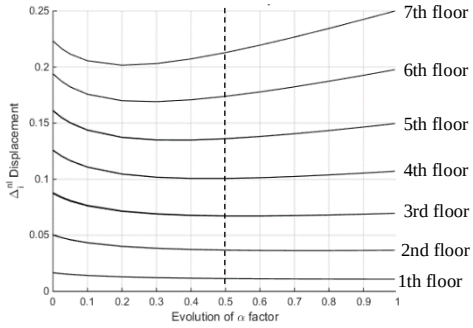

d. Maximum absolute Floor – displacement evolution

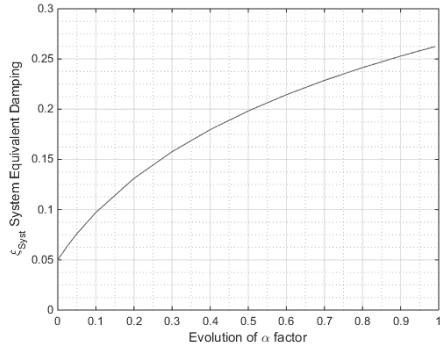

e. Structure Equivalent damping evolution

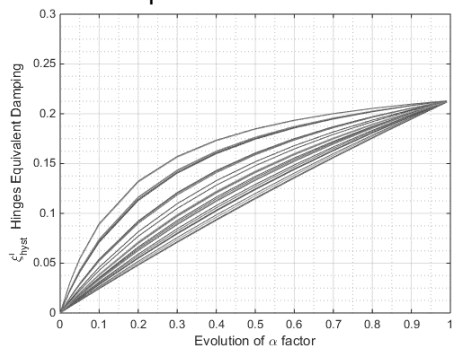

f. All hinges hysteretic damping evolution

Figure 6.24. Analysis for PBSD with the DLA.
Combination and superposition for a wide range of alpha factor

Figure 6.25.a shows the structure deformation as displacement and rotation demand for which the damaged sections should be designed. Maximum bending moment for the selected damage factor are plot in Figure 6.25.b. For this example, the accuracy of the method is shown in Figure 6.26, Table 6.18, Table 6.19 and

Table 6.20. The displacement, rotation and bending moment computed by the DLA are compared with the result of non-linear time history analysis. It can be observed that all columns remain elastic as it is shown in Table 6.20. As observed, bending moments are lower than the computed by DLA (Figure 6.25.b. and Table 6.20) and the plastic rotation are negligible. The based shear obtained in the DLA is 1234.9 KN, a difference of 14% lower respect to time-history analysis. Although the approximation may be regarded as good, it should be highlight that the spectrum of the scaled acceleration presents a similar difference with respect to the design spectrum (11%) in the region of the first vibration mode of the structures. Finally, in this example the concept of strong columns – weak beams is achieved accounting a performances based design for a given hazard.

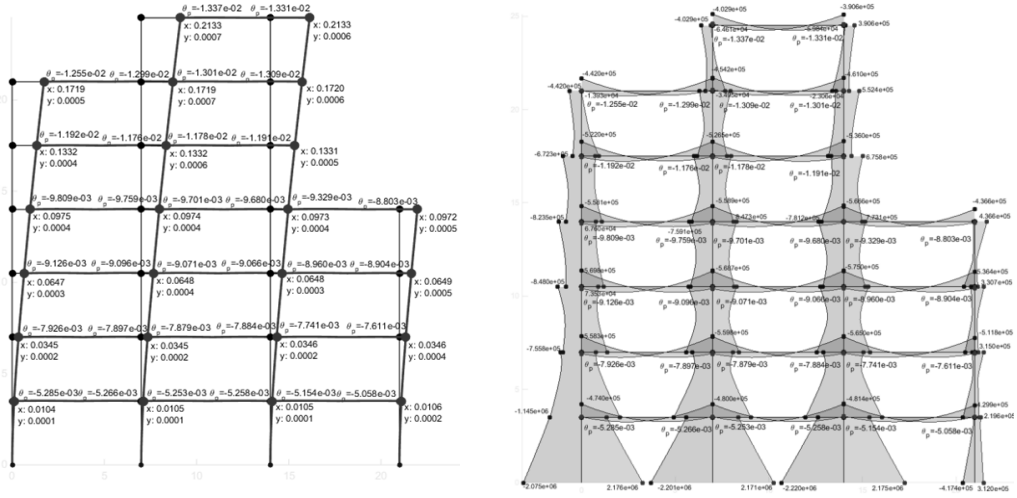

a. Displacement deformed shape b. Bending moment law

Figure 6.25. Deformation and internal forces result for the DLA with a damage factor ($\alpha = 0.5$)

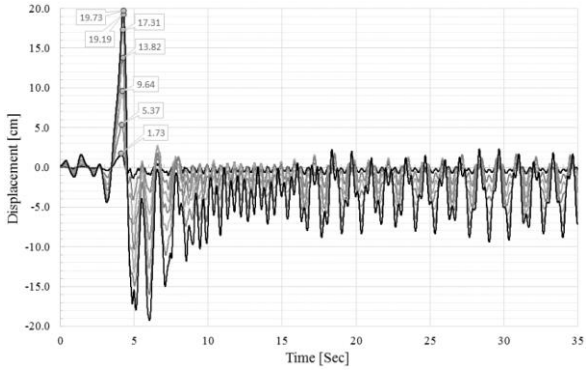

Figure 6.26. Non – linear time – history displacement of all the storey

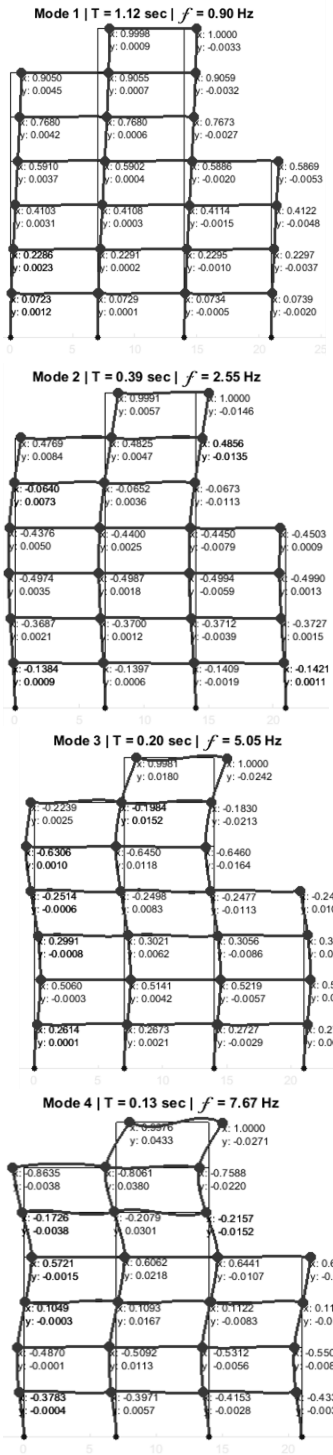

c. Elastic structure

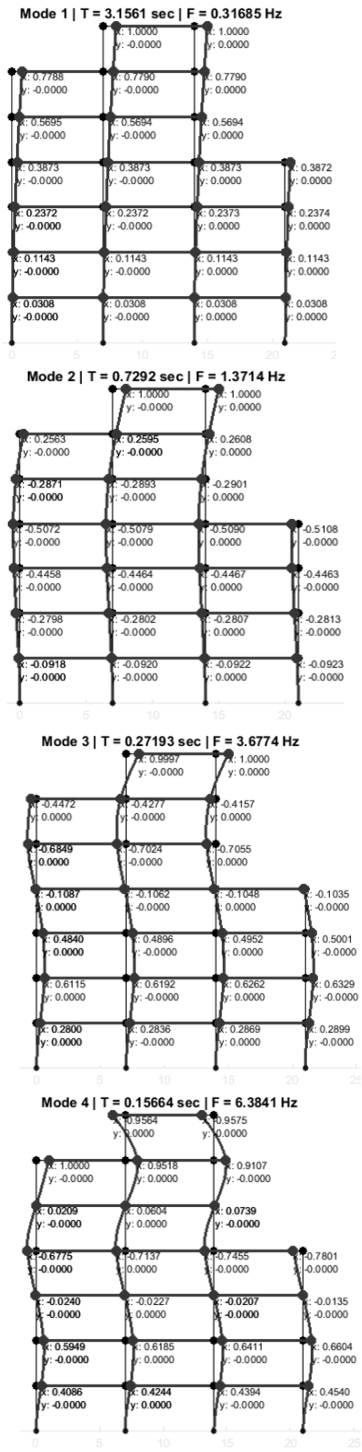

d. Auxiliary structure

Figure 6.27. Comparison of vibration modes of elastic and auxiliary structure

Table 6.18. Ductility demand (θ_d) [rad] from non-linear time–history analysis (NLTH) and non-linear static analysis (PO), compared to the DLA design

Hinge ID	**25H1**	**25H2**	**26H1**	**26H2**	**27H1**	**27H2**	**28H1**	**28H2**
PO	0.00261	0.00688	0.00234	0.00234	0.00180	0.00651	0.00786	0.00851
NLTH	0.00551	0.00716	0.00541	0.00718	0.00529	0.00678	0.00808	0.00878
DLA	0.00529	0.00527	0.00525	0.00526	0.00515	0.00506	0.00793	0.00790
Hinge ID	**29H1**	**29H2**	**30H1**	**30H2**	**31H1**	**31H2**	**32H1**	**32H2**
PO	0.00786	0.00848	0.00749	0.00760	0.00717	0.00943	0.00738	0.00932
NLTH	0.00815	0.00873	0.00778	0.00783	0.00775	0.00998	0.00799	0.00985
DLA	0.00788	0.00788	0.00774	0.00761	0.00913	0.00910	0.00907	0.00907
Hinge ID	**33H1**	**33H2**	**34H1**	**34H2**	**35H1**	**35H2**	**36H1**	**36H2**
PO	0.00718	0.00763	0.00632	0.00894	0.00653	0.00864	0.00561	0.00702
NLTH	0.00766	0.00932	0.00774	0.01001	0.00788	0.00977	0.00679	0.00810
DLA	0.00896	0.00890	0.00981	0.00976	0.00970	0.00968	0.00933	0.00880
Hinge ID	**37H1**	**37H2**	**38H1**	**38H1**	**39H1**	**39H2**	**40H1**	**40H2**
PO	0.00270	0.00648	0.00246	0.00246	0.00670	0.00106	-	0.00412
NLTH	0.00878	0.00790	0.00856	0.00803	0.01001	0.00699	0.01039	0.00832
DLA	0.01192	0.01176	0.01178	0.01191	0.01255	0.01299	0.01301	0.01309
Hinge ID	**41H1**	**41H2**						
PO	-	0.00193						
NLTH	0.01195	0.00951						
DLA	0.01337	0.01331						

Table 6.19. Maximum displacement [cm] for non-linear time – history analysis (NLTH) and non-linear static analysis (PO), compared with the prediction using the DLA design

Story	**7**	**6**	**5**	**4**	**3**	**2**	**1**
PO	21.61	20.11	17.52	13.75	9.58	5.28	1.63
NLTH	19.73	19.19	17.31	13.84	9.63	5.36	1.73
DLA	21.33	17.20	13.31	9.72	6.49	3.46	1.06

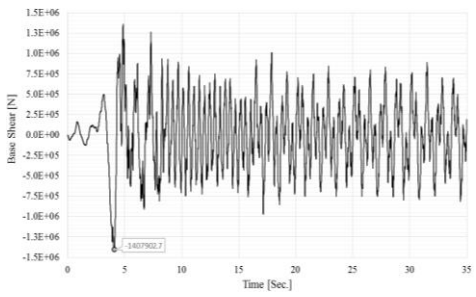

a. Non – linear time – history of the base shear

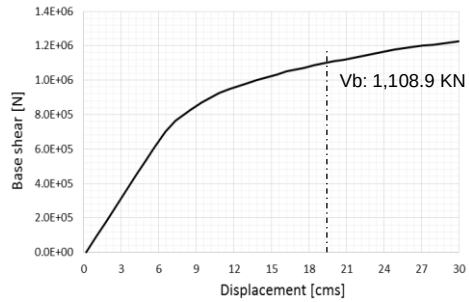

b. Pushover curve

Figure 6.28. Non – linear base shear

Table 6.20. Maximum bending moment [KN/m] in plastic hinge for NLTH and PO, compared with the prediction using the DLA design

Hinge ID	**25H1**	**25H2**	**26H1**	**26H2**	**27H1**	**27H2**	**28H1**	**28H2**	**29H1**	**29H2**
PO	127.51	484.04	126.28	482.00	127.59	434.34	82.09	552.17	73.06	553.92
NLTH	475.77	484.68	473.83	486.45	478.66	434.89	549.45	552.90	542.28	555.60
DLA	474.00	479.97	471.44	481.37	478.17	429.89	558.33	559.82	549.43	565.04
Hinge ID	**30H1**	**30H2**	**31H1**	**31H2**	**32H1**	**32H2**	**33H1**	**33H2**	**34H1**	**34H2**
PO	68.85	512.81	134.14	554.93	119.23	557.92	112.03	529.14	140.25	542.23
NLTH	542.76	514.00	550.17	556.37	542.35	560.81	542.77	530.54	539.94	546.50
DLA	550.21	511.85	569.82	568.75	557.09	574.97	558.07	536.40	558.08	558.85
Hinge ID	**35H1**	**35H2**	**36H1**	**36H2**	**37H1**	**37H2**	**38H1**	**38H2**	**39H1**	**39H2**
PO	117.51	549.19	103.14	442.03	147.73	507.18	138.78	514.90	80.22	436.97
NLTH	525.93	552.14	521.71	444.33	508.92	510.64	501.91	518.18	444.34	447.45
DLA	539.01	566.56	535.40	436.62	521.99	526.52	513.54	536.00	442.03	454.25
Hinge ID	**40H1**	**40H2**	**41H1**	**41H2**	**1H1**	**7H1**	**14H1**	**21H1**		
PO	55.45	446.53	14.23	380.28	1678.8	1796.7	1814.9	346.9		
NLTH	468.42	455.69	412.50	397.14	1846.9	1971.6	1996.9	375.7		
DLA	470.80	460.97	402.85	390.64	2175.8	2200.7	2220.3	417.37		

The accuracy of the compared internal forces as bending moment, ductility demand as plastic rotation and nodal displacement with NLTH and pushover analyses, were predicted with a good accuracy, they are showed in Table 6.18 Table 6.20, respectively. Columns remain elastic in all cases, some yielding are present; however those yielding belongs to values that represent crack; the moment rotation curvature of those yielding zone in columns showed that the maximum rotation are before the yielding point.

6.5 6-Storey building with complex vertical irregularities [Example 4]

In this example, a 6-storey building with vertical irregularities is studied. The building is subjected to a gravity load of 56 KN/m in all beams and the seismic actions. The detailing of section are shown in Table 6.21 and modal properties of the structures is shown in Table 6.22. The structural layout and height of this example, are chosen in order to evaluate the accuracy of the DLA method for complex concrete structure.

Hence, to obtain an uniform the reinforced layout, the design objective is set to produce similar bending moments in stories 1 and 2. After analyzing the evolution of maximum bending moment demand, the α factor was select as 0.6. To achieve this design of redistribution demand of plastic rotation in some beam is reached 1.2e-2 rad.

Table 6.21. Geometry of elements sections of elastic (E) and auxiliary structure (A)

Element		Edge	Story	Width [mm]	Height [mm]	Length [mm]
Column	C1	A-B-C-D-E	1-6	800	800	3500
Beam	V1	A to B	1-6	400	600	7000
Beam	V2	B to C	1-2	400	600	5000
Beam	V3	C to D	1-4	400	600	6000
Beam	V4	D to E	1-5	400	600	7000

Table 6.22. Modal properties of elastic (E) and auxiliary structure (A)

Mode	Periods [sec.]		Mass participation factor [%]	
	(E)	(A)	(E)	(A)
1	0.687	1.517	60.22	34.58
2	0.453	0.535	11.78	37.58
3	0.199	0.245	14.80	07.73
4	0.132	0.152	03.59	10.45

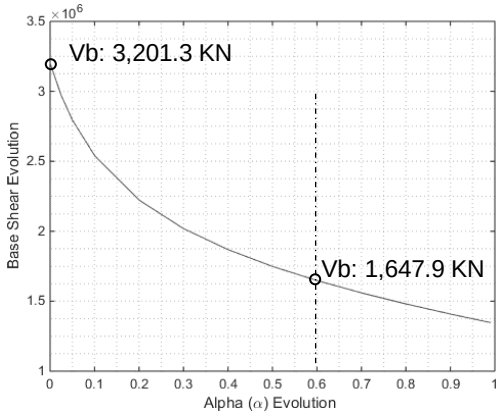

a. Base shear evolution

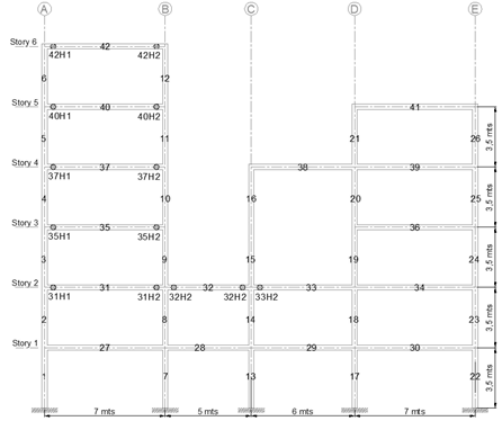

b. Mechanism proposed

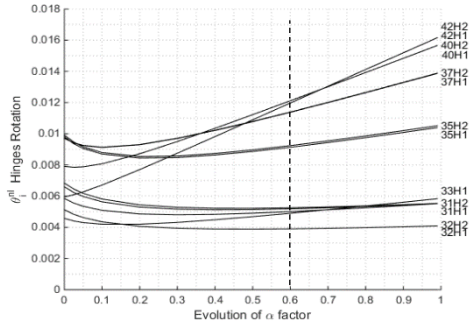

c. All hinges plastic rotation evolution

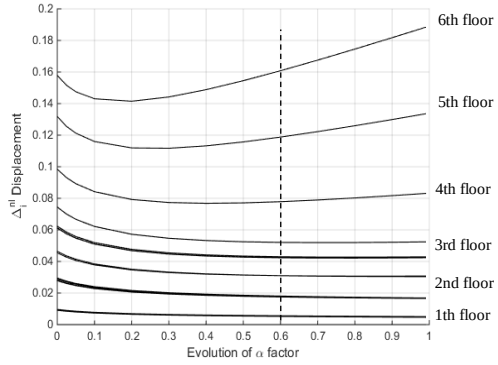

d. Maximum absolute Floor – displacement evolution

Figure 6.29. Analysis for PBSD with the DLA.
Combination and superposition for a wide range of alpha factor

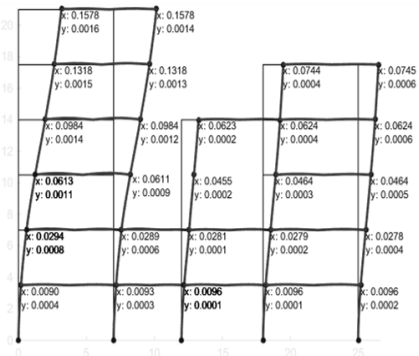

a. Elastic maximum displacement

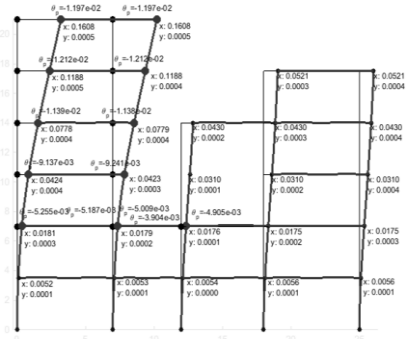

b. Inelastic maximum displacement

Figure 6.30. Comparison of elastic and Inelastic displacement obtained with the DLA design

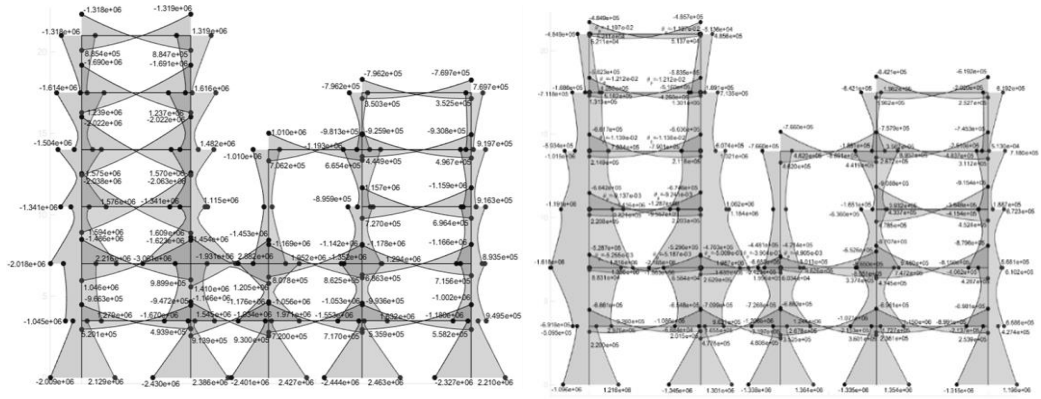

a. Elastic maximum seismic moment b. Inelastic maximum seismic moment

Figure 6.31. Comparison of elastic and Inelastic bending moment obtained with the DLA design

Table 6.23. Ductility demand (θ_d) [rad] from non-linear time–history analysis (NLTH) and non-linear static analysis (PO), compared to the DLA design

Table 6.23.a. Beams rotations

Hinge ID	**27H1**	**27H2**	**28H1**	**28H2**	**29H1**	**29H2**	**30H1**	**30H2**
PO	7.16e-4	2.49e-4	4.24e-4	5.92e-4	7.00e-4	5.64e-4	7.78e-4	4.43e-4
NLTH	2.76e-3	3.12e-3	2.95e-3	2.95e-3	2.82e-3	3.03e-3	2.76e-3	3.18e-3
DLA	-	-	-	-	-	-	-	-
Hinge ID	**31H1**	**31H2**	**32H1**	**32H2**	**33H1**	**33H2**	**34H1**	**34H2**
PO	4.80e-3	4.35e-3	4.64e-3	3.04e-3	4.25e-3	2.95e-4	3.38e-4	2.03e-4
NLTH	6.34e-3	6.85e-3	6.24e-3	5.62e-3	6.41e-3	2.93e-3	2.62e-3	2.85e-3
DLA	5.25e-3	5.19e-3	5.00e-3	3.90e-3	4.90e-3	-	-	-
Hinge ID	**35H1**	**35H2**	**36H1**	**36H2**	**37H1**	**37H2**	**38H1**	**38H2**
PO	7.15e-3	6.70e-3	-	-	8.53e-3	7.89e-3	-	-
NLTH	9.98e-3	1.09e-3	2.26e-3	2.62e-3	1.33e-2	1.44e-2	1.35e-3	2.39e-3
DLA	9.14e-3	9.24e-3	-	-	1.14e-2	1.14e-2	-	-
Hinge ID	**39H1**	**39H2**	**40H1**	**40H1**	**41H1**	**41H2**		
PO	-	-	9.04e-3	8.45e-3	-	-		
NLTH	2.20e-3	2.71e-3	1.56e-2	1.66e-2	2.39e-3	2.93e-3		
DLA	-	-	1.21e-2	1.21e-2	-	-		

Figure 6.31 shows, by means of the maximum bending moment distribution, how higher vibration modes are affecting storey 2 and 3, showing higher bending forces comparing to the elastic bending moment diagrams.

Table 6.23.b. Columns rotations

Hinge ID	1H1	2H1	3H1	4H1	5H1	6H1	7H1	8H1
PO	1.26e-4	-	-	-	-	-	4.07e-4	1.08e-4
NLTH	3.07e-3	-	1.35e-3	1.86e-3	1.13e-3	5.03e-4	3.03e-3	-
DLA	-	-	-	-	-	-	-	-
Hinge ID	**9H1**	**10H1**	**11H1**	**12H1**	**13H1**	**14H1**	**15H1**	**16H1**
PO	-	-	-	-	3.86e-4	1.66e-4	-	-
NLTH	5.23e-4	1.09e-3	4.13e-4	-	3.08e-3	-	1.64e-3	-
DLA	-	-	-	-	-	-	-	-
Hinge ID	**17H1**	**18H1**	**19H1**	**20H1**	**21H1**	**22H1**	**23H1**	**24H1**
PO	4.84e-4	2.21e-5	-	-	-	5.44e-4	1.35e-4	-
NLTH	3.05e-3	2.77e-3	1.48e-3	6.82e-4	7.59e-4	2.89e-3	-	1.74e-3
DLA	-	-	-	-	-	-	-	-
Hinge ID	**25H1**	**26H1**						
PO	-	-						
NLTH	4.39e-4	3.24e-4						
DLA	-	-						

Table 6.24. Maximum displacement [cm] for NLTH and PO, compared with the prediction using the DLA design

Story (Edge A)	6th	5th	4th	3rd	2nd	1st
PO	16.18	12.47	8.67	5.08	2.22	0.67
NLTH	24.11	17.91	12.18	7.29	3.38	1.57
DLA	16.08	11.88	7.79	4.23	1.79	0.53
Story (Edge D)	**6th**	**5th**	**4th**	**3rd**	**2nd**	**1st**
PO	-	5.16	4.47	3.46	2.14	0.74
NLTH	-	9.07	7.72	5.99	3.81	1.60
DLA	-	5.21	4.30	3.10	1.75	0.56

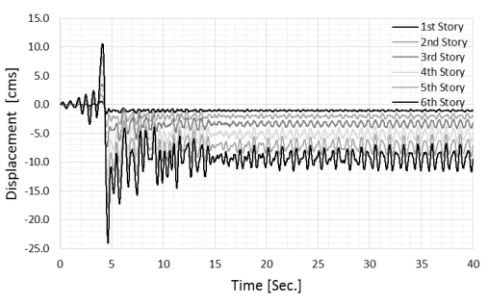

a. Non – linear time – history of displacement of edge A

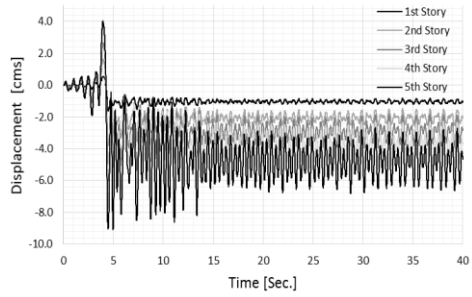

b. Non – linear time – history of displacement of edge E

Figure 6.32. Non – linear time – history of displacement floors

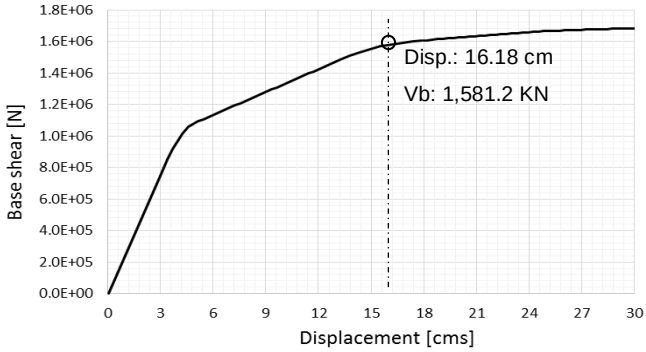

Figure 6.33. Non-linear incremental static (Pushover) curve

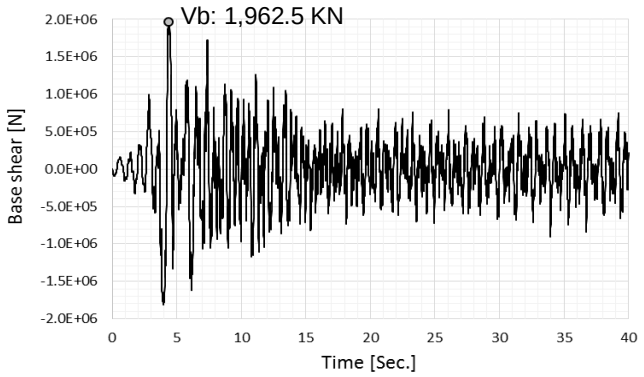

Figure 6.34. Non – linear time – history of the base shear

Figure 6.29.a shows the reduced base shear in "x" direction computed with the DLA method. It is shown that it fits well the base shear obtained from pushover analysis (Figure 6.33) and, compared to the maximum base shear of NLTH (Figure 6.34), the accuracy is still close to the prediction. It should be highlight that, for the selected α value, the storey displacement is practically the same as what will have been obtained with an elastic design (Figure 6.29). Table 6.23 shows some yielding in columns hinges by very small rotation; however, it may be considered as negligible.

Table 6.25. Maximum bending moment [KN/m] in plastic hinge for non-linear time – history analysis (NLTH) and non-linear static analysis (PO), compared with the prediction using the DLA design

Table 6.25.a. Beams bending moment

Hinge ID	**27H1**	**27H2**	**28H1**	**28H2**	**29H1**	**29H2**	**30H1**	**30H2**
PO	213.78	640.09	471.71	710.22	343.88	680.03	229.87	679.41
NLTH	662.60	615.24	704.61	689.50	683.63	655.71	689.52	653.86
DLA	666.10	658.80	709.9	726.8	688.2	696.1	696.1	698.1
Hinge ID	**31H1**	**31H2**	**32H1**	**32H2**	**33H1**	**33H2**	**34H1**	**34H2**
PO	87.03	527.33	265.94	448.54	60.62	636.37	410.43	854.35
NLTH	536.99	539.31	484.01	456.16	432.36	574.32	858.41	745.30
DLA	528.7	529.6	476.3	448.1	421.1	652.6	870.7	879.6
Hinge ID	**35H1**	**35H2**	**36H1**	**36H2**	**37H1**	**37H2**	**38H1**	**38H2**
PO	225.82	682.24	379.94	363.49	218.83	674.95	303.36	594.23
NLTH	682.78	696.17	892.78	757.22	690.04	695.53	753.75	705.69
DLA	664.2	674.6	908.8	915.4	661.7	663.6	766.0	757.9
Hinge ID	**39H1**	**39H2**	**40H1**	**40H1**	**41H1**	**41H2**	42H1	42H2
PO	154.76	601.95	135.50	596.56	88.43	488.53	533.23	498.20
NLTH	740.05	665.38	615.02	619.17	638.27	616.58	514.76	517.82
DLA	757.9	745.3	582.3	583.5	642.1	619.2	484.9	485.7

Table 6.25.b. Columns bending moment

Hinge ID	**1H1**	**2H1**	**3H1**	**4H1**	**5H1**	**6H1**	**7H1**	**8H1**
PO	1217.5	748.91	1232.41	733.25	224.31	62.64	1340.8	1077.38
NLTH	1208.31	906.78	1807.35	1404.48	786.66	422.18	1336.15	994.81
DLA	1216.10	691.80	1816.5	1416.2	793.4	168.6	1345.3	1086.6
Hinge ID	**9H1**	**10H1**	**11H1**	**12H1**	**13H1**	**14H1**	**15H1**	**16H1**
PO	1708.80	800.31	472.97	207.08	1353.3	1239.14	176.40	261.02
NLTH	2155.36	1281.63	786.03	491.31	1349.67	1179.20	792.80	315.26
DLA	2165.3	1287.7	790.1	516.0	1364.5	1244.5	801.3	270.1
Hinge ID	**17H1**	**18H1**	**19H1**	**20H1**	**21H1**	**22H1**	**23H1**	**24H1**
PO	1353.12	1139.2	258.14	84.53	16.55	1311.04	876.51	318.30
NLTH	1340.99	1125.03	940.98	394.49	354.60	1302.67	772.36	804.30
DLA	1354.6	1150.6	948.0	392.3	356.2	1315.5	899.1	815.0
Hinge ID	**25H1**	**26H1**						
PO	91.48	8.43						
NLTH	394.41	252.38						
DLA	394.8	251.0						

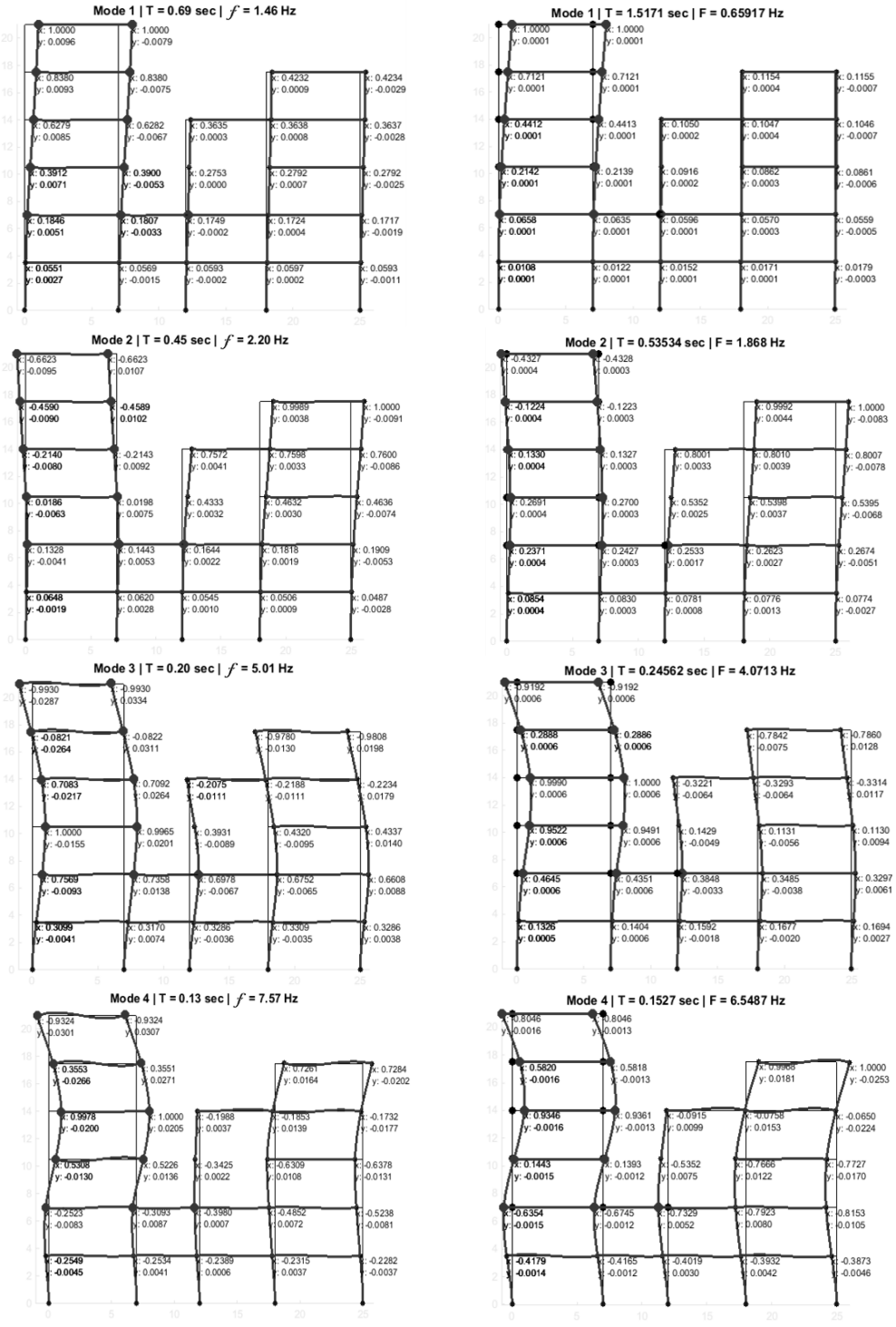

a. Elastic structure b. Auxiliary structure

Figure 6.35. Comparison of vibration modes of elastic and auxiliary structure

6.6 3D building with vertical and horizontal irregularities [Example 5]

This section presents a 3D model of a RC structure with plan and vertical irregularities. The aim, is to show the accuracy of the DLA method applied to a complex layout structure. The seismic load was applied in "x" direction; however, the result components in both directions are account for by the non-linear analysis and the validation methodology. Design loads are shown in Table 6.27, elements' cross section in Table 6.26 and modal properties in Table 6.28. The building layout is shown in Figure 6.36. The decision of distribution and damage intensity was based on the design objective of redistributing the bending moments on some beams and by reducing internal forces on columns. As it is demonstrated in the previous example, this concept gives a considerable redistribution of internal force but not an important plastic rotation. With this design objective and after analyzing the evolution of bending moment, the factor α is taken as 0.4, and the maximum rotation is 5e-3 rad.

Table 6.26. Geometry of elements sections of elastic (E) and auxiliary structure (A)

Element		Story	Width [mm]	Height [mm]	Length [mm]
Column	C1	1-3	500	500	3500
Beam	VL1	1	400	600	7000
Beam	VT1	1	300	500	5000
Beam	VL2	2	400	600	7000
Beam	VT2	2	300	500	5000
Beam	VL3	3	400	600	7000
Beam	VT3	3	300	500	5000

Table 6.27. Distributed load [KN/m] in elements

ELE ID	Load	ELE ID	Load	ELE ID	Load	ELE ID	Load
27	-10.00	36	-28.00	45	-5.00	54	-5.00
28	-10.00	37	-10.00	46	-19.00	55	-5.00
29	-14.00	38	-10.00	47	-10.00	56	-14.00
30	-24.00	39	-14.00	48	-10.00	57	-5.00
31	-10.00	40	-5.00	49	-28.00	58	-5.00
32	-10.00	41	-5.00	50	-10.00	59	-7.00
33	-24.00	42	-7.00	54	-10.00		
34	-10.00	43	-12.00	52	-14.00		
35	-10.00	44	-5.00	53	-7.00		

Table 6.28. Modal properties of elastic (E) and auxiliary structure (A)

Mode	Periods [sec.]		Mass participation factor [%]	
	(E)	(A)	(E)	(A)
1	0.4240	0.63706	1.587	52.619
2	0.3772	0.42062	60.167	1.806
3	0.2882	0.30849	24.626	28.538
4	0.1518	0.15584	0.019	11.471
5	0.1311	0.15180	9.296	0.0059

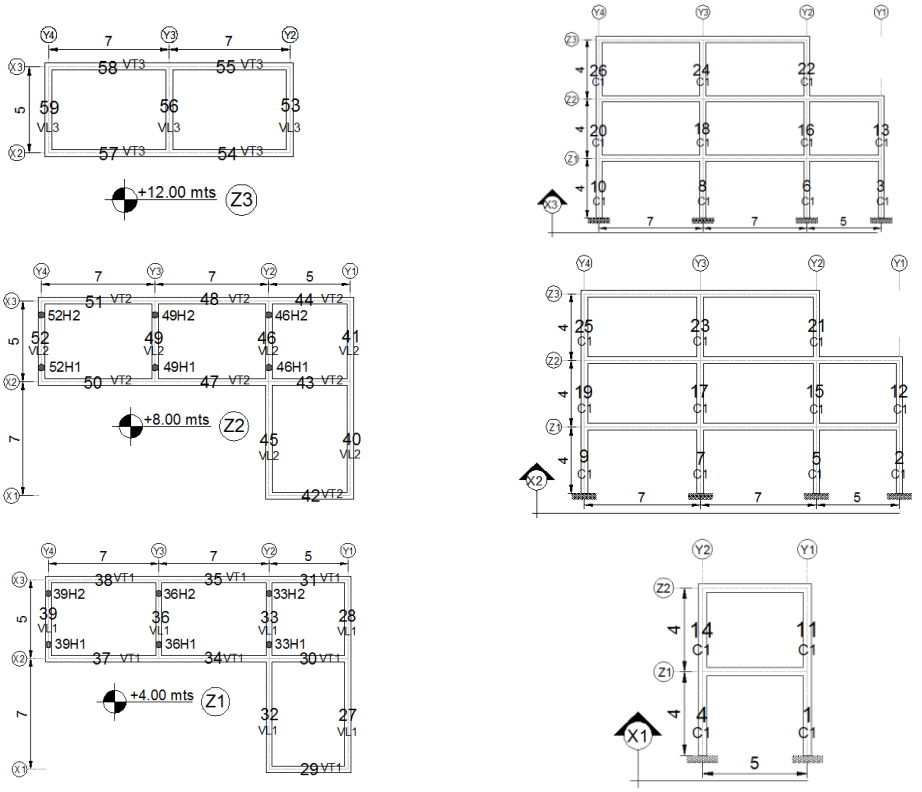

a. Plan views b. Elevation views

Figure 6.36. 3D model layout

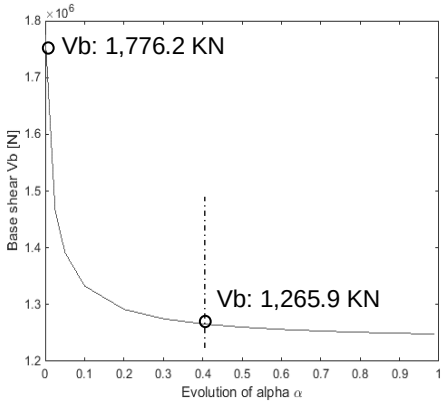

a. Base shear evolution

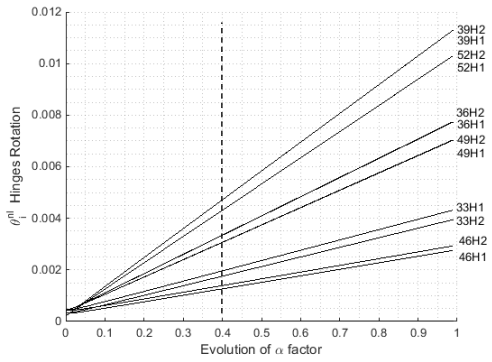

b. Rotation evolution in hinges

Figure 6.37. Analysis for PBSD with the DLA.
Combination and superposition for a wide range of alpha factor

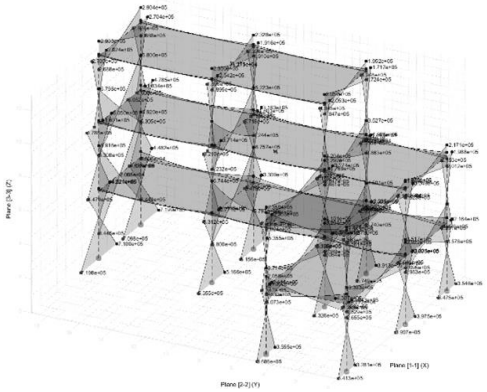

a. Elastic bending moment

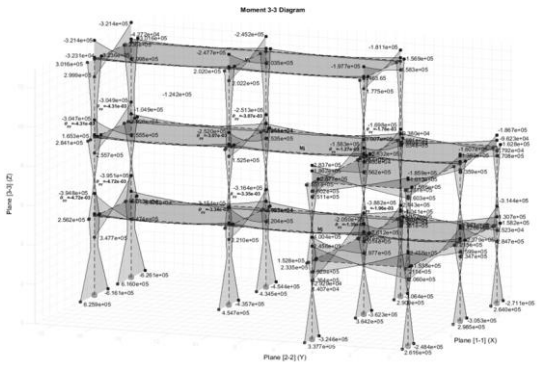

b. Combined (Inelastic) bending moment

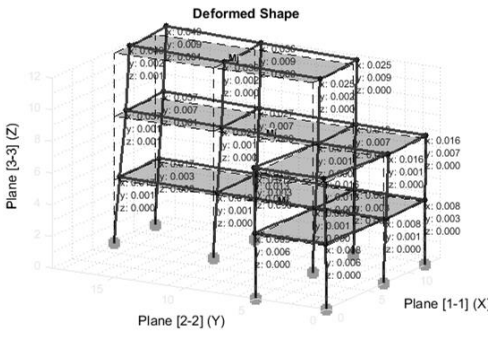

c. Elastic displacement

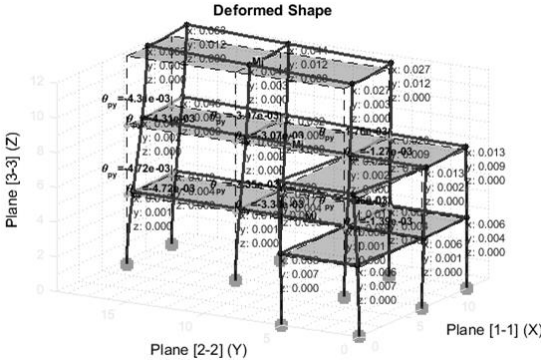

d. Combined (Inelastic) displacement

Figure 6.38. Comparison of Inelastic maximum bending moment diagrams and displacement computed with the DLA with the elastic solution

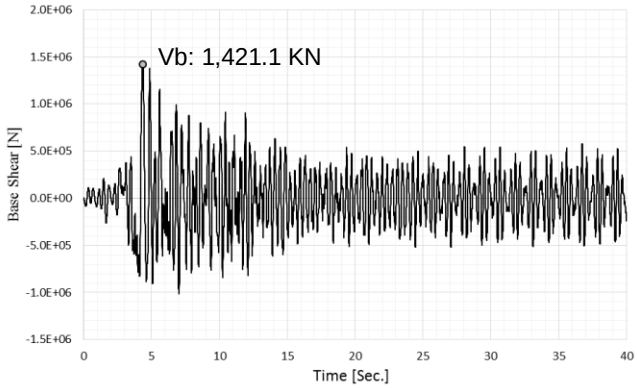

Figure 6.39. Non – linear time – history of the base shear

The designed reinforcement was selected in order to redistribute the internal forces in the 1st and 2nd story longitudinal beams. Inelastic maximum bending moment diagrams can be compared with the elastic bending moment in Figure 6.38. It worth emphasizing the fact of activating a low quantity of hinges allows reaching the maximum reduction of internal forces with low value of α factor (Figure 6.37). The deformation for the elastic and inelastic structure have a similar shape; however, if the damage was introduced in other location, deformation shape could be different than the elastic.

Table 6.29. Ductility demand (θ_d) [rad] from non-linear time–history analysis (NLTH) and non-linear static analysis (PO), compared to the DLA design

Table 6.29.a. Beams rotations

Hinge ID	**33H1**	**33H2**	**36H1**	**36H2**	**39H1**	**39H2**
PO	2.97e-3	3.49e-3	3.68e-3	3.80e-3	3.86e-3	3.93e-3
NLTH	3.41e-3	4.85e-3	3.61e-3	4.76e-3	4.09e-3	4.74e-3
DLA	1.96e-3	1.39e-3	3.34e-3	3.35e-3	4.72e-3	4.73e-3
Hinge ID	**46H1**	**46H2**	**49H1**	**49H2**	**52H1**	**52H2**
PO	1.25e-3	1.66e-3	1.90e-3	2.05e-3	2.24e-3	2.30e-3
NLTH	3.42e-3	4.71e-3	3.83e-3	4.98e-3	4.87e-3	5.47e-3
DLA	1.27e-3	1.76e-3	3.07e-3	3.07e-3	4.31e-3	4.31e-3

Table 6.29.b. Columns rotations

Hinge ID	**1H1**	**2H1**	**3H1**	**4H1**	**5H1**
PO	-	4.1e-3	4.35e-3	4.56e-3	4.41e-3
NLTH	3.35e-3	3.26e-3	3.29e-3	2.77e-3	2.66e-3
DLA	-	-	-	-	-
Hinge ID	**6H1**	**7H1**	**8H1**	**9H1**	**10H1**
PO	4.74e-3	7.73e-3	4.85e-3	4.87e-3	4.93e-3
NLTH	2.65e-3	1.64e-3	1.53e-3	1.65e-3	1.73e-3
DLA	-	-	-	-	-

Table 6.30. Maximum displacement [cm] for non-linear time – history analysis (NLTH) and non-linear static analysis (PO), compared with the prediction using the DLA design

Story (Edge X3-Y3)		3rd	2nd	1st
PO	**x**	**4.53**	**3.75**	**2.11**
	y	0.41	0.31	0.10
NLTH	**x**	**5.56**	**3.84**	**1.70**
	y	1.36	0.94	0.42
DLA	**x**	**4.40**	**3.20**	**1.30**
	y	1.20	0.90	0.40
Story (Edge X2-Y1)		3rd	2nd	1st
PO	**x**	**-**	**3.24**	**1.92**
	y	-	0.57	0.20
NLTH	**x**	**-**	**3.77**	**1.75**
	y	-	1.83	0.83
DLA	**x**	**-**	**2.0**	**0.80**
	y	-	1.7	0.70

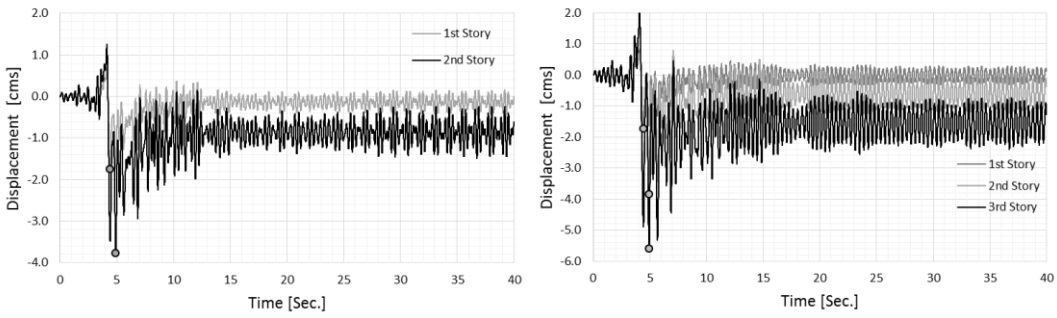

a. Non – linear time – history of displacement of edge X3-Y3

b. Non – linear time – history of displacement of edge Y2-X1

Figure 6.40. Non – linear time – history of displacement floors

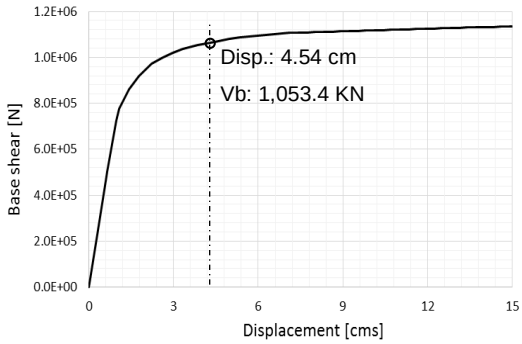

Figure 6.41. Non-linear incremental static (Pushover) curve for the top story in edge X3-Y3

Table 6.31. Maximum bending moment [KN/m] in plastic hinge for non-linear time – history analysis (NLTH) and non-linear static analysis (PO), compared with the prediction using the DLA design

Table 6.31.a. bending moment on beams

Hinge ID	**33H1**	**33H2**	**36H1**	**36H2**	**39H1**	**39H2**
PO	84.6	185.62	186.83	272.12	297.15	338.64
NLTH	175.50	185.65	269.71	271.85	338.9	340.04
DLA	214.3	205.0	315.4	316.4	394.8	395.1
Hinge ID	**46H1**	**46H2**	**49H1**	**49H2**	**52H1**	**52H2**
PO	69.62	145.37	127.17	216.81	216.72	261.47
NLTH	135.09	145.48	215.47	215.87	262.22	263.03
DLA	169.8	158.3	251.3	252.0	304.7	304.9

Table 6.31.b. Bending moments on columns

Hinge ID	**1H1**	**2H1**	**3H1**	**4H1**	**5H1**
PO	147.45	225.74	164.55	172.18	220.10
NLTH	241.6	283.35	250.16	309.34	334.41
DLA	261.6	305.3	264.0	337.7	364.2
Hinge ID	**6H1**	**7H1**	**8H1**	**9H1**	**10H1**
PO	130.54	179.40	181.70	231.96	232.89
NLTH	277.48	410.17	408.17	561.69	561.27
DLA	306.4	454.7	454.4	625.9	626.1

By analyzing Table 6.29, the maximum of plastic rotations obtained in PO and NLTH are reached. Table 6.31 shows the bending moment result of the NLTH and PO analysis, which are slightly lower (7.2%-10%) than DLA prediction. The base shear prediction in Figure 6.37.a, is 11% lower than NLTH (Figure 6.39) and 16.7% bigger than PO (Figure 6.41). Finally, the displacement obtained with the DLA, is compared as well with the two non-linear analysis. Table 6.30 shows two directional displacements due to the torsional effect. In spite the existence of this torsional displacement in the building, the DLA shows a good approximation of inelastic displacement.

CHAPTER 7

CONCLUSIONS

7.1 General conclusions

The main objective of this Thesis was to develop a direct performance based seismic design method for concrete structures. This general objective was achieved with enough accuracy for design purposes, by extending the non-linear static design (NLSD) methodology, based on a double linear analysis (DLA), to seismic loads and 3D effects. Thus, a “Double Linear Seismic Analysis” (DLSA) for performance based seismic design method was developed. The method was applied to concrete structures.

The methodology proposed was validated through a number of design examples whose performance was assessed by means of Non-Linear Time-History (NLTH) and incremental static non-linear analysis, i.e. Push-Over (PO). In this way, the accuracy of the method was demonstrated. Furthermore, the methodology of selecting damage was used as an assessment method. Thereby, it was confirmed that the DLA methodology is capable of capturing the effects of higher vibration modes when the structure behavior is non-linear. It was possible to obtain how the pattern of maximum storey seismic load changes along the height during damage process with reasonable precision for design purposes. Likewise, those results highlight the importance of considering the redistribution of lateral forces in order to avoid underestimation forces on elements in middle stories; as it may lead to not ensuring of the “strong column – weak beam” criterion and the consequent formation of undesired plastic hinges on columns.

The main hypothesis on which the method is based is that the non-linear response can be approximated, for design purposes, by two linear analyzes of the elastic and the auxiliary models, and the adequate superposition of both. The latter is carried out by means of a damage factor (α). Based on the results of this Thesis, this hypothesis can be considered as valid.

The α factor allows for a simple representation of the variations of the damage intensity distribution, redistribution of internal forces and energy dissipation, for varying values of α. Hence, it allows supporting design decisions and may be useful for optimization.

7.2 Specific conclusions

Based on the analyses carried out in this research, the following specific conclusions can be drawn:

- A direct performance based seismic design procedure for 2D and 3D irregular structures was developed. This method accounts for energy dissipation and redistribution of internal forces in the design process. For which, the decision of the intensity and damage location is decided in early design phases by the designer.

- The proposed method assures the distribution of hinge location selected by the designer. In the case of damage located in beams, the “weak beam-strong column” criterion is accounted for, considering the redistribution of internal forces in the system.

- The NLTH and PO analysis demonstrated that DLA captures the effects of higher vibration modes, activated after the structure behavior is inelastic.

- The examples carried out in this thesis, show that the more regular the structure layout is, the contribution of the effects of high vibration modes increase more after the inelastic behavior begins, compared to irregular structures. This can be explained by the fact that the participation factor of modes higher than the fundamental one in the auxiliary structure, simulating the presence of plastic hinge distribution.

- The proposed equation for the superposition of the response of the elastic and auxiliary models allows for a simple separation of the effects of the nonlinear behavior; i.e., force reduction and displacement increment, into components due to redistribution and dissipation. The importance of each component was observed to be dependent on the damage intensity parameter (α). This

provides basis for design decisions on increasing ductility, hysteresis loops, seismic devices, etc.

- In all the considered examples, beams where the elements were damage was produced. In the most of the cases, columns remained elastic; although, in some situations, minor yielding was observed in these columns with very small plastic rotations. By slightly reducing the elastic column stiffness, column yielding did not take place. This suggests that the consideration of crack stiffness in non-linear analysis should be include.

- Due to redistribution of forces, as the damage evolves without the formation of hinges on columns, the resistance demand on columns keeps increasing after first yielding of the beams on the ends of the columns. Hence, depending on the selected distribution of hinges, height and extend of damage (or ductility demand), the ratio of column resistance demand to the yielding strength of beams in the floor varies. It was observed that this ratio can be considerably larger than the overstrength factors in current design codes. This result is in agreement with the observations of other researches, Moehle (2015), Vielma (2008), (Franchin , et al., 2016), among others, that reported that code overstrength factors do not totally guarantee the strong column-weak beam criterion on tall buildings.

- The ratio of columns strength demand to beam yielding strength ratio varies along the building height. Its maximum value is sensitive to the current distribution of lateral forces. This suggests that a non-constant overstrength factor may be needed to avoid the formation of plastic hinges in columns.

- The shape of the seismic load pattern is sensitive to the damage parameter (α). For larger values of α (large damage), significant differences on the distribution of force in the non-damaged system may be observed.

7.3 Recommendations for future research

After conducting the research, some topics of possible improvement of the method have been identified. In the following, recommendation for future research in some ways are the given:

- In chapter 6, it was observed that the accuracy of the DLA was adequate for design purposes, providing improved information of the time dependent and non-linear response. However, design recommendation should be studied by means of parametric analyzes and safety factors should be calibrated based on target reliabilities, and the considerations of the system and seismic variability.

- In the cases of a hinged beam, redistribution of bending moments takes place in columns. In the validation cases, all columns were designed with the needed strength. Despite this, a safety gap between the column strength demand and yielding strength of beams for real designs. The role of overstrength factors and a calibration format for this coefficient should be calibrated for designing with the DLA method.

- The proposed methodology is able to account for different structural technologies for connection, hysteresis, use of seismic devices, etc. A study related to the use single or combine techniques should be carried out to derive recommendations and guidelines. Likewise, retrofitting procedure with hysteretic device could be developed, i.e., the work of Benavent-Climent (2011).

- In some structural systems, such as inverted pendulum, hinges may only take place in columns. However, this may produce a mechanism in the auxiliary structure and modal analysis cannot be carried out on it. Therefore, a pertinent improvement of the methodology is to include yielding stiffness in the column

hinges, so that it will be possible to exploit a complete mechanism, exploiting the base columns strength and ductility capacity.

- Second order effects has been neglected in the analysis conducted in this research. However, its inclusion in the linear analyses of the elastic and auxiliary system is possible by means of the geometric stiffness matrix. It is suggested that a research regarding the inclusion of second order effects in the design with the DLA method should be carried out.

- The maximum response for each structure is obtained by modal analysis. In this thesis the SRSS method was used. Other modal combination should be investigated for non-well separate frequencies in higher vibration modes.

- As recently suggested in Wilson (2015), it is currently possible to carry out linear time-history analysis with a low computational cost. Although, this may provide significant improvement in the uncertainties related to modal response combination, this will not include the effects related to the nonlinear response. The DLA method may provide an interesting tool to estimate the nonlinear response in the transient analysis. Therefore, it is suggested to carry out a research on the adaptations of the DLA method for use together with linear time history analysis as alternative to spectral analysis.

- The DLA method was here applied and validated for one direction modal dynamic spectral demand. Moreover, the directionality of the seismic hazard should be investigated, including the effects of the vertical component, as this may affect the formation of hinges in columns.

- Finally, it is recommended to investigate the use of the evolution curves, which are easily generate by the DLA to optimize a performance based earthquake design. Evolution plots for multiple seismic demands corresponding to different return periods, may be plot in the same graphic. Hence, the DLA may be used as a design tool for multiple design objectives.

REFERENCES

ACI Committee 318, 2014. *Building Code Requirements for Structural Concrete and Commentary (ACI 318-14)*: American Concrete Institute.

Akiyama, H., 1999. *Metodología de proyecto sismorresistente de edificios basafa en el balance energético.* Barcelona: Reverté.

Antoiou, S. & Pinho, R., 2004. Development and verification of a displacement-based adaptive pushover procedure. *Journal of Earthquake Engineering,* 8(5), pp. 643-661.

ATC-40, 1996. Seismic evaluation and retrofit of buildings, Report Nº40 ATC-40. *Applied Technology Council, Redwood City, CA.*

Ayala, G. A., Castellanos, H. & Lopez, S., 2012. A displacement-based seismic design method with damage control for RC buildings. *Earthquakes and Structures,* 3(3), pp. 413-434.

Bairán, J., Marí, A. & Duarte , N., 2011. Diseño no lineal de pórticos de hormigón. *V Congreso de ACHE,* pp. 1-10.

Bairán, J. & Marí, A. R., 2010. Proyecto de estructuras de hormigón armado con armaduras de alta ductilidad. *Instituto para la promoción de armaduras certificadas (IPAC),* p. 165.

Benavent-Climent , A. & Zahran, R., 2009. An energy-based procedure for the assessment of seismic capacity existing frames: Application to RC wide beam systems in Spain. *Soil Dynamic and Earthquake Engineering,* Volume 30, pp. 254-367.

Benavent-Climent, A., 1997. *An energy-based damage model for seismic response of steel structures,* Tokio: Universidad de Tokio. Tesis doctoral.

Benavent-Climent, A., 2007. An energy-based damage model for seismic response of steel structures. *Earthquake Engineering and Structural Dynamics ,* Volume 36, pp. 1049-1064.

Benavent-Climent, A., 2011. An energy-based method for seismic retrofit of existing frames using hysteretic dampers. *Soil Dynamics and Earthquake Engineering,* Volume 31, pp. 1385-1396.

Bento, R., Falcao, S. & Rodrigues, F., 2004. Non - Linear static procedures in performance based seismic design. *13th World Conference on Earthquake Engineering ,* Issue Paper No. 2522.

Bermudez, C. A., Hurtado, J. E., Barbat, A. H. & Pujades, L. G., 2012. Smart scaling of accelerograms applied to the study of steel buildings. *World Conference on Earthquake Engineering, 15th WCEE.*

Bertero, R. D. & Bertero, V. V., 2001. Performance-based seismic engineering: the need for a reliable conceptual comprehensive approach. *Earthquake Engineering & Structural Dynamics ,* 31(3), pp. 627-652.

Biondini, F., Titi, A. & Toniolo, G., 2012. Pseudo-dynamic test and numerical simulations on a full-scale prototype of a multi-storey precast structure. *World Conference on Earthquake Engineering, 15th WCEE.,* Issue 15th.

Blandon, C., 2004. Equivalent viscous damping equation for direct displacement based design. *Master Thesis, Rose School, Pavia.*

Bojorquez, E., Teran-Gilmore, A., Ruiz, S. E. & Reyes-Salazar, A., 2011. Evaluation of structural reliability of steel frames: Inter-story drift versus plastic hysteretic energy. *Earthquake Spectra,* 27(3), pp. 661-682.

Cheng , F. Y., 2001. Matrix Analysis of Structural Dynamics. In: New York, USA: Marcel Dekker, Inc., p. 997.

Chopra, A. K., 2007. *Dynamics of structures - Theory and applications to earthquakes engineering.* Third ed. New Jersey: Prentice Hall.

Chopra, A. K. & Goel, R. K., 2001. Direct displacement-based design: use of inelastic vs elastic design spectra. *Earthquake Spectra,* 17(1), pp. 47-64.

Chung, J. & Hubert, G. M., 1993. A Time Integration Algorithm for Structural Dynamics with Improved Numerical Dissipation: The Generalized-α Method. *ASME Journal of applied Mechanics,* Volume 60, pp. 371-375.

Clough, R. W. & Penzien, J., 1993. *Dynamics of Structures.* 2nd edition ed. New York: McGraw-Hill.

Council Building Seismic Safety, 1997. *NEHRP Guidelines for the Seismic Rehabilitation of Buildings, FEAM-273.* Federal Emergency Management Agency: Washington, DC: s.n.

Dalhquist, G., 1963. A Special stability problem for linear multistep methods. *BIT,* Volume 3, pp. 27-43.

Dokainish, M. A. & Subbaraj, K., 1989. A survey of direct time-integration methods in computational structural dynamics. I. Explicit Methods. *Computers & Structures,* 32(6), pp. 1371-1386.

Dwairi, H. M., Kowalsky, M. J. & Nau, J. M., 2007. Equivalent damping in support of direct displacement-based design. *Journal of earthquake Engineering,* Issue 11, pp. 512-530.

EHE-08, 2008. Instrucción del Hormigón Estructural, Comisión Permanente del Hormigón. *Ministerio de Fomento.*

Eurocode-2, 1992. Design of concrete structures.,. *BS EN 1992-1-1:2004 - Design of concrete structures. General rules and rules for buildings,* : .

Eurocode-8, 2004. Part 1: General rules, seismic actions and rules for buildings. In: *Eurocode 8: Design of structures for earthquake resistance.* : The European Standard EN 1998-1:2004, p. .

Fajfar, P., 2000. A Nonlinear Analysis Method for Performance Based Seismic Design. *Earthquake Spectra ,* 16(3), pp. 573-592.

FEMA 273 , 1997. Guidelines for the seismic rehabilitation of buildings. *Federal Emergency Management, Washington, USA.*

FEMA P-58, 2012. Seismic Performance Assessment of buildings. *Federal Emergency Management, Washington, USA.*

Franchin , P., Molaioli, F. & Petrini, F., 2016. Improvement gradient-based equivalent linear procedure for probabilistic displacement-based design of RC structures, accounting for damage-induced stiffness degradation.

Franchin, P. & Pinto, P. E., 2012. Method for probabilistic Displacement-Based Design of RC Structures. *Journal of Structural Engineering,* 138(5), pp. 585-591.

Ghorbanirenani, I., 2010. Experimental and numerical investigation of higher mode effects on seismic inelastic response of reinforced shear walls. *Ph.D. Thesis, Ecole Polythecnique, Montreal, Canada.*

Ghorbanirenani, I., 2011. Experimental and numerical investigation of higher mode effects on seismic inelastic response of reinforced shear walls. *Ph.D. Thesis, Ecole Polythecnique, Montreal, Canada.*

Grant, D. N., Blandon, C. & Priestley, M. J. N., 2004. Modeling inelastic response in direct displacement-based design. *Report No. ROSE 2004/02, European School of Advanced Studies in Reduction of Seismic Risk.*

Gulkan, P. & Sozen, M. A., 1974. Inelastic Responses of Reinforced Concrete Structure to Earthquake Motions. *ACI,* 71(12), pp. 604-610.

Hilber, H. M., Hughes, T. J. & Taylor, R. L., 1977. Improved numerical dissipation for time integration algorithms in structural dynamics. *Earthquake Engineering and Structural Dynamics,* Volume 5, pp. 283-292.

Houbolt, J. C., 1950. A recurrence matrix solution for the dynamic response of elastic aircraft. *Journal of the Aeronautical Sciences,* Volume 17, pp. 540-550.

Hughes, T. J. R., 1987. *The Finite Element Method: Linear Static and Dynamic Finite Element Analysis.* Englewood, New Jersey: Prentice-Hall.

Jacobsen, P. C., 1930. Steady forced vibrations as influenced by damping. *ASCE Journal of Engineering Mechanics Division,* 1(52), pp. 103-116.

Javadein, S. I. & Taghinezhad, R., 2007. *Evaluation of lateral load pattern in pushover analysis VI.* UK: Wessex Institute of Technology.

Jingjiang, S., Ono, T., Yangang, Z. & Wei, W., 2003. Lateral load pattern in pushover analysis. *Earthquake Engineering and Engineering Vibration,* 2(1), pp. 99-107.

Kappos, A. J. & Stefanidou, S., 2010. A deformation-based seismic design method for 3D R/C irregular buildings using inelastic dynamic analysis. *Bulletin of Earthquake Engineering,* 8(4), pp. 875-895.

Kassimali, A., 1999. Matrix analysis of structures. In: Illiloins, USA: CL Engineering, p. 592.

Khoshnoudian, F., Mestri, S. & Abedinik, F., 2011. Proposal of lateral load pattern for pushover analysis of RC buildings. *Computational Methods in Civil Engineering ,* 2(2), pp. 169-183.

Kowalsky, M. J., 1994. Displacement based seismic design - a methodology for seismic design applied to RC bridge columns. *Master's Thesis, University of California.*

Liao, W.-C., 2010. *Performance - based plastic design of earthquake resistant reinforced concrete moment frames.* Michigan : Ph.D. Thesis - University of Michigan.

Luu, H., Léger, P. & Trembalay , R., 2014. Seismic shear demand of moderately ductile RC shear walls considering higher modes effects. *Proceeding of the 9th International Conference on Structural Dynamics, EURODYN ,* pp. 451-458.

Maniatakis, C. A., Psycharis, I. N. & Spyrakos, C. C., 2013. Effect of higher modes on the seismic response and design of moment resisting RC frame structures. *Engineering Structures,* Volume 56, pp. 417-430.

Mendoza Pérez, M., 2011. *Desarrollo y validación de un método de evaluación y diseño sísmico basado en desempeño para edificios de concreto reforzado.* s.l.:Tesis Doctoral Universidad Nacional Autónoma de México.

Moehle, J., 2015. *Seismic Design of reinforced concrete buildings.* United State of America: McGRaw-hill.

Newmark, N. M., 1959. A Method of Computation for Structural Dynamics. *ASCE Journal,* Volume 85, pp. 67-94.

Pampanin, S., 2012. Living a New Era in Earthquake Engineering: targeting damage-resisting solutions to meet societal expectations. *Australian Earthquake Engineering Society Conference.*

Panagiotakos, T. B. & Fardis, M. N., 1999. DEFORMATION-CONTROLLED EARTHQUAKE-RESISTANT DESIGN OF RC BUILDINGS. *Journal of Earthquake Engineering,* 3(4), pp. 495-518.

Panagiotou, M., 2008. *Seismic design, testing and analysis of reinforced concrete wall buildings.* Ph.D. Thesis, Dept. of Structural Eng., Univ. of California–San Diego: USD.

Panagiotou, M. & Restrepo, J. I., 2007. Lessons learn from the UCSD full-scale shake table testing on a 7-story residential building slice. *SEAOC convention proceedings,* pp. 57-73.

Panagiotou, M. & Restrepo, J. I., 2009. Dual-Plastic hinge design concept for reducing higher mode effects on high-rise cantilever wall buildings. *Earthquake Engineering and Structural Dynamics,* Volume 38, pp. 1359-1380.

Panagiotou, M. & Restrepo, J. I., 2011. Displacement-Based Method of Analysis for Regular Reinforced-Concrete Wall Buildings: Application to a Full-Scale 7-Story Building Slice Tested at UC-San Diego. *Journal Structural Engineering ASCE,* 137(6), pp. 677-690.

Park, R. & Paulay, T., 1975. *Reinforced Concrete Structures.* New York: John Wiley and Sons.

Park, Y. J., Ang, A. H. & Wen, Y. K., 1987. Damage-limiting aseismic design of buildings. *Earthquake Spectra,* 3(1), pp. 1-26.

Paz, M., 1998. *Structural Dynamics: Theory and Computation.* 4th Edition ed. Louisville, KY: Springer Science & Business Media.

Paz, M. & Leigh, W., 2001. Integrated matrix analysis of structures: Theory and Computation. In: United State of America: Kluwer Academies Publishers, p. 315.

Priestley, M., Calvi, G. & Kowalsky, M., 2007. *Direct displacement based seismic design of structures.* Pavia: IUSS Press, Instituto Universitario di Studi di Pavia.

Priestley, M. J. N., 2000. Performance based seismic design. *12th World Conference on Earthquake Engineering. Auckland, New Zeland.*

Priestley, M. J. N. & Kowalsky, M. J., 2000. Direct displacement based seismic design of concrete buildings. *Bulleting of the New Zealand society for earthquake engineering,* 33(4), pp. 421-444.

Rodenblueth, E. & Herrera, I., 1964. On a kind of hysteresis damping. *Journal of the Engineering Mechanics Division,* Issue 90, pp. 37-48.

Rodiguez, H., Varum, H., Arede, A. & Costa, A., 2012. A comparative analysis of energy dissipation and equivalent viscous damping of RC columns subjects to uniaxial and biaxial loading. *Engineering Structures,* Issue 35, pp. 149-164.

Rosenblueth, E., 1951. *A basis for aseismic design.* Doctoral Thesis, University of Illinois : .

SEAOC, 2000. Vision 2000 - Performance based seismic engineering of buildings. *Structural Engineering Association of California.*

Sullivan, T. J., 2011. An Energy-Factor Method for the Displacement-Based Seismic Design of RC Wall Structures. *Journal of Earthquake Engineering,* 15(7), pp. 1083-1116.

Tremblay, R. et al., 2008. Seismic response of multi-storey reinforced concrete walls subjected to eastern North America high frequency ground motions. *14th WCEE.*

Tremblay, R. et al., 2005. Multi-Purpose earthquake simulation testing set-up for seismic forces resisting systems of multi-story buildings. *Proceedings First International Conference on Advances in Experimental Structural Engineering, Nagoya, Japan ,* Issue Paper No. 533.

Vielma Perez, J. C., 2008. Caracterización del comportamiento sísmico de edificios de hormigón armado mediante la respuesta no lineal. *Doctoral Thesis. Universitat Politècnica de Catalunya UPC. Barcelona.*

Wilson, E., 2015. Termination of the response spectrum method RSM.. *www.edwilson.org/History/ Termination.pdf..*

Wilson, E. L., 1968. *A computer program for the dynamic stress analysis of underground structures,* University of California, Berkeley: SESM Report no.68-1, Division of Structural Engineering Structural Mechanics.

Wilson, E. L., Der Kiureghian, A. & Bayo, E. P., 1981. A replacement for the SRSS method in seismic analysis. *Earthquake Engineering and Structural Dynamics,* Volume 9, pp. 187-194.